Post-stack seismic inversion in reservoir quality assessment: petrophysical aspects of acoustic impedance

by

Emmanuel Kobina Gyasi

B.S., Kwame Nkrumah University of Science and Technology, 2020

A THESIS

submitted in partial fulfillment of the requirements for the degree

MASTER OF SCIENCE

Department of Geology
College of Arts and Sciences

KANSAS STATE UNIVERSITY
Manhattan, Kansas

2025

Approved by:

Major Professor
Dr. Abdelmoneam Raef

Copyright

Abstract

The Morrison Northeast field produces hydrocarbon from the thin Viola formation: Among the 12 wells that have been drilled into the Viola formation, five of them have proven to be non-producing. This problem of well placement is caused in part by complex seismic amplitude responses arising from both the constructive and destructive interference reflectors waveform (tuning effects) and petrophysical and diagenetic reservoir rock heterogeneities. It is therefore consequential to understand acoustic impedance variation in relation to well-logs petrophysical analysis, to guide placement of new wells and/or enhanced oil recovery programs.

This study illuminates the utility of acoustic impedance rock property in mapping the variation of reservoir porosity and facies. It is noteworthy that acoustic impedance is independent of stratigraphic thickness and is strongly dependent on porosity variations within the Viola carbonates. Significant correlations of impedance to porosity for leverage well placement planning in the development of Morrison Field. This study has also provided insights on needed seismic phase adjustments (+70) for more accurate time-to-depth conversion of the Viola-Top seismic horizon. The 3D seismic data has undergone spectral whitening to boost the seismic resolution by broadening the spectral bandwidth and flattening the amplitude spectrum. Seismic horizons were retracked, a synthetic to seismic well ties were established, a representative wavelet was derived to improve inversion accuracy, and an inverted acoustic impedance log was obtained at well locations.

Finally, beyond conventional inversion techniques, this study presents data driven machine learning approaches to predict impedance values in areas lacking well control. Providing a robust framework for improving hydrocarbon exploration and production efficiency. The significance of this workflow lies in establishing a workflow that enhances the reservoir quality assessment,

offering practical solutions for optimizing well placement and maximizing hydrocarbon recovery in complex geological settings based on acoustic impedance-reservoir porosity relationships and improved accuracy of time-to-depth conversion.

Table of Contents

List of Figures

List of Tables

Acknowledgements

I would like to express my sincere gratitude to my advisor, Dr. Abdelmoneam Raef, for his guidance, support, and encouragement throughout my research.

I am also grateful to my committee members, Dr. Behzad Ghanbarian and Dr. Claudia Adam for their valuable feedback and insights.

I appreciate Kansas State University for providing the resources and opportunity to complete this work.

Special thanks to the Geology Department for their generous financial support and for fostering an excellent learning environment. Your commitment has been instrumental in helping me achieve my academic goals.

Lastly, my heartfelt gratitude goes first to my family, and to my friends for their unwavering support and motivation during this journey.

Dedication

This piece of achievement is wholeheartedly dedicated to my mother, I owe you everything.

Chapter 1 - Introduction

3D seismic data has revolutionized the petroleum industry by providing clear structural images of the subsurface and probing subsurface lithology and pore-fluid effects, leading to several benefits in exploration, field development and production. It reduces the risk of drilling dry or marginal exploration wells by identifying potential targets and their size, enabling robust basis for well placement for enhanced flow rates and efficient drainage, also helping development programs of rejuvenating mature fields with declining production by identifying bypassed oil and gas high-success rate prospects. Seismic reflection data interpretation enables continued updating of reservoir models continuously, and it facilitates effective reservoir management (Nestvold, 1996).

Acoustic impedance inversion of P-wave seismic reflection data has been utilized in reservoir characterization because of the merit of converting a seismic amplitude dataset to reservoir acoustic impedance, which is a rock property quantified as the product of rock bulk density and P-wave seismic velocity (e.g., Erryansyah et al., 2020). It is invaluable to estimate acoustic impedance, especially in the case of a thin reservoir, such as the Viola limestone, where seismic amplitudes would suffer from thin layer interference effects, otherwise referred to as tuning effects (e.g., Widess, 1973; Papageorgiou and Chapman, 2021).

Tuning effects in seismic exploration describe the changes in the seismic reflection amplitudes and waveforms that occur when a subsurface layer's thickness is less than one-quarter of the dominant wavelength of the seismic wave used to image it. This phenomenon arises from the interference between the reflected waves from the top and bottom of the thin layer (Li & Guo, 2007; Roden et al., 2017). These reflected waves, depending on the layer thickness, can interfere constructively, resulting in a stronger amplitude, or destructively, leading to a weaker amplitude or completely obscuring the amplitude which is both bad for seismic interpretation (Adriansyah & McMechan, 2002).

The interference pattern is influenced by the layer thickness relative to the seismic wavelength, the acoustic impedance contrast at the layer boundaries and the shape of the seismic wavelet (Roden et al, 2017; Brown et al., 1986).

Tuning has a significant impact on seismic resolution and the utility of seismic amplitudes in reservoir characterization. Seismic resolution refers to the ability to distinguish between separate features in the subsurface. The tuning thickness defines the limit of vertical resolution, one-fourth of the dominant wavelength. Layers thinner than the tuning thickness become increasingly difficult to resolve individually as their top and bottom reflections interfere and overlap (Roden et.al., 2017). In the early stages of this study, we aimed at improving the resolution of the 3D seismic data set that covers the Morrison NE field in Clarks County producing hydrocarbon from the thin layered Viola limestone formation.

The Viola Limestone is a shelf carbonate deposit that formed in the Middle Ordovician period in a warm, tropical, shallow marine environment (Bornemann et al., 1982; Vohs, 2016). The Viola is found throughout Texas, Oklahoma, Nebraska, Missouri and Kansas (Carlson & Newell, 1997). It is a significant petroleum reservoir in Oklahoma and Kansas (Linares & Totten, 2016). The Viola limestone does not have a consistent topographic expression. Instead, the topography of the Viola is largely controlled by an erosional unconformity that separates it from the overlying Maquoketa formation (Vohs, 2016). The erosional period contributed to the development of significant variations in thickness and secondary porosity vugs in the upper portion of the Viola Limestone. These vugs, which are irregular holes that cut across grains and cement boundaries, are responsible for much of the porosity and permeability of the Viola limestone making it a suitable reservoir rock, also generating paleotopographic traps where hydrocarbons accumulate (Vohs, 2016).

The variable thickness of this formation (Fig1.1) gives rise to the seismic-amplitude problem of most thin hydrocarbon reservoirs (tuning effects). Conventional ways of tackling this problem is dependent on seismic attributes that suffer from tuning. This study explores other data-driven options outside the scope of seismic attributes to better understand the petrophysical aspects of reservoir quality and optimal well placements within the Morrisson NE field. This study revealed that the reduction in impedance values, associated with more porous areas within the study area indicates substantial hydrocarbon saturations.

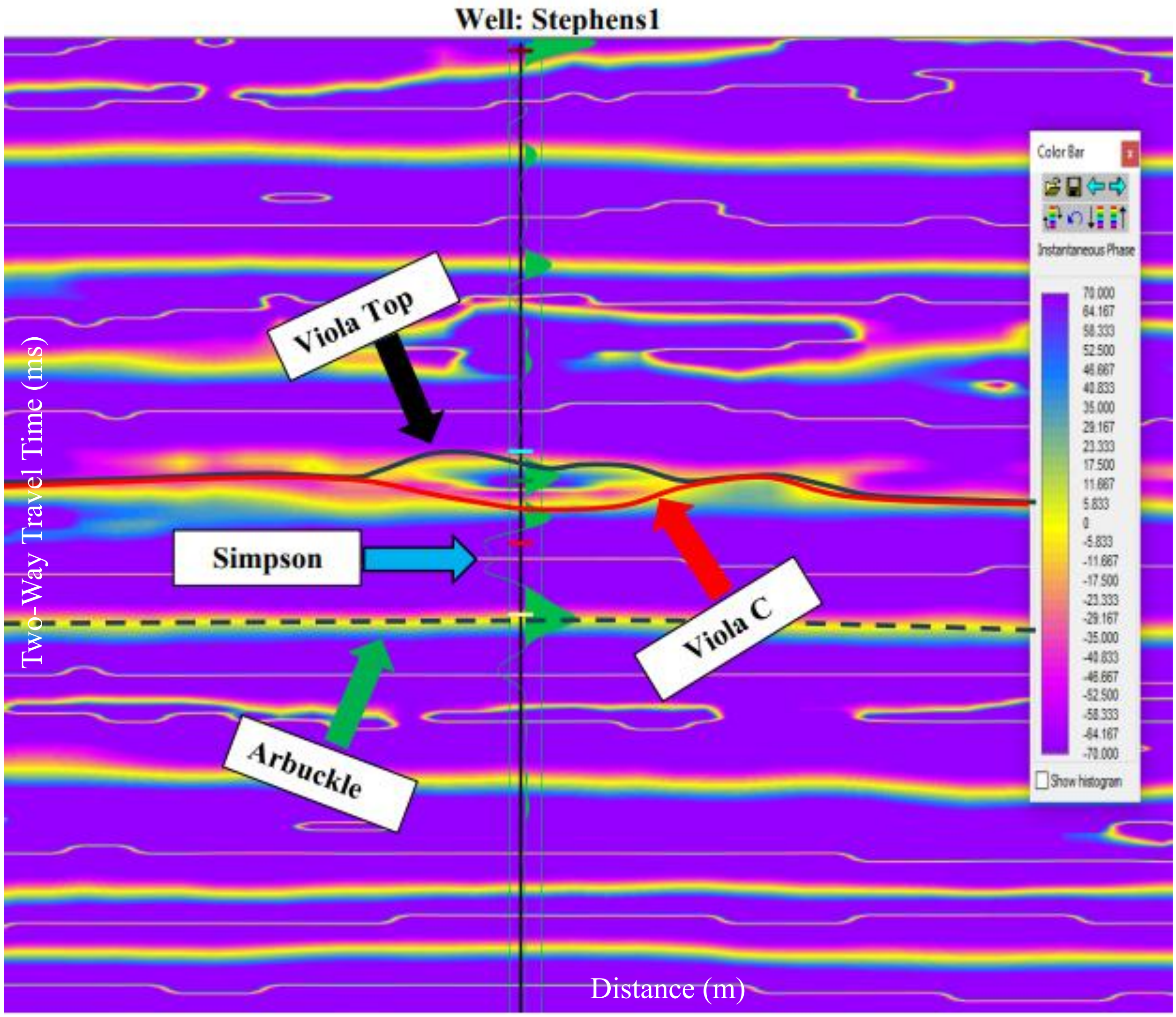

Figure 1.1: Instantaneous phase cross section across Stephens1 along with its synthetic. The Viola limestone thickens and splits (seismic doublet) into two peaks named Viola Top (black line) and Viola C (red line) around the well. and Arbuckle (black dashed line) is a strong peak with a consistent instantaneous phase. Phase angles are represented by the color bar on the right. (Jallow, 2024)

1.1 Problem Statement

Thin layer interference renders seismic amplitude variation dependent on stratigraphic thickness among other factors. Acoustic seismic inversion of a 3D survey is likely to circumvent the problem of thin layer interference by producing a rock property parameter (acoustic impedance) (Fig1.2), which is a function of mainly lithofacies porosity in case of Viola limestone of this study area.

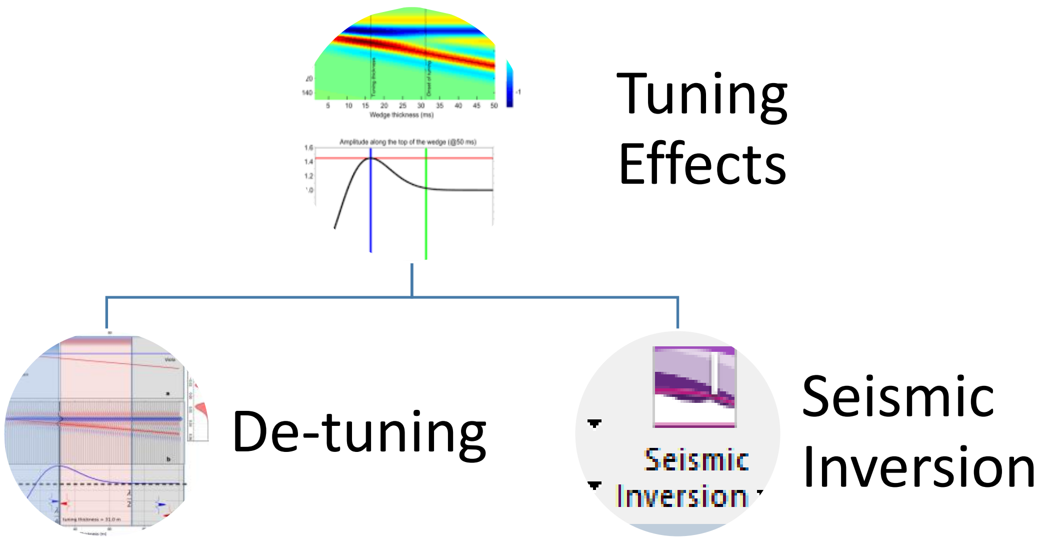

Figure 1.2: A visual representation of hypothesis. Seismic inversion provides an unconventional route to solve tuning effects challenges

1.2 Previous Study

St. Clair (1981, &1985) examined cores of the Viola limestone in Barber and Pratt counties which lie to the east of the Morrison NE field, contributing significantly to our understanding of the formation's depositional environments and diagenetic processes. Based on his observations, he identified four distinct, mappable units within the Viola Limestone. He proposed that the Viola limestone was deposited in a fluctuating pattern of marine transgressions and regressions, and identified several diagenetic processes, including dolomitization, and silicification that changed the original texture and composition of the limestone. St. Clair's work, though not explicitly focused on the Morrison NE field, but his proposal is consistent with

Bornemann et al.'s (1982) findings and provides a framework for understanding the vertical variations observed in the Viola limestone within the Morrison NE field.

Richardson (2013) revealed from his studies on the Herd Viola trend in Comanche County that hydrocarbon production from the Viola Limestone is not solely determined by structural traps but significantly influenced by the preservation of its upper portion, which is characterized by porous dolomite. Richardson has attributed this preservation to an erosional unconformity between the Viola limestone and the overlying Maquoketa/Kinderhook section. Thus highlighted the importance of the subsurface mapping techniques in predicting the optimal conditions for porosity preservation in the Viola limestone and emphasized that the Viola produces from a paleotopographic trap and observed from regional studies, a correlation between the geologic conditions in Herd pool and other Viola pools in Comanche and Clark counties encompassing the Morrison NE field.

Vohs (2016) sought to understand the reservoir heterogeneities and hydrocarbon entrapment settings within the Viola limestone, investigated if unique attributes could be identified in producing wells that could guide exploration in other areas within the Viola. Additionally, he explored whether reprocessing seismic data could have led to better drilling decisions, potentially avoiding dry holes and poorly producing wells. He confirmed Richardson's (2013) paleotopographic traps in Viola oil production, observed a strong correlation between low amplitude anomalies and producing wells, and created tuning thickness charts for wavelets extracted at each well within the survey area. These charts can help differentiate between amplitude anomalies caused by thin beds and those caused by actual changes in reservoir properties. Linares (2016) conducted petrographic analysis of the Viola limestone, examining drill-cutting samples from Stephen's Ranch within the Morrison NE field, focused on the relationship between the depositional environment, diagenetic alterations, and reservoir quality of the Viola.

Raef et al., (2019) characterized the relationship between lithofacies and reservoir quality, focusing on the distribution and characteristics of these productive dolomitized zones, by employing petrophysical and petrographic methods coupled with unsupervised machine learning approach based on five seismic attributes consistent with Ca-Mg ratio and the observed variation in sonic transit time (DT log) with porosity increase.

Victor (2020) used ultrasonic velocity measurements on core samples to determine the elastic properties of the Viola Limestone. He used both P-wave and S-wave velocities, providing insights into the stiffness and its response to seismic waves, and integrated his laboratory derived ultrasonic velocity measurements with in-situ well log data to understand core-scale elastic properties and the larger-scale measurements obtained from well logs. To understand how changes in pore fluid composition affects Viola’s elastic properties, he applied Gassmann’s fluid replacement model, that indicated that the impact of hydrocarbon saturation on seismic properties becomes more significant in zones with higher porosity. This observation suggests that porosity plays a crucial role in amplifying the seismic detectability of hydrocarbons within the Viola Limestone.

Jallow (2024) suggested focusing on areas characterized by structural highs, substantial thicknesses, and persistently low amplitudes after detuning.

Chapter 2 - Geological Setting and Background

2.1 Study Area

The study area for the Viola Limestone is the Morrison Northeast Field of Clark County in south-central Kansas (Fig 2.1). This area is where the Hugoton Embayment of the Anardarko Basin, located to the southwest, meets the Central Kansas Uplift and Pratt Anticline to the east (Fig 2.2). The 3D seismic survey conducted in this field covers an area of approximately seven and half square miles (Vohs, 2016). It includes 320 from 1001 to 1320 inlines running west to east and 380 crosslines running south to north, with a bin spacing of 82.5 feet.

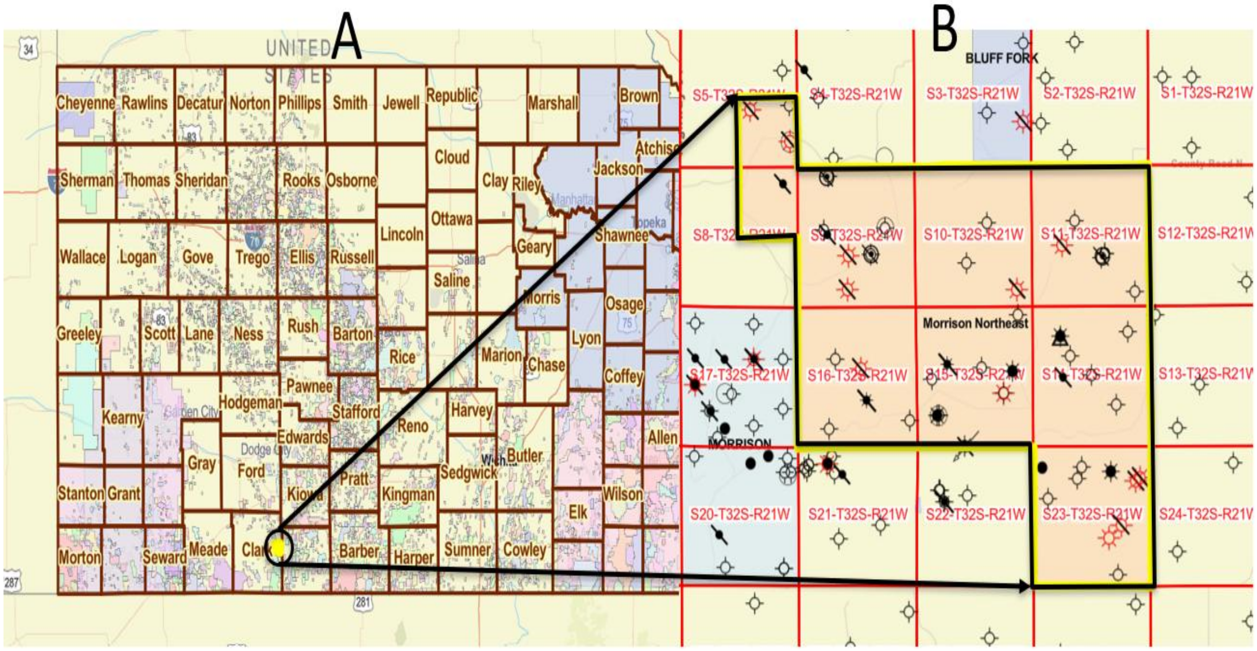

Figure 2.1: Regional and local map of the study area in Clark County, Kansas. (A) The map of Kansas, with county boundaries outlined in brown. The yellow dot circled in black marks the location of the study area within Clark County. (B) A zoomed-in section of Clark County showing the Morrison Northeast Field, delineated by yellow and black borders. The map includes township and range grid labels (e.g., T32S-R21W) and various drilling wells marked within the field and its surroundings. The black arrows illustrate the transition from the regional to the local scale of the study area.

Figure 2.2: Anardarko Basin map. Red star indicates the approximate location of the study area within Clark County, Ks. (Modified after Ball, 1991)

2.2 Stratigraphic Setting

The stratigraphic setting (Fig 2.3) in the Morrison Northeast field of Clark County, Kansas, includes several key formations from the Cambrian and Ordovician periods. The stratigraphic units in descending order within this field include the upper Ordovician Maquoketa Shale, middle Ordovician Viola limestone, middle Ordovician Simpson group and the lower Ordovician/Cambrian Arbuckle group. That is, the Viola limestone, which is the reservoir of interest is sandwiched above and beneath by Maquoketa shale and the Simpson group respectively. The Arbuckle creates a distinctive seismic signature that aids in the mapping of other relevant horizons.

Maquoketa Shale

The Maquoketa shale is primarily a gray, dense limestone. However, it includes pale green or greenish-gray dolomitic shale, gray pyritic shale, and gray or buff dolomite (Cole,1975). This formation is relatively thin, averaging 20 to 25 feet thick in the study area (Vohs, 2017, Victor, 2020, Jallow,2024). However, it can thicken significantly in east- central Kansas, where it reaches over 170 feet. This variation in thickness is likely due to post-depositional erosion (Cole 1975). The Maquoketa shale unconformably overlies the Viola Limestone and prevents the escape of hydrocarbons from the reservoir (Richardson, 2013, Raef et. al., 2019). Despite its importance as a seal, the Maquoketa Shale is often difficult to identify on well logs (Richardson, 2013). This difficulty arises from its variable lithology and the lack of distinctive features.

Viola Limestone

The Viola limestone is a middle Ordovician formation that serves as the primary producing formation in the study area. This formation was deposited in a warm, tropical marine setting, likely during the high stand of a large inland sea that covered much of the North American interior during this time (Raef et. al., 2019; Bornemann et al., 1982). The Viola Limestone is characterized by its complex mineralogy and lithology. It is composed of varying amounts of limestone, dolomite and chert (Bornemann et al., 1982). This complex composition leads to variable porosity and permeability throughout the formation, making the identification of productive zones challenging. This formation is informally divided into four distinct zones or lithofacies, labeled A to D zones as illustrated in Figure 2.3.

The “A” zone is typically a thin bed of 10 to 30 feet, that includes chert fragments, cryptocrystalline limestone, and fine to medium crystalline, sucrosic dolomite, that can be easily identified under the binocular microscope (Linares, 2016). Vugs within the “A” zone are associated with good porosity and permeability, making it a good reservoir rock (Goebel, 1968). The “B” zone is characterized by a predominance of dolomite and can be up to 100 feet thick (Linares, 2016) it consists of cherty dolomite with intercrystalline porosity (Hagood, 2019).

The “C” and “D” zones are non- productive zones beneath the “A” and “B” zones. These zones are denser and more crystalline, lacking the productive porosity of the upper zones (Linares, 2016). Porosity in the Viola is primarily controlled by the presence of irregular cavities formed by dissolution due to the subaerial exposure of its uppermost part (vugs), and fractures created by tectonic stresses. The most productive zones, particularly “A” zone, are associated with the preservation of porous dolomitized facies, abundant vugs and a favorable paleo topographic setting that traps hydrocarbons as seen in Figure 2.4 below (Richardson, 2013).

Simpson Formation

The middle Ordovician Simpson Group stratigraphic unit within the study area lies beneath the Viola Limestone. While this formation is not a known significant hydrocarbon producer, its lithology and stratigraphic position impact on the characteristics of the Viola Limestone reservoir. The Simpson Group is typically divided into three informal units based on their dominant lithology: the upper Simpson unit that is characterized by a mix of shale and limestone. It often includes two hard blocky shale layers separated by a soft, chalky, fossiliferous limestone with poor porosity. The middle unit features the upper Simpson sand, which is fine grained, poorly sorted, sub-rounded sandstone composed primarily of quartz grains with abundant shale inclusions. The thick shale layer in this unit is roughly about 60 feet similar to that of the upper Simpson. The base of the Simpson formation is defined by the lower Simpson sand.

Arbuckle Formation

The Arbuckle stratigraphic unit encompasses sedimentary rocks from the Cambrian to the lower Ordovician age in subsurface Kansas (Cole, 1975). Its depths range from about 500 feet in southeastern Kansas to over 5000 feet in southwestern Kansas, with a general thickening trend from north to south. The thickest recorded section is 1390 feet in southeastern Kansas (Cole, 1975). The diverse lithology that makes up this formation include dolomite variations (sandy and cherty), sandstones primary found in the oldest subsurface rocks, often as quartz sandstone and sandy carbonate rocks (Cole, 1975). The strong contrast in acoustic impedance between the Arbuckle and the overlying Simpson formation creates a distinct seismic reflector, aiding in the mapping of subsurface stratigraphy and identifying potential traps in overlying units within the study area (Vohs, 2016).

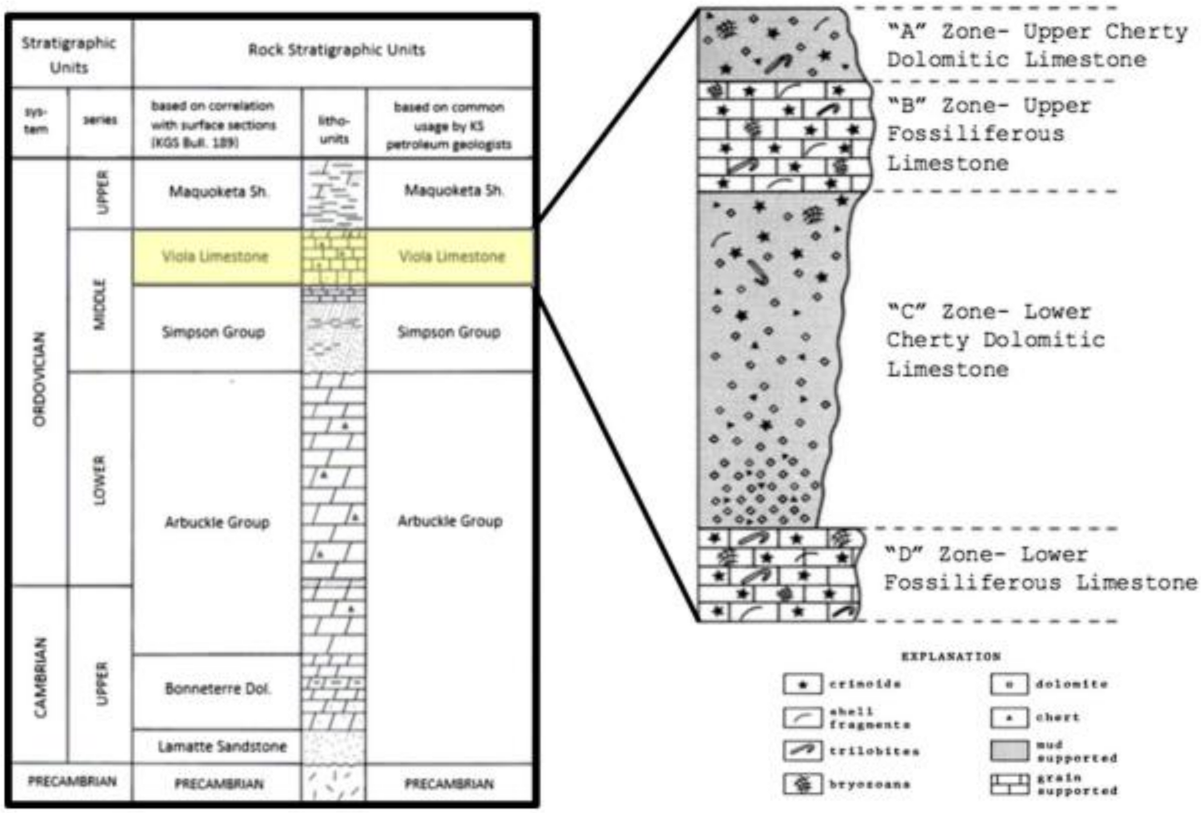

Figure 2.3: Stratigraphic column showing formations of interest in the study area and the four distint lithofacies within the Viola (Raef et. al., (2019), modified after Cole (1975))

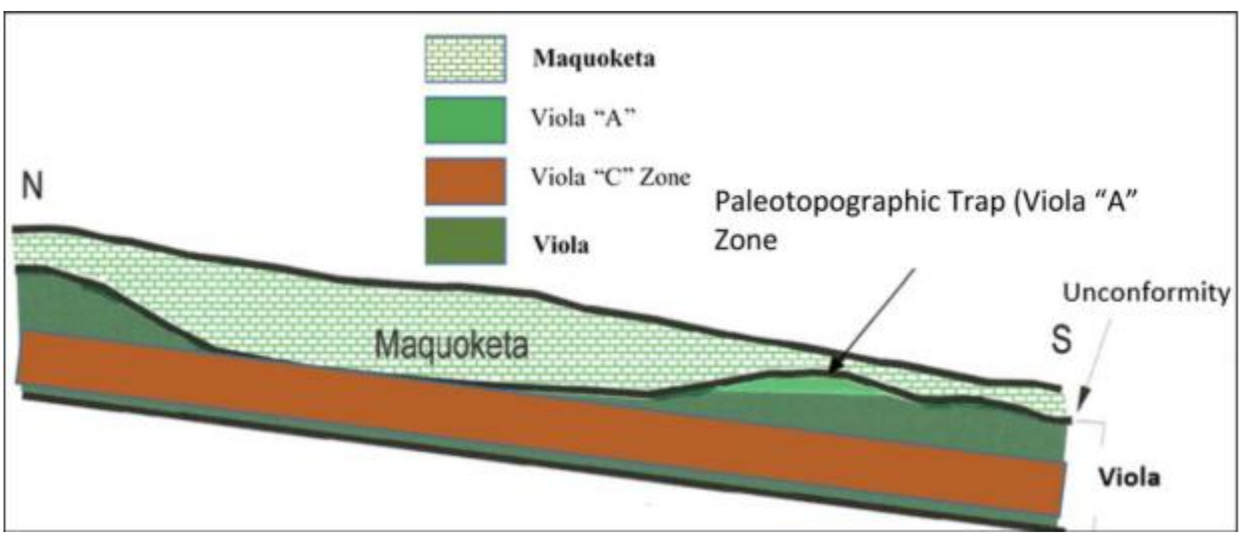

Figure 2.4: Idealized cross section showing paleotopographic traps within the Viola of the Herd Field, Comanche County, Ks. The Herd Field is approximately fifteen miles east of the study area (modified after Richardson (2013))

2.3 Seismic Resolution

Seismic resolution refers to the ability to distinguish between two features that are close together (Herron, 2011). It applies to both seismic data and the products of interpreting seismic data, such as maps, in both temporal and spatial domains (Herron, 2011). The temporal resolving power of seismic data is described by the tuning thickness of the data, based on the fundamental equation that relates velocity, dominant frequency and wavelength.

Vertical Resolution

The ability to distinguish separate reflections from the top and bottom of a thin bed is vertical resolution. The Rayleigh limit of vertical resolution is one-quarter of the seismic signal's wavelength, tuning thickness is the point at which the composite amplitude from the top and base of a bed is maximized (Herron, 2011). When the bed thickness is above the tuning thickness, the seismic responses from the top and base of the bed are separate and distinct, or resolved. Below the tuning thickness, the waveform of the composite response does not change, but its amplitude decreases as the bed thickness decreases. Koefoed (1981) proposed that the width of the main lobe, the side lobe ratio or peak-to-trough ratio, and the amplitude of oscillations control vertical resolution, whereas the temporal resolution of a broadband wavelet with a white spectrum is controlled by its highest terminal frequency (Kallweit, 1982). An event that is detectable may or may not be resolvable because resolution is primarily a problem of frequency band, whereas detection is principally one of acquisition (Kallweit, 1982).

Horizontal Resolution

This is the ability to separate two features that are close together on a map or cross-section laterally across the subsurface. The spatial resolving power of seismic data is usually described in terms of the Fresnel zone, defined as the portion of a reflector from which reflected energy can reach a detector within one-half wavelength of the first reflected energy (Herron, 2011). The greater the Fresnel zone the worse the lateral resolution and vice versa. Seismic migration collapses or reduces the size of the Fresnel zone and moves dipping reflectors to their true locations, improving lateral resolution (Rost & Thomas, 2009; Herron, 2011).

2.4 Inverse Q-filtering

Inverse Q-filtering is a seismic data processing technique that addresses the issue of anelastic attenuation, which causes a loss of amplitude and bandwidth in seismic data as the wave travel through the Earth (Schoepp et al., 1998). As seismic waves travel through the Earth, they experience a decay that increases with time, diminishing both amplitude and bandwidth, referred to as anelastic attenuation (Schoepp et al., 1998). This is due to the Earth's materials absorbing the energy of the seismic waves, with higher frequencies being attenuated more than lower frequencies (Djanawir & Langitan, 2004). The quality factor, or Q, is a measure of attenuation (Sheriff, 1994). Inverse Q filtering aims to compensate for the effects of anelastic attenuation, it attempts to restore the attenuated energy of the seismic signal in a time-variant manner. By so doing, it increases the bandwidth and improves the resolution of seismic data (Djanawir & Langitan, 2004; Chopra et al., 2011). The inverse Q filtering works by applying a filter that is the inverse of the attenuation function. This compensates for the loss of high-frequency signals and the broadening of the wavelet shape that occurs as seismic waves travel the subsurface. When combined with deconvolution, inverse Q filtering compensates for the effects of attenuation, as deconvolution solves the problem of reverberation in the presence of noise, particularly in low signal to noise ratio areas (Peacock & Treitel, 1969).

2.5 Stacking & Spectral Whitening

Stacking plays a significant role in improving signal-to-noise ratio and imaging quality of seismic data (G. Liu et al., 2009). There are two orders of operations for common seismic processing, pre stack and post stack. The former entails conducting the seismic processes before adding the seismic traces (stacking) whilst the latter means the data is processed after stacking.

To maximize resolution in the seismic data processing sequence, wavelet processing to zero phase and post-stack spectral whitening are most critical (Morris, 1995). Post-stack spectral whitening enhances or boosts high frequencies that were attenuated by the stacking process itself (Morris, 1995). Spectral Whitening is a seismic data processing technique that aims to flatten the frequency spectrum of seismic data and improve its bandwidth loss introduced during data acquisition and processing. This process is crucial for enhancing the interpretability and to precondition seismic data to meet the theoretical assumptions of Amplitude Versus Offset (AVO) analysis (Nagarajappa et. al., 2009; Chopra & Marfurt, 2018; Maulana et. al., 2022). As it compensates for spectral bandwidth loss caused by factors like Normal Moveout (NMO) stretch, creating a spectrum that is non-stationary with offset and time, where far offsets undergo frequency loss reducing resolution and continuity of AVO attributes (Nagarajappa et. al., 2009). Spectral balancing, which is a variation of spectral whitening is a deconvolution tool used to pre-condition post-stack seismic data in the inversion process (Maulana et. al., 2022), as is the case with this research.

2.6 Jallow's (2024) Detuned Seismic Amplitude

Jallow (2024) developed a data-driven method to remove the effects of thin-layer tuning on seismic horizon attributes in the Viola carbonate reservoir of the Morrison NE field in Clark County, Kansas. He used a statistical approach to determine tuning error, synthetic wedge models to simulate the tuning effect on seismic attributes and a machine learning technique to automate the identification and removal of tuning effects. This study revealed that areas with structural highs, substantial thicknesses, and low amplitudes after detuning are potential areas for hydrocarbon production. Specifically, hydrocarbon-producing wells (S1, S2, S4, S6, & S7) that were masked by high amplitude anomalies before detuning, showed lower amplitudes after detuning. Nonproducing wells S5 and S8, which had been identified as promising drilling targets due to structural highs, showed high amplitudes even after detuning, suggesting the absence of hydrocarbons. Detuning also identified areas where instantaneous frequency peaks are associated with hydrocarbon saturation rather than with tuning effects. The above deductions was built on the knowledge from Raef (2001), that zones of decreasing amplitude has high instantaneous frequency values and indicate the presence of hydrocarbons.

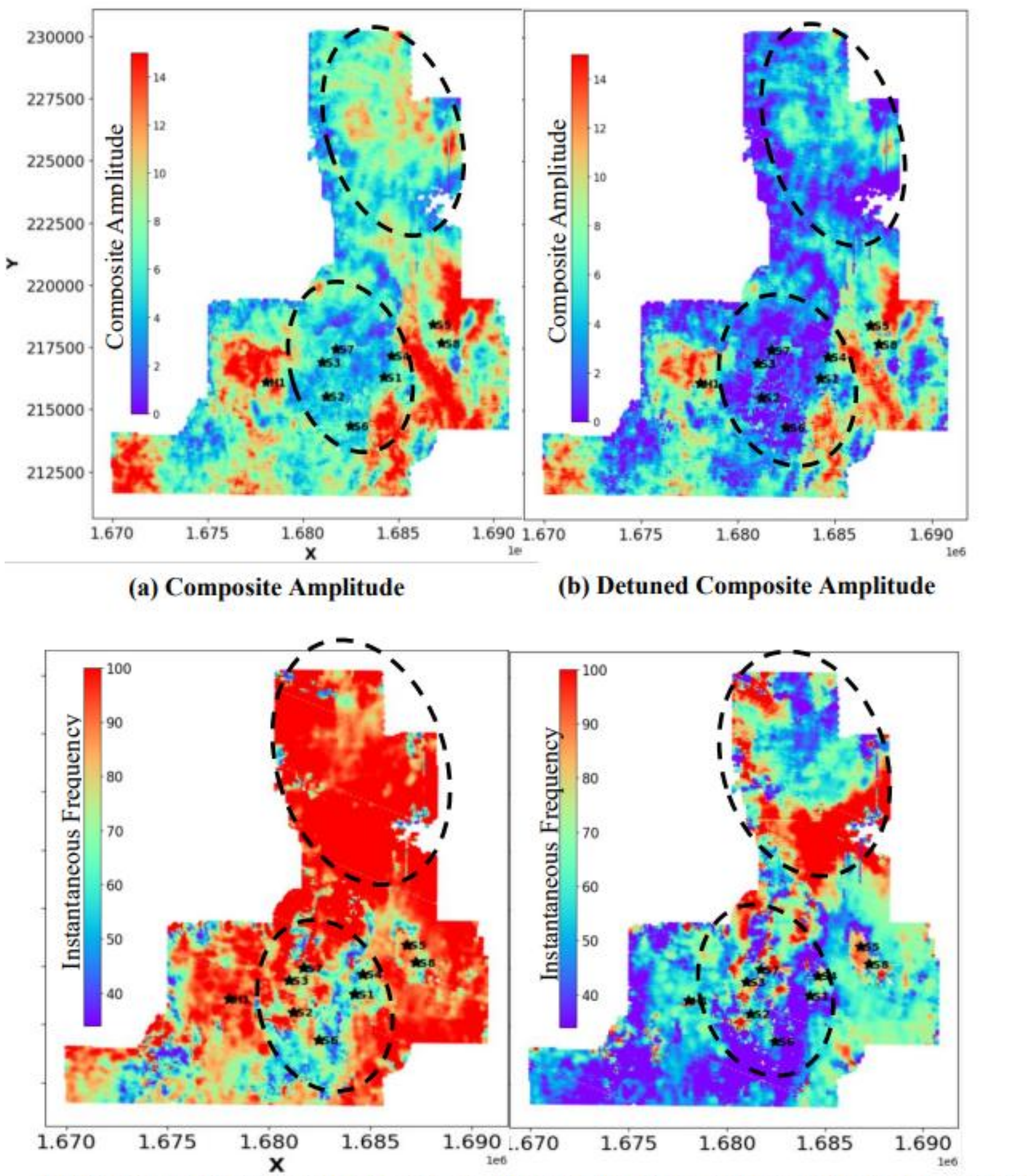

(a) Composite Amplitude (b) Detuned Composite Amplitude

(c) Composite Instantaneous Frequency (d) Detuned Composite Instantaneous Frequency.

Figure 2.5: Original and corrected attributes from statistical method (Jallow, 2024).

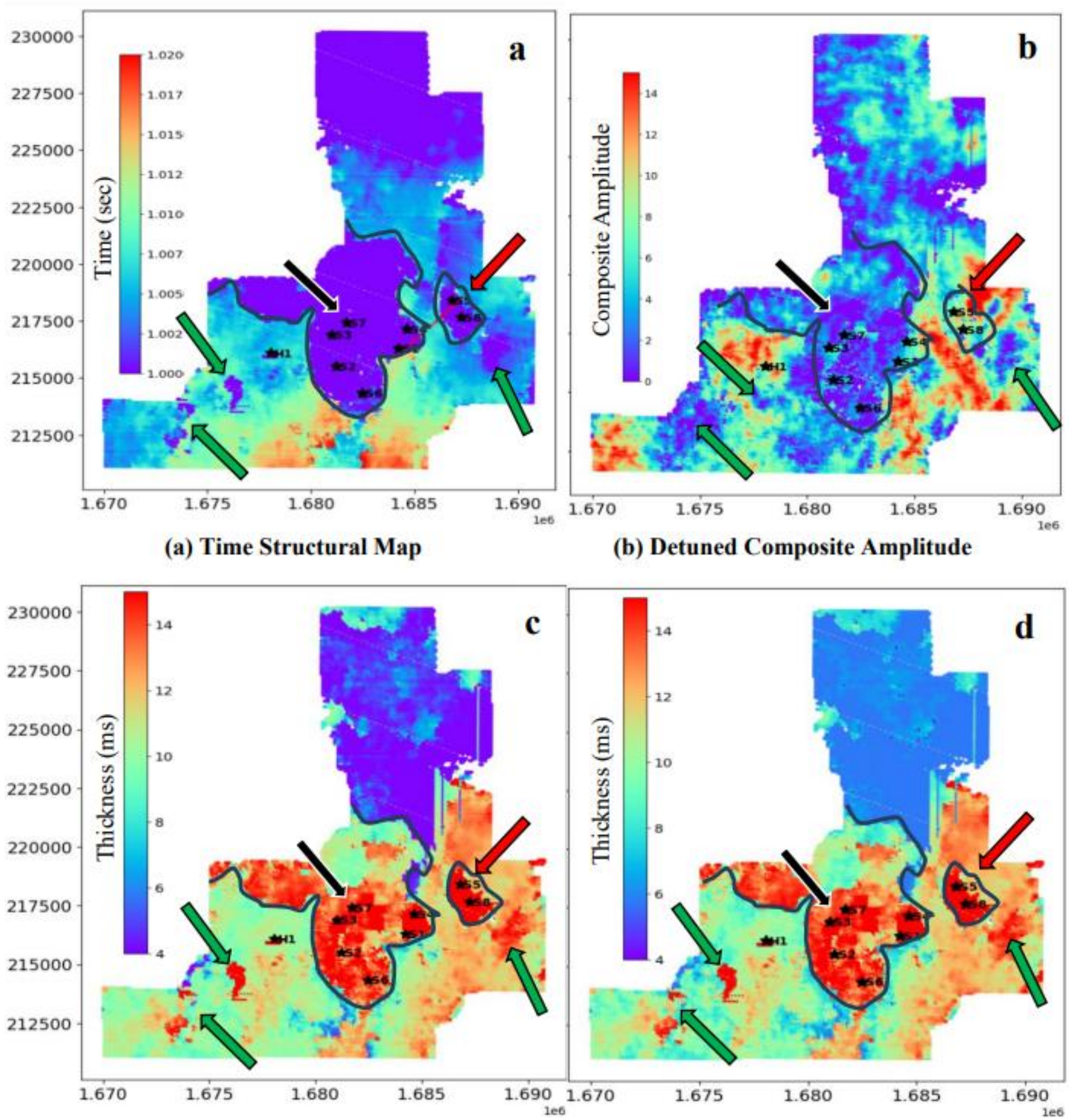

Figure 2.6: Well locations superimposed on the time structural map (a), detuned composite amplitude map (b), original isochrone map (c) and Detuned isochrone map (d) highlighting the correlation between structural highs, high thicknesses, and well locations originally targeted for drilling. Producing wells (black arrows), nonproducing wells (red arrows) and potential drilling zones (green arrows) are highlighted (Jallow, 2024)

Chapter 3 - Data and Methods

3.1 3D Seismic Data

This study utilized a 3D seismic reflection data volume covering the Morrison NE field, in Clark County Kansas, acquired in 2010 by Coral Coast Petroleum. This seismic survey was conducted to explore the optimal conditions for hydrocarbon field development and production. The seismic data volume (Fig 3.1) contains 320 inlines, and 380 crosslines with acquisition geometry of 82.5ft x 82.5ft bin size, 2ms sampling rate and a data length of 2 seconds. The data also had an original spectral bandwidth of 15Hz to 84Hz. The seismic phase was established through 1d synthetic seismic modeling and well-to-seismic matching and was corrected to zero-phase angle to improve resolution and time-to-depth conversion accuracy. The bandwidth of the seismic data and the resolution have further been enhanced through a spectral whitening workflow.

3.2 Wireline Logs

Well logs, otherwise referred to as wireline logs (Fig 3.2), are recordings of any rock formation characteristics made against depth traversed by a measuring equipment lowered on a cable (wireline) into a wellbore ("1. Review of Basic Concepts," 1984). Well logs provide information about both geological and petrophysical properties of rock strata which can be used to evaluate porosities and saturations of reservoir rocks, and for depth correlations (1. Review of Basic Concepts," 1984). In this study, the well logs were used for 1D forward modelling, lithology Cross plots and simulated annealing inversion. Sonic (DT) and density (RHOB) logs were fed into the seismic inversion feature in S & P Global Kingdom software to invert the seismic response at the well locations to acoustic impedance logs.

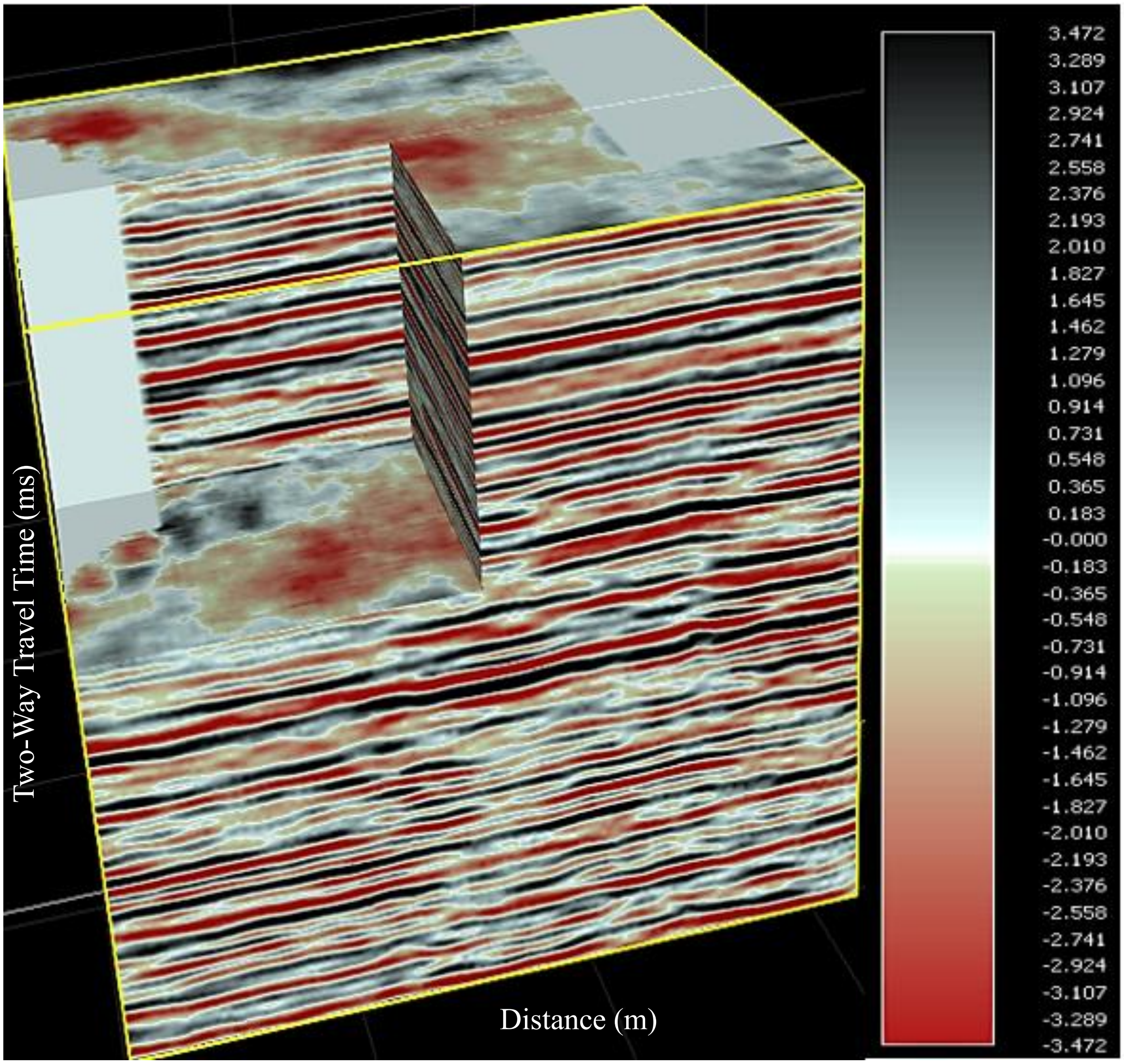

Figure 3.1: Stephens Ranch 3D seismic volume with inlines and crosslines in a 3D view

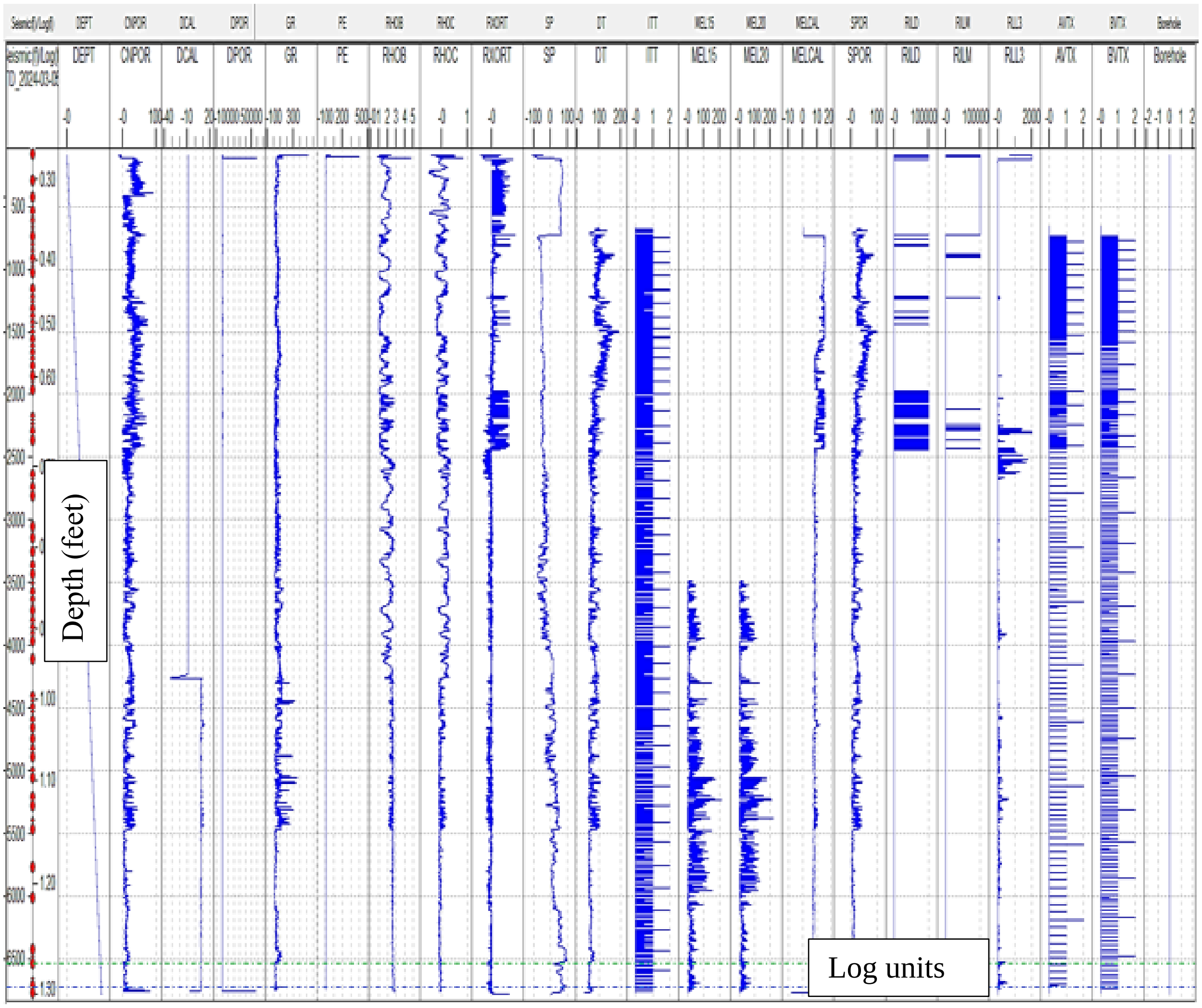

Figure 3.2: Well log display, showing multiple petrophysical logs plotted against depth. The depth scale (in feet) is displayed on the leftmost column, with various log curves recorded in blue across multiple tracks. The logs include gamma-ray (GR) resistivity (RILD, RILM, RLLD), density (RHOB), neutron porosity (DPOR), sonic (DT), spontaneous potential (SP), and several other derived petrophysical parameters.

3.3 Phase Shift Adjustments

Phase shift in seismology refers to the change in the phase of a seismic wave, which can occur due to post-critical angle incidence at underground discontinuities (Zhang et al., 2012). Changes in phase of seismic data manifests as non-zero phase wavelets (Fig 3.3) which is not ideal for interpretation, most interpreters prefer zero-phase wavelets deduced from a phase corrected data because, it is symmetrical with most of its energy concentrated in its central lobe, less ambiguity to associate observed waveforms with subsurface structures, better resolution, maximum amplitude occurs at the center of the waveform and coincides with time horizon, and a horizon track drawn at the center of the wavelet coincides with the travel time to subsurface interface causing reflections. To obtain all these benefits, we applied an average phase adjustment of (+70) to correct for the phase of the seismic data.

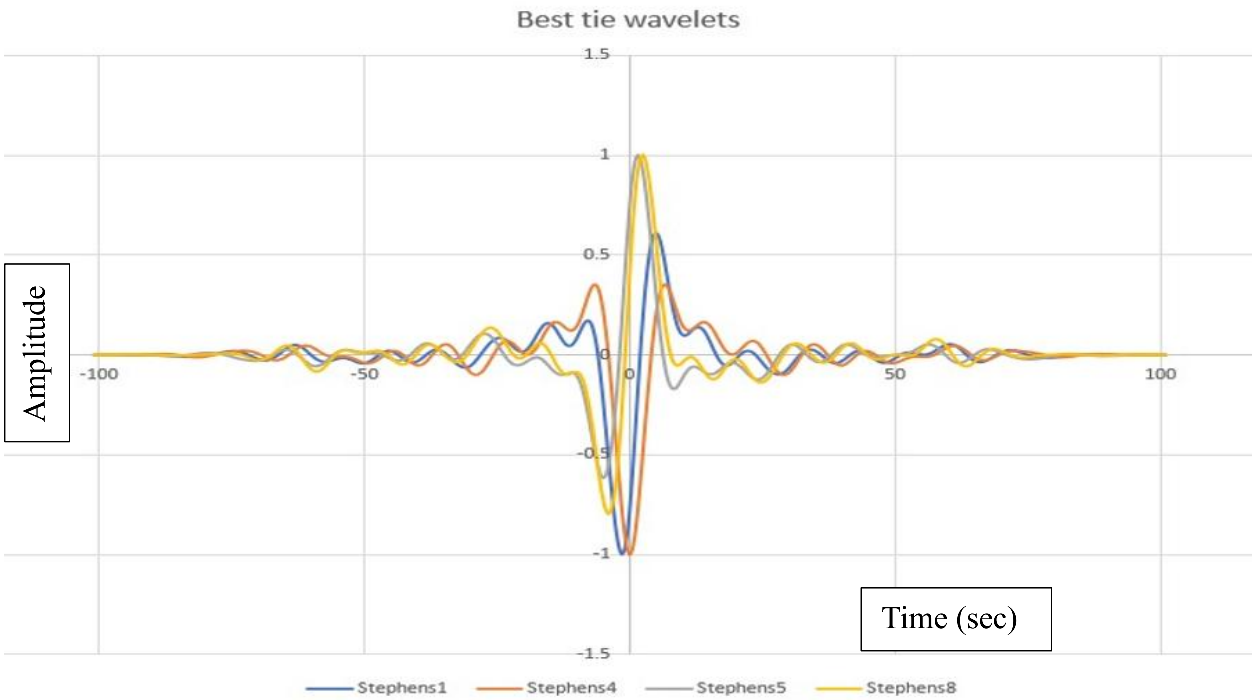

Figure 3.3: Non-zero phase wavelets, which is non-symmetrical with unequal side lobes extracted from Stephens 1 (blue), Stephens 4 (orange), Stephens 5 (green) and Stephens 8 (yellow) wells.

3.4 Seismic Wavelet Extraction

A seismic wavelet is a fundamental component of seismic data linking seismic data and subsurface geological features (Cui & Margrave, 2014). It represents the acoustic pulse disturbance that propagates outward from a source such as a dynamite explosion (Ricker, 1953). Seismic resolution is limited by the time breadth of the seismic wavelet. When wavelets overlap significantly, they can be difficult to interpret, resulting in a loss of resolution (Ricker, 1953). We used the S & P Global Kingdom suite's frequency extraction method to extract wavelets from seismic data within a radius of ten seismic traces around each well location (Fig 3.4). These wavelets have different shapes (Fig 3.5). The wavelets were used to generate synthetic seismograms and for seismic inversion phase at the well locations.

3.5 1D Seismic Synthetic Modelling (Seismic-to-Well Tie)

A seismic-to-well tie is a process of calibrating well log data with seismic data (White & Simm, 2003). Well logs, such as sonic (DT) are measured at high frequencies and fine depth sampling intervals, while seismic data have a lower frequency range and coarser sampling interval (Singh, 2008). This allows the higher-resolution data from the well to interpret the lower-resolution data and vice versa (Jallow, 2024). It is frequent practice to stretch and squeeze the synthetic seismogram to force a tie, but this is not technically justifiable without confirmatory evidence (Singh, 2008). We stretch due to travel time reduction resulting from the fact that the sonic log frequency is several orders of magnitude higher (higher velocities) than that of the seismic data, and squeeze due to transit time increase arising from drilling problem as diameter of wellbore might increase due to caving in. The goal of a seismic-to-well tie is to achieve an optimal match between seismic data and well log data without relying on methods such as stretch-and-squeeze (Singh, 2008).

The 3D seismic reflection dataset volume and well logs that cover the Morrison NE field, Clark County, Kansas, were utilized to generate synthetic seismograms that represent the subsurface geology of the study area. With minimal stretch and squeeze, and in some cases with no stretch and squeeze, we adjusted the model until a good match (correlation coefficient) was established with the seismic data (Fig 3.6). This gave depth relationship to the seismic data in time, allowing a better estimate of the formations of interest and the subsequent mapping of these horizons for seismic attribute extraction.

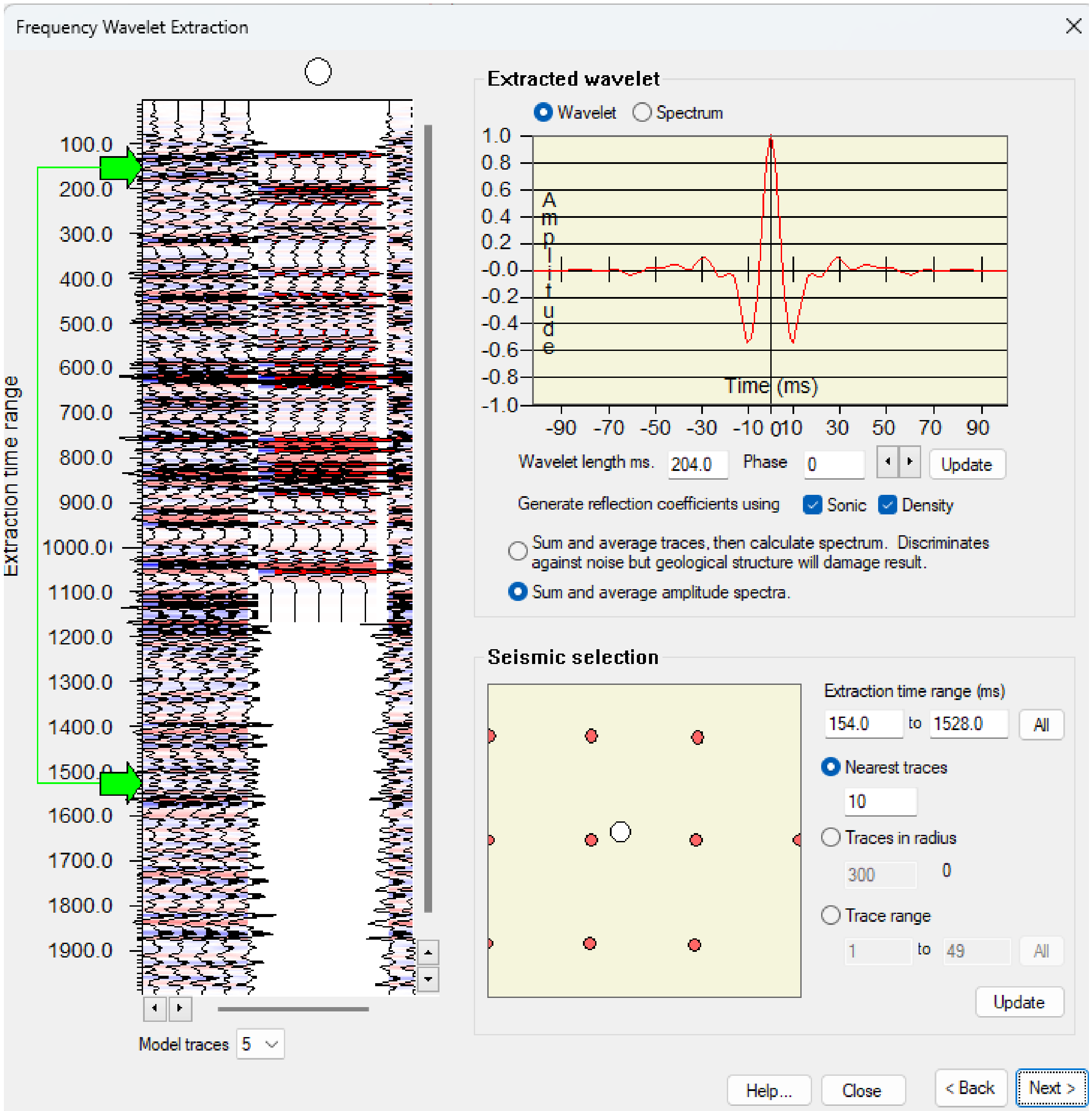

Figure 3.4: Frequency wavelet extraction process with an extraction time range of 154ms to 1528ms around 10 seismic traces.

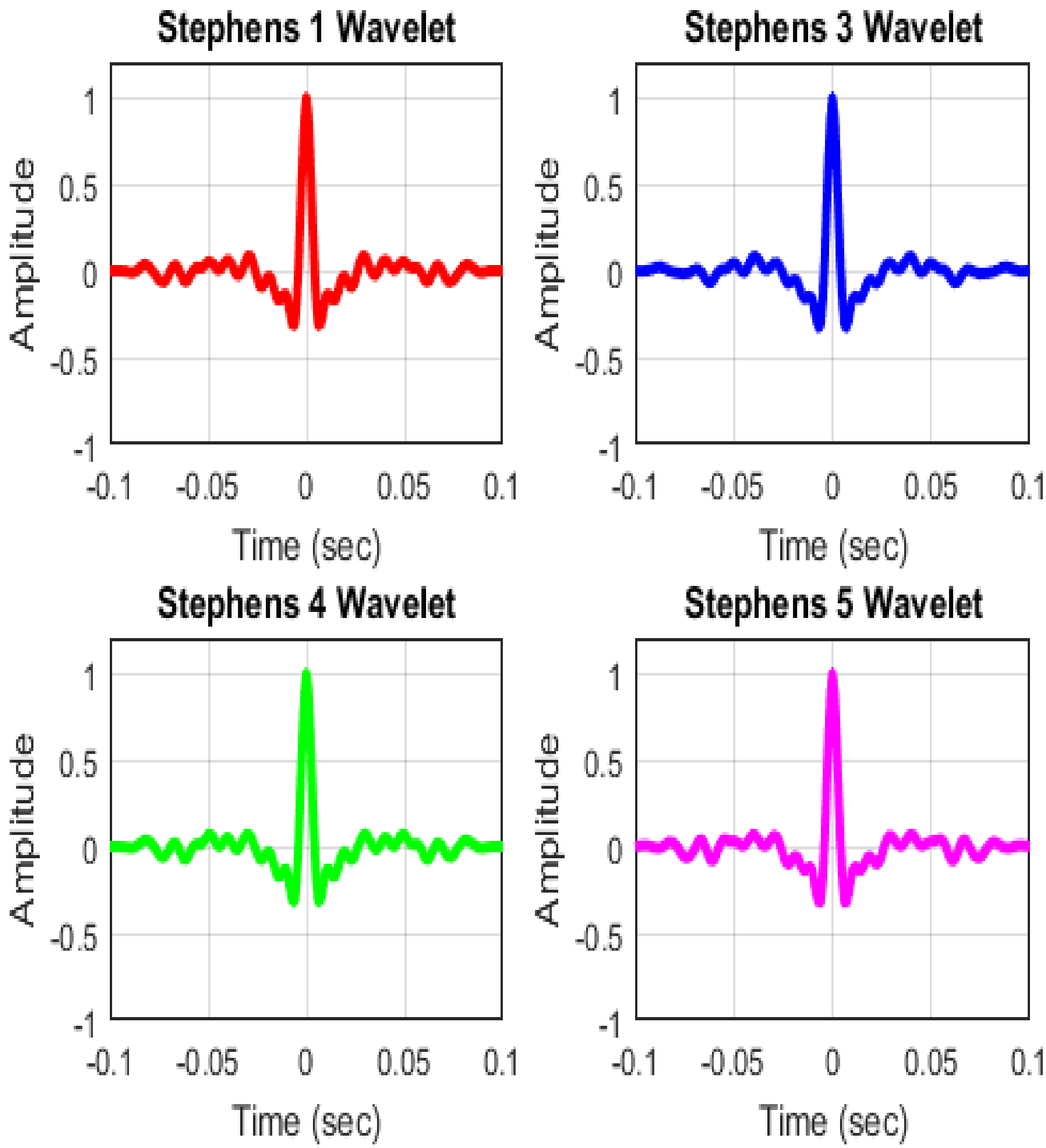

Figure 3.5: Frequency extracted wavelets for Stephens 1, Stephens 3, Stephens 4, and Stephens 5. Each subplot displays a distinct wavelet with variations in amplitude, frequency content and number side lobes (Matlab R2016b, Mathworks®).

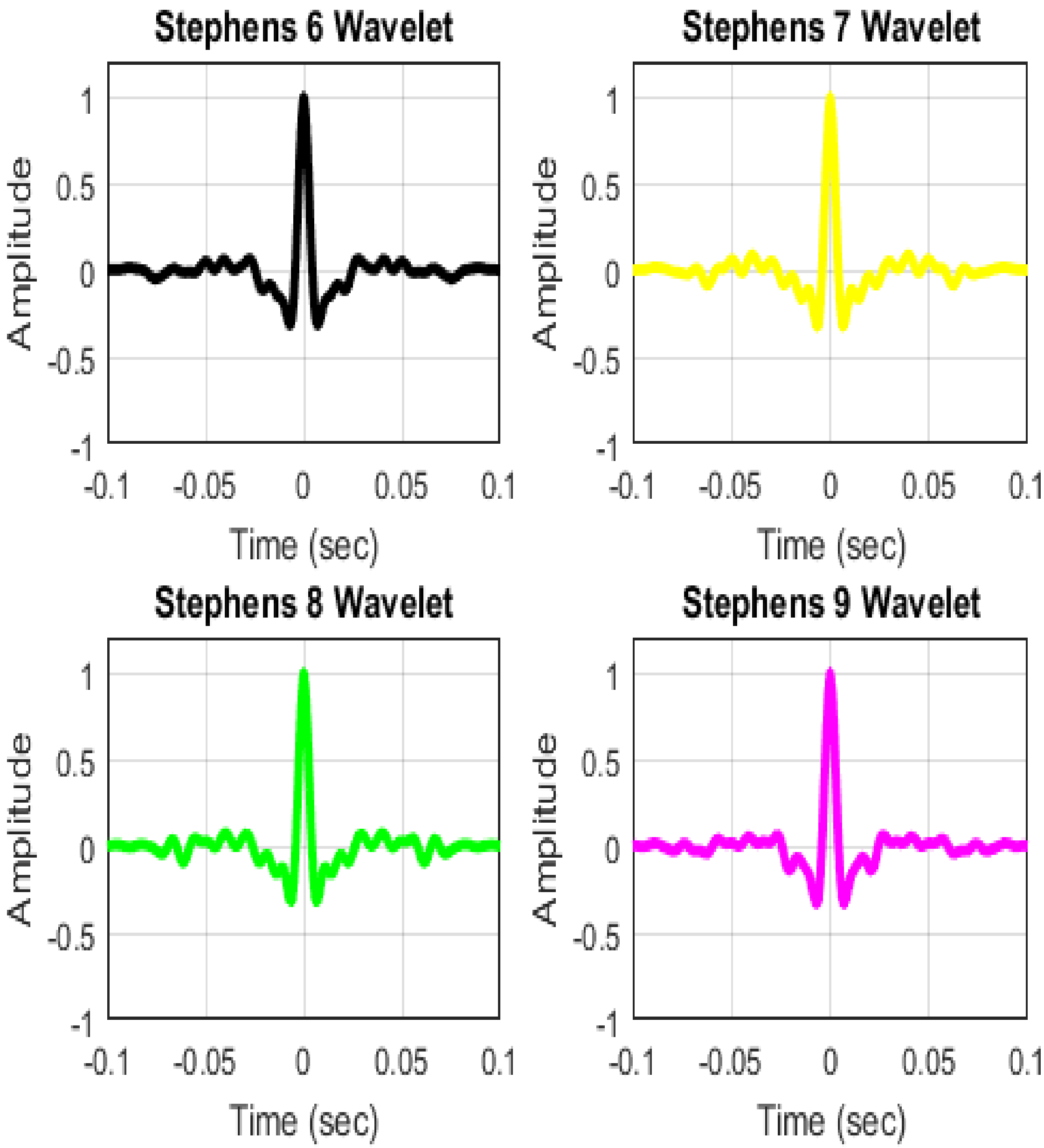

Figure 3.6: Frequency extracted wavelets for Stephens 6, Stephens 7, Stephens 8, and Stephens 9. Each subplot displays a distinct wavelet with variations in amplitude, frequency content and number side lobes (Matlab R2016b, Mathworks®).

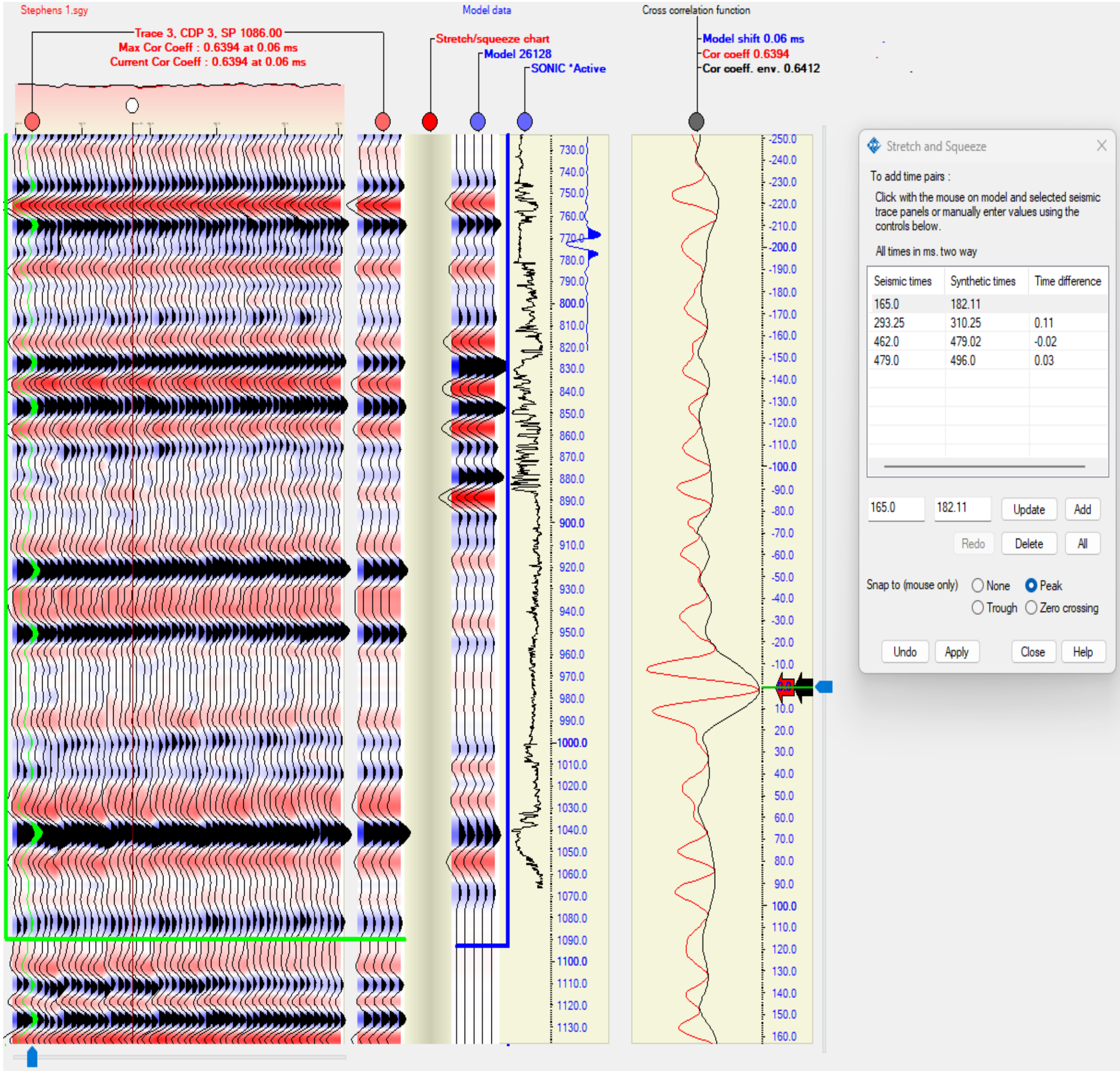

Figure 3.7: Seismic well tie analysis, comparing synthetic and observed seismic data to improve time-depth relationships. The leftmost section displays seismic traces with waveforms in red and black, representing the original seismic data. The central panel shows a sonic log, which has been used to generate the synthetic seismogram. The rightmost panel contains a cross-correlation function, which evaluates the alignment between the synthetic and real seismic data. The correlation coefficient (0.6394 at 0.06 ms shift) and the stretch/squeeze adjustment panel, which allows for fine-tuning of the time alignment between seismic and synthetic data

3.6 Horizon Mapping

Horizons are interfaces with distinct mineral densities and porosity characteristics between material layers, visible as high and low bands in seismic reflection data (Patel et. al., 2010). Identifying and delineating subsurface interfaces as seismic events that represent changes in rock properties across (crosslines) and along (in lines) seismic reflection dataset is called horizon mapping.

We remapped the Viola, Simpson and Arbuckle horizons aided by the alignment of the formation top and generated synthetic overlay on the appropriate seismic reflectors. In addition, we mapped 7 new horizons (Fig 3.8) visible as high band reflectors, used to create time and depth grids to generate an alternative test velocity volume. These mapped reflections were used to generate time structure maps that can be used to extract attributes. All mapping was done manually with the manual feature in Kingdom other than the available automatic horizon picking tools because automatic horizon mapping methods may struggle with seismic faults, weak reflections, and varying wavelet characteristics (Figueiredo et al., 2007).

3.7 Seismic Resolution Enhancement

To improve the resolution of the seismic reflection dataset, we subjected the original seismic reflection dataset to spectral whitening using the S & P Global Kingdom Geophysics tool, to obtain amplitude spectrums having close to a flat peak (reduce ringing) and broaden the original spectrum's frequency bandwidth, thereby enhancing the resolution of the data. Overall, three sets of bandwidth spectral whitening were applied to the original data, guided by the spectral bandwidth of the original spectrum. The three whitened spectra were analyzed and that which enhanced the original seismic response by reducing the interference effect of thin layer beds was selected for further evaluation in preparation for the next phase leading to the seismic inversion process.

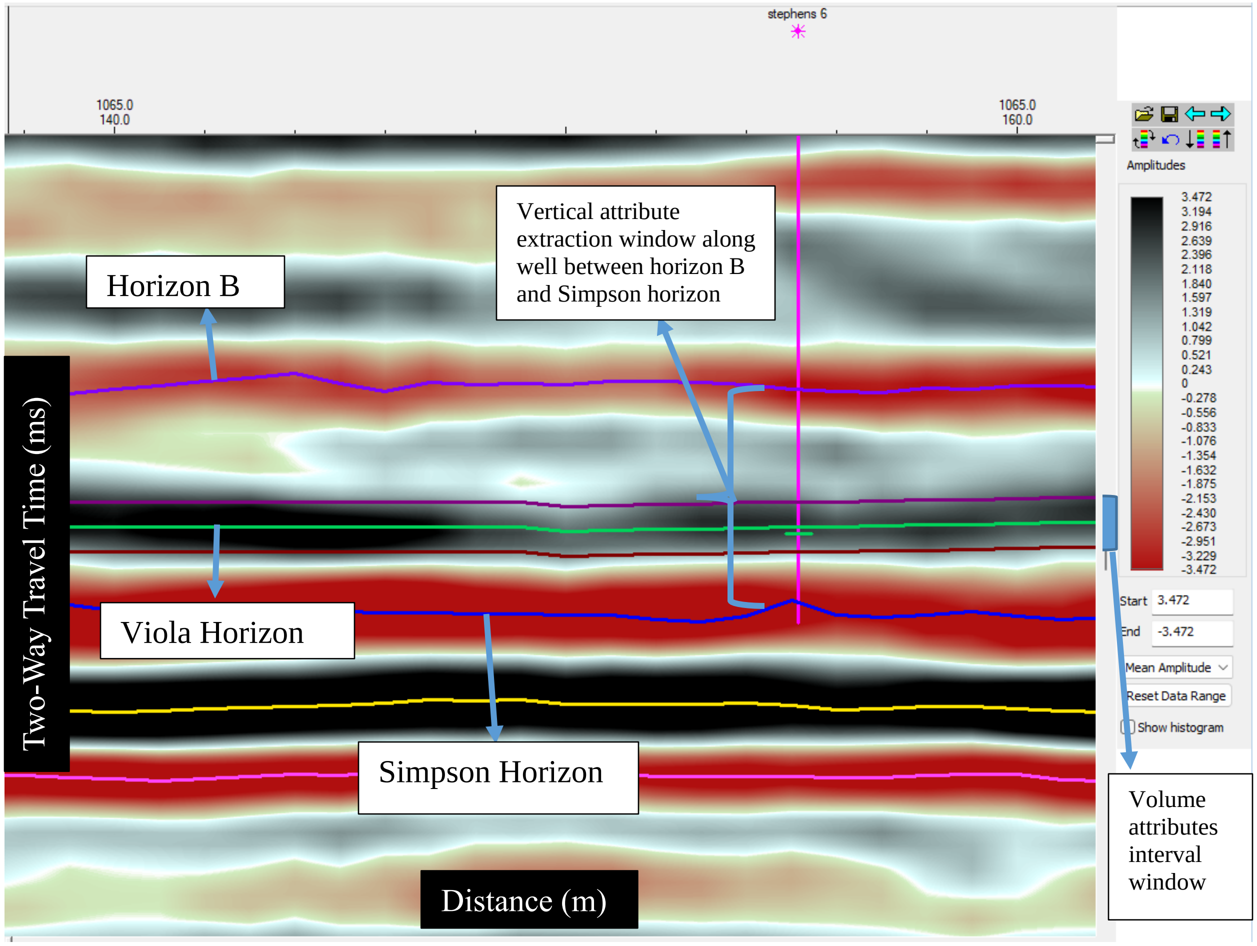

Figure 3.8: Some mapped horizons showing vertical extraction window along wells used for training machine learning models and volume extraction window above and beneath the Viola top horizon.

3.8 Model – Based Acoustic Inversion

Acoustic impedance inversion is the process of transforming observed seismic reflectivity and measured well-data into acoustic impedance layer data (Campbell et al., 2015). The inversion of seismic data to acoustic impedance has become a standard tool for the prediction of reservoir properties (Ali et al., 2017). There are several seismic inversion methods broadly grouped under pre-stack and post-stack (Fig 3.9). Pre-stack inversion can be used to see the effect of fluid changes in amplitude to offset, whereas post-stack inversion, in this case model based can restore lost low and high frequencies by correlating seismic data with seismic responses from geological models (Erryansyah et al., 2020). The fundamental interpretive benefit of any form of seismic inversion is that interface information is converted to interval information. Hence, inverted seismic is representative of the rock layers, rather than rock boundaries.

Another way to look at inversion is to consider it as the technique for creating a model of the Earth using seismic data as input (Russell, 1990). As such, it can be considered as the opposite of the forward modelling technique (Fig 3.10), which involves creating a synthetic seismic section based on a model of the Earth, or in the simplest case, using a sonic log as a one-dimensional model. According to Bouharket (2017), the main aim for post-stack acoustic inversion is to estimate a model for acoustic impedances from seismic data that will help in better understanding rock properties and providing continuous information that cannot be obtained from well locations, which is an important input for reservoir characterization. In this study we followed Wang et al. (2022) flow diagram (Fig 3.11) of model-based acoustic impedance using the S & P Global Kingdom Software to obtain the inversion results at the well locations to be applied to the whole data volume. Compared with other inversion methods, model-based acoustic impedance inversion strengthens the description of thin reservoir horizontal and vertical changes (Wang et al., 2022).

We fed the S & P Global Kingdom software with sonic (DT) and bulk density (RHOB) logs at each well location, a time-depth chart created by generating synthetic models for each well, the survey data and a macromodel (Fig 3.12) to produce the calculated resampled impedance log at individual well locations.

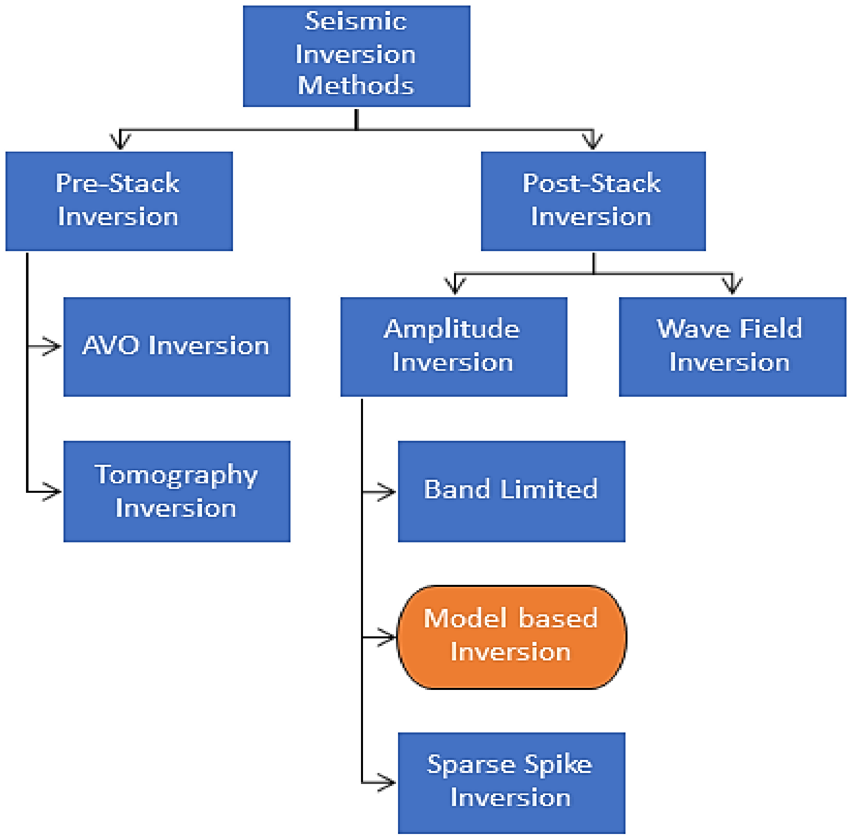

Figure 3.9: Hierarchical classification of seismic inversion methods, categorized into pre-stack and post-stack inversion techniques. Model-based and sparse spike inversion are highlighted as key approaches for impedance estimation (Erryansyah et.al., 2020)

3.9 Seismic Attributes Extraction

Seismic attribute is a quantitative measure of a seismic characteristic of interest (Chopra & Marfurt, 2005). Its extraction is the technique used to calculate useful information from seismic data that reflects the physical and lithological characteristics of reservoirs from different perspectives (Zhonghua, 2017). It involves processing and transforming seismic signals into varieties of seismic attributes that relate to in more specific ways to the subsurface geological features related to lithology identification, reservoir description, and oil and gas detection (Xiong et al., 2024). Extracting independent seismic attributes is essential for quantitative seismic facies analysis and reservoir prediction (Liu et al., 2010). In this study, we extracted five different instantaneous attributes (Fig 3.13 to 3.17) labeled A-E for the Viola reservoir horizon, with preset Kingdom parameters under the rock-solid attribute's module (Fig 3.18). The calculated attribute, at a 2ms sampling interval along the various wells between the mapped "Horizon B" above and the mapped Simpson Horizon, were exported as ASCII format seismic attributes file. This file of attributes "learning feature" was utilized for the input features for training machine learning model. These same attributes were also extracted between a window of 4ms above and beneath the Viola top horizon (Fig 3.8) and fed to the trained model for impedance volume predictions.

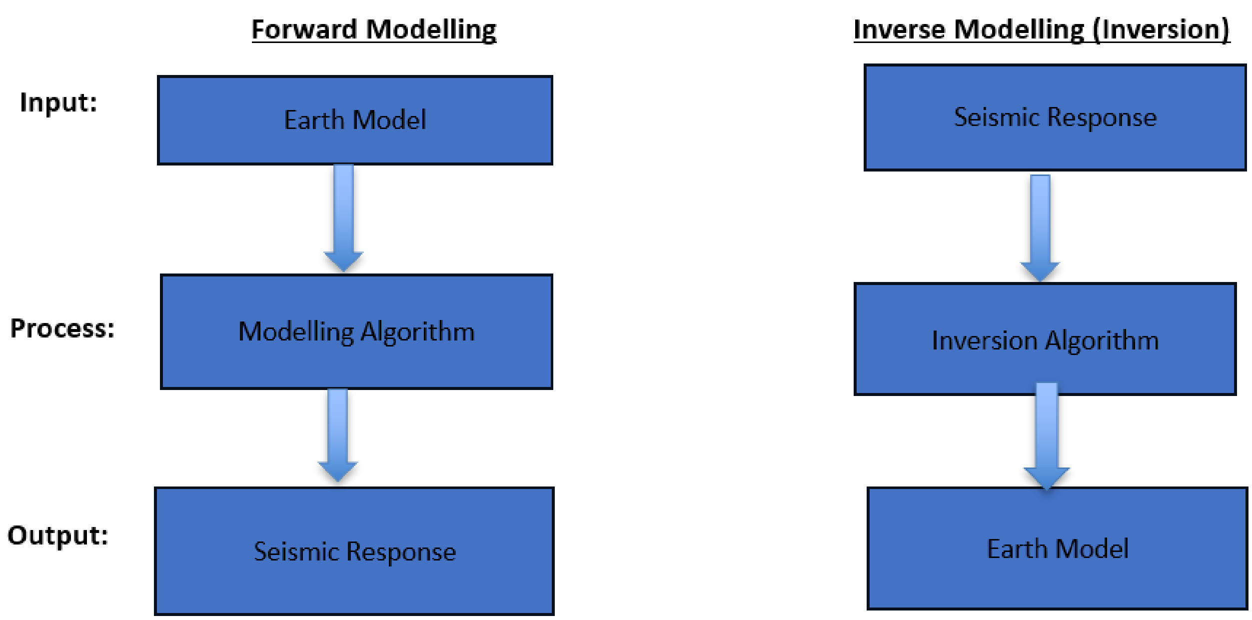

Figure 3.10: Inverse and forward modelling algorithms (from Russell, 1990).

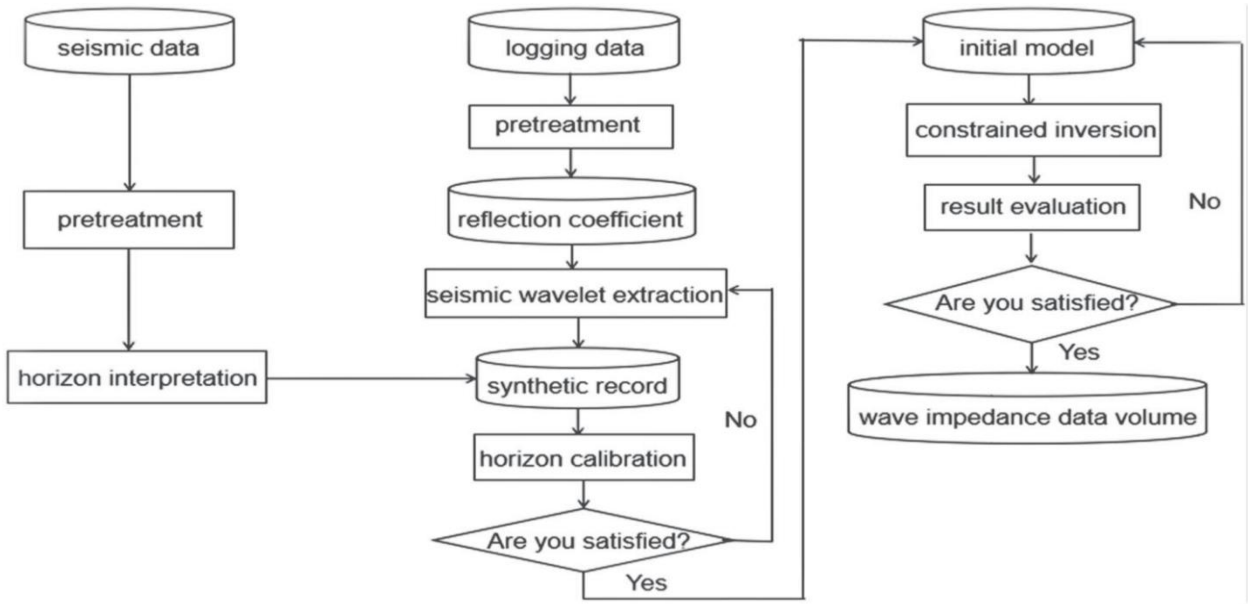

Figure 3.11: Model based acoustic inversion workflow adopted for research. It illustrates the seismic inversion workflow, integrating seismic and well log data to estimate subsurface wave impedance (Wang et. al., 2022)

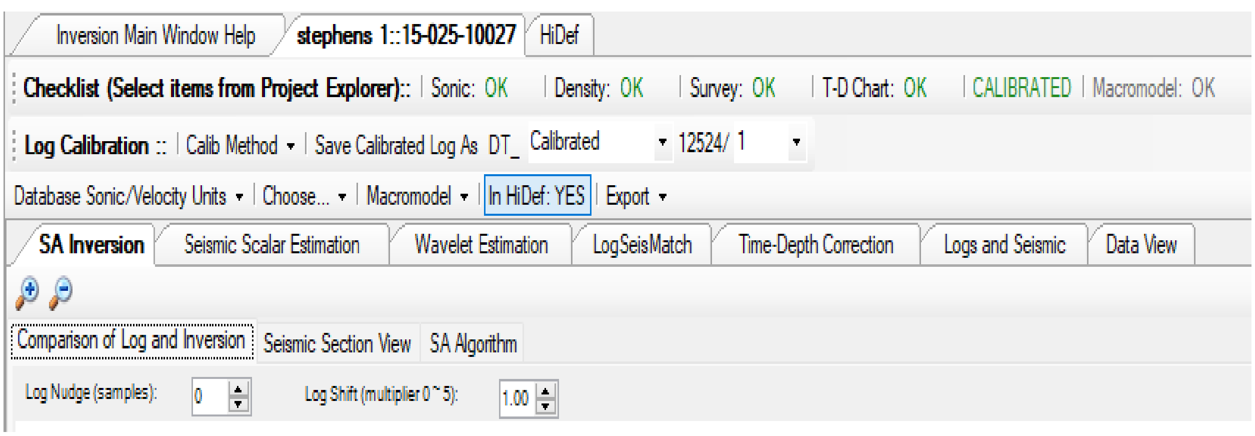

Figure 3.12: Kingdom inversion window input checklist, showing selected sonic and density logs, loaded survey data, time-depth (T-D) chart and macromodel.

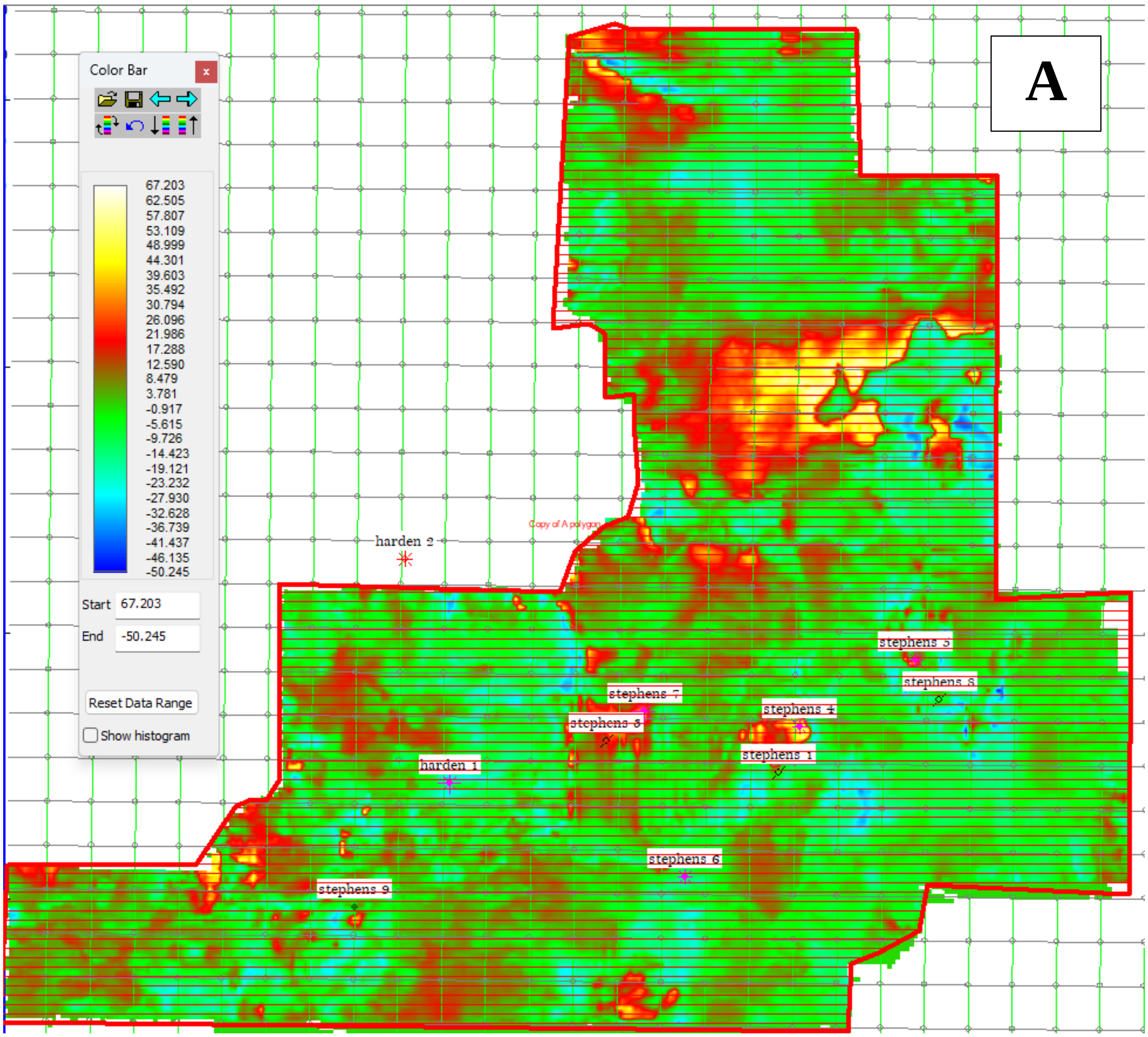

Figure 3.13: Dominant frequency instantaneous attribute map of the Viola top horizon. Dominant frequency values are represented by the color bar on the left

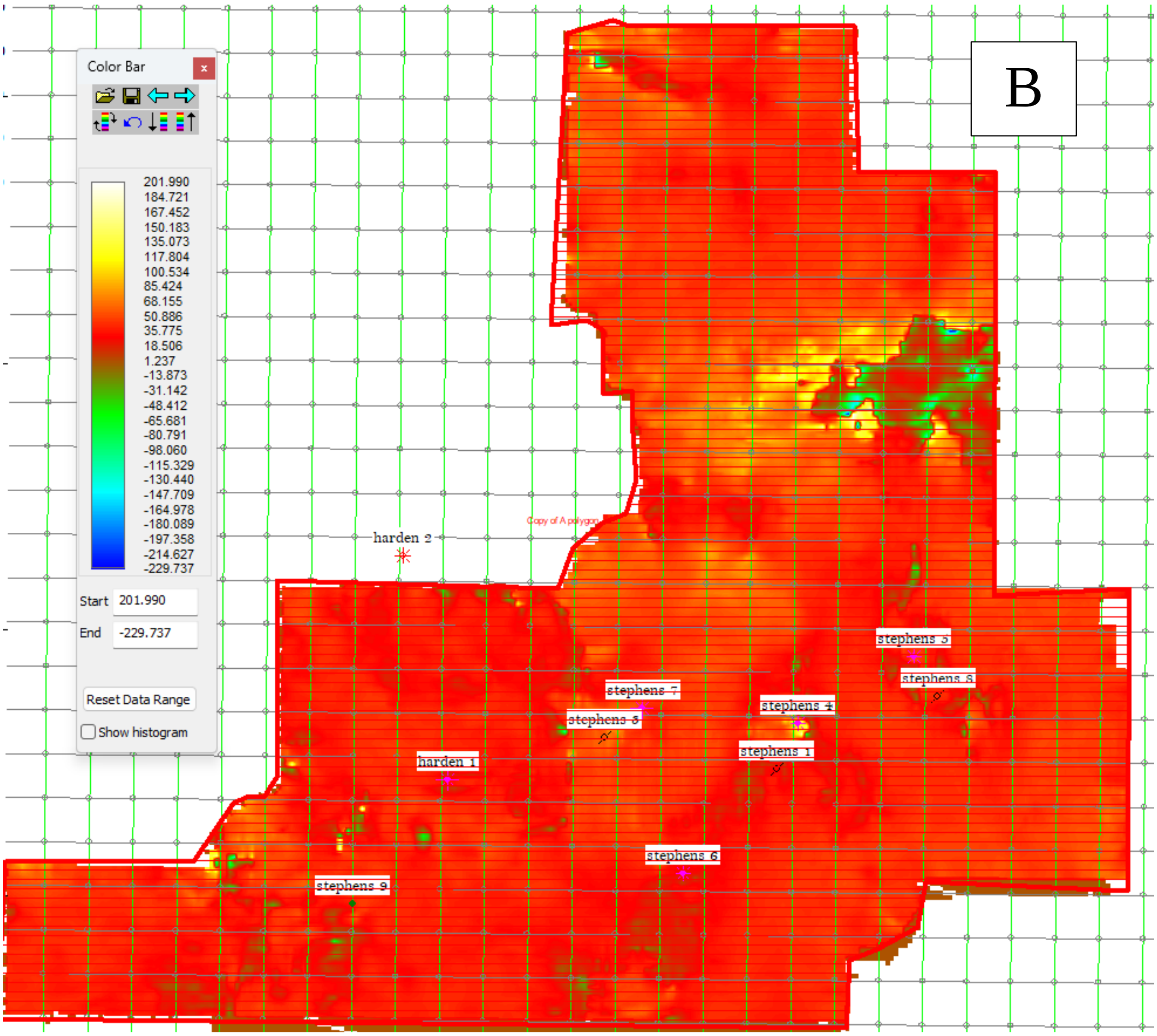

Figure 3.14: Instantaneous frequency attribute map of the Viola top horizon. Instantaneous frequency values are represented by the color bar on the left.

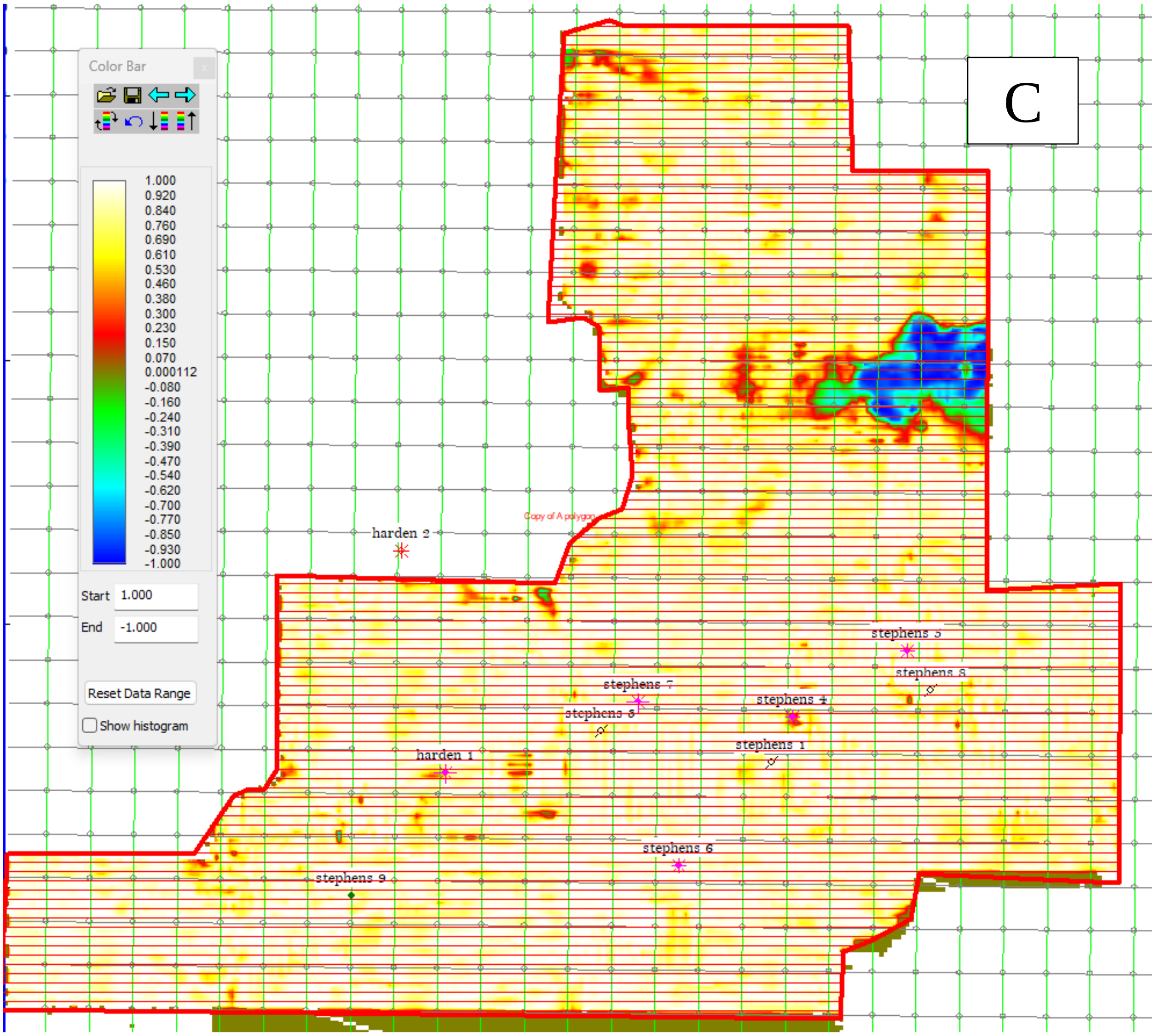

Figure 3.15: Normalized amplitude instantaneous attribute map of the Viola top horizon. Normalized amplitude values are represented by the color bar on the left

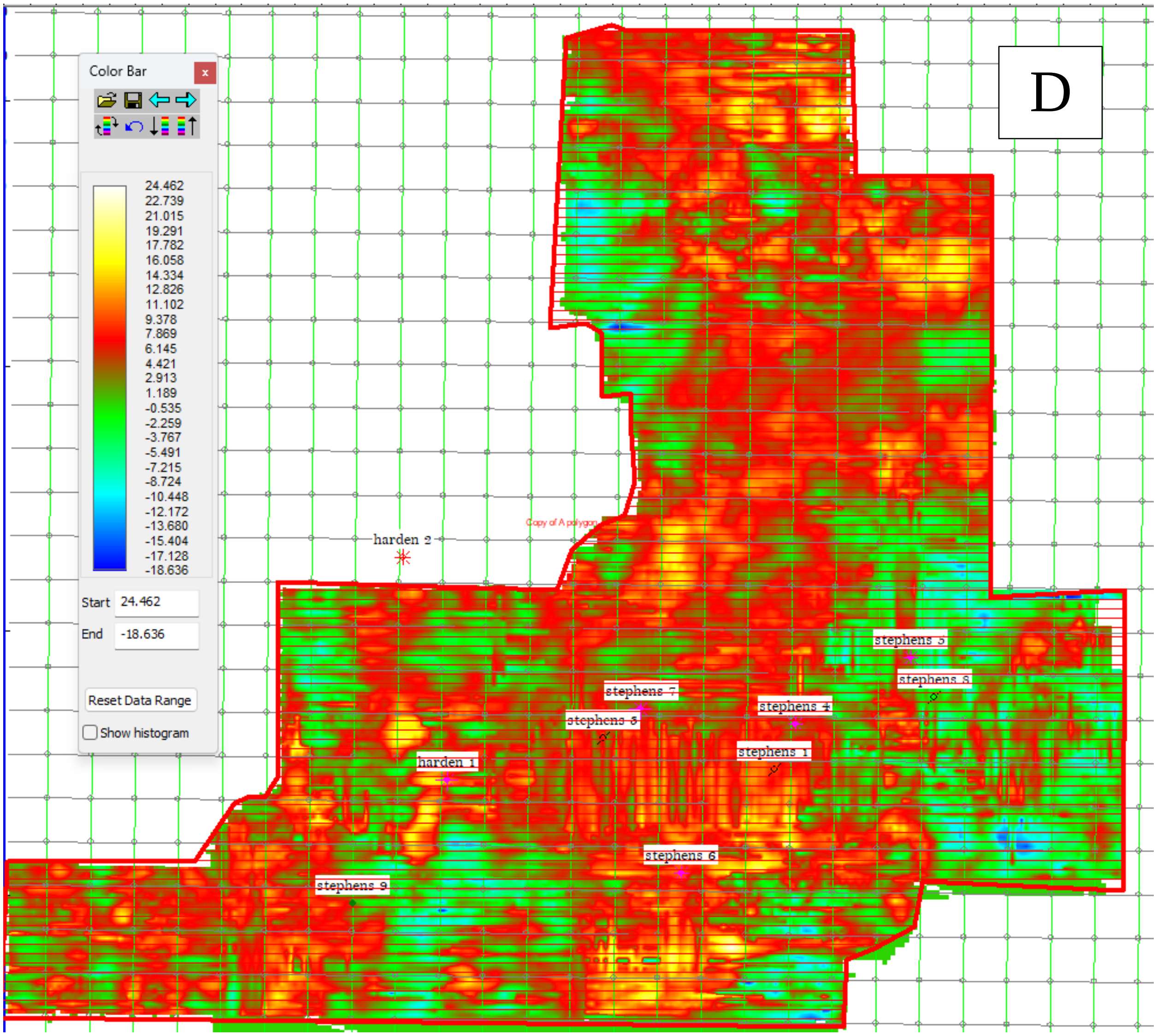

Figure 3.16: Relative acoustic impedance instantaneous attribute map of the Viola top horizon. Relative acoustic impedance values are represented by the color bar on the left

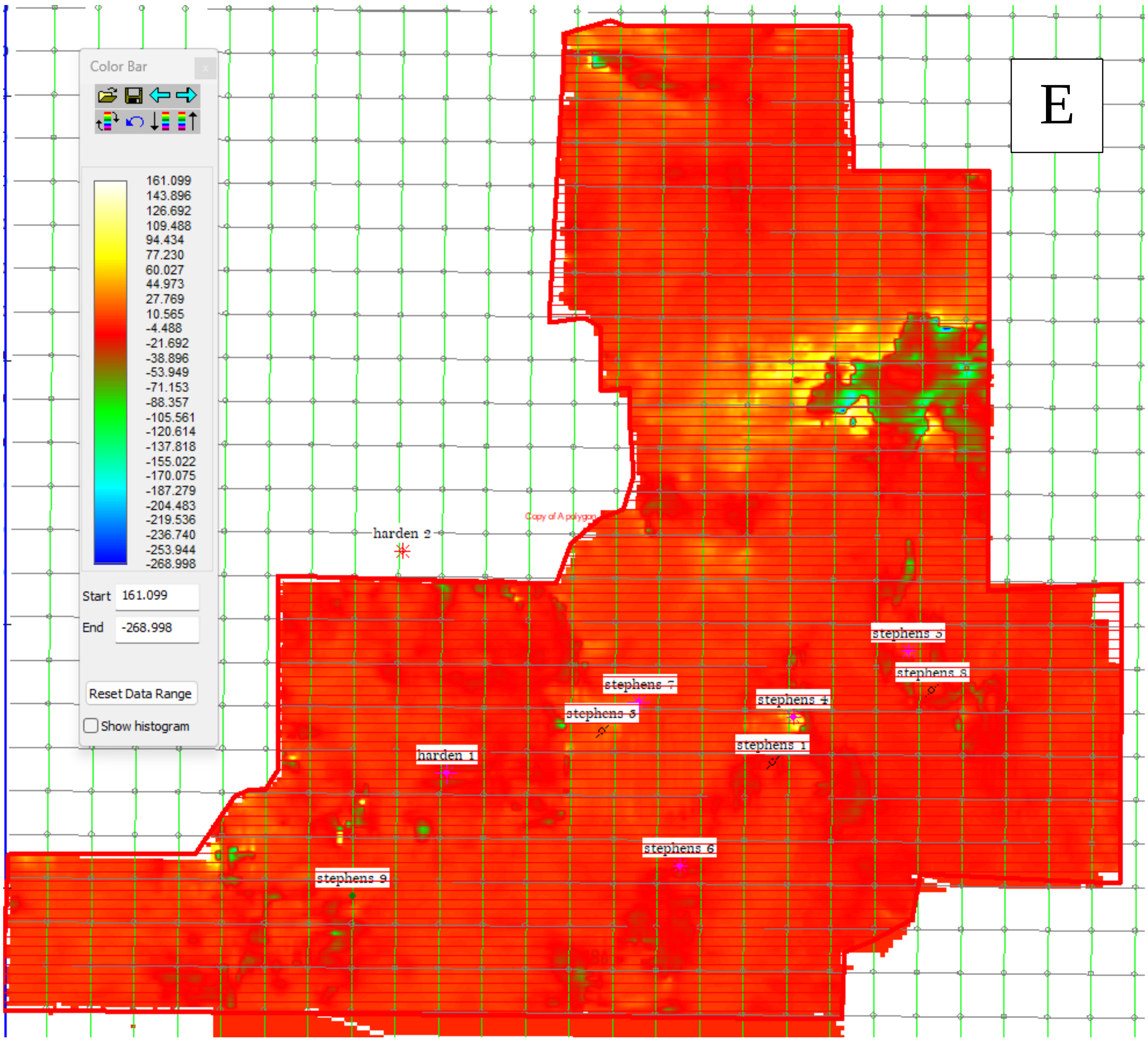

Figure 3.17: Thin bed indicator instantaneous attribute map of the Viola top horizon. Thin bed indicator values are represented by the color bar on the left

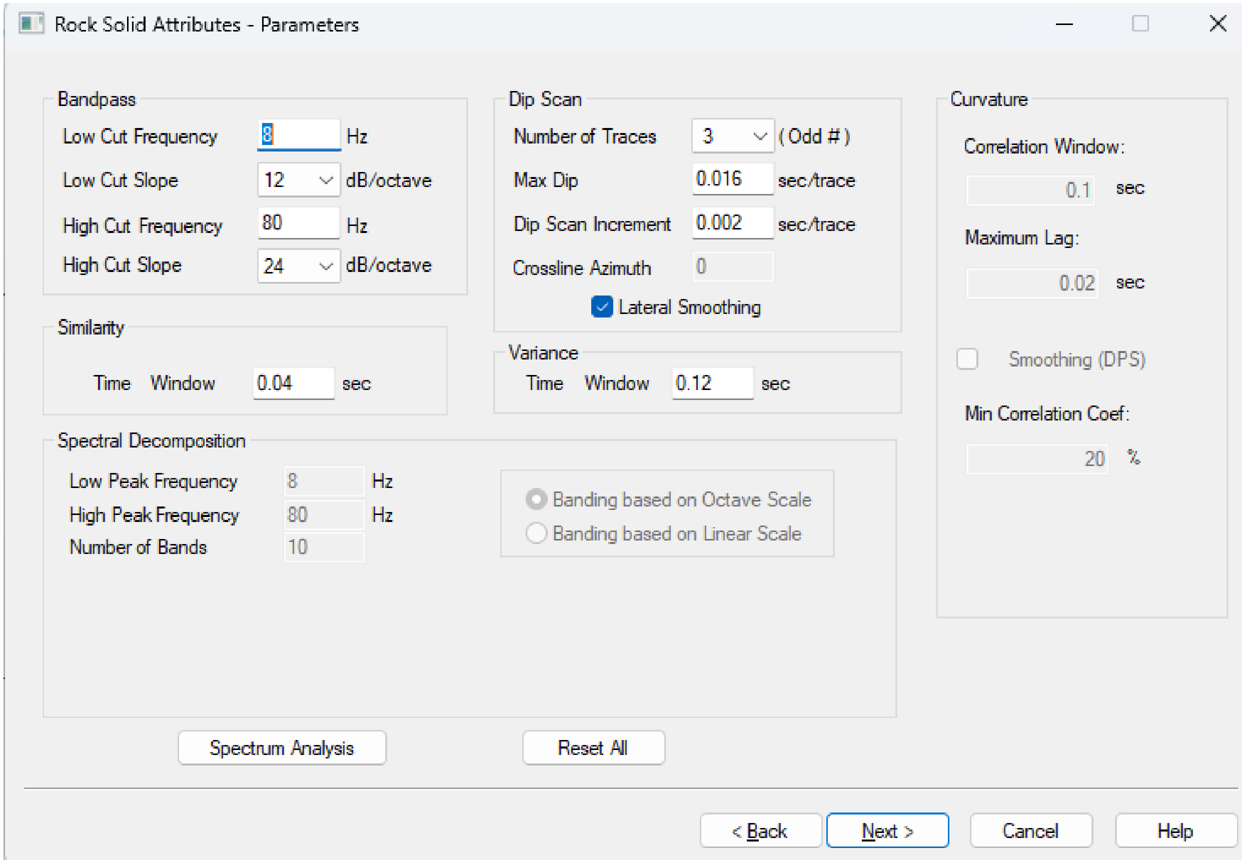

Figure 3.18: Instantaneous attributes extraction parameters from rock solid attributes feature in S & P Global Kingdom software.

3.10 Supervised Machine Learning for Seismic Inversion

The five extracted instantaneous seismic attributes from for Viola horizon time window that are: dominant frequency, instantaneous frequency, relative acoustic impedance, thin bed indicator, and normalized amplitude, along the Stephens 1, 3, 4, 5, 6, 7, 8 and 9 wells were used as input features, and the resampled impedance log values obtained from the seismic inversion results at each well location with corresponding time intervals as that of the input features were used as target labels. The data was standardized by Z – score normalization to improve model performance and training stability, ensuring that all features contribute equally to the model's learning process. Especially for the neural networks model used in this study where the output needs to be on a specific scale.

The dataset was split randomly into training and test sets. 20% of the dataset was used for testing the model, whilst 80% was used for training and validation. We built two machine learning models and assessed its performance using regression metrics.

Neural Networks

Neural networks are powerful techniques for solving problems in pattern recognition, data analysis and control (Bishop, 1994). They are an interconnected assembly of simple processing elements (units or nodes) loosely based on the animal neuron, these elements, possess high processing speeds stored in the interunit connection strengths, or weights, obtained by adaptation to, or learning from a set of training patterns (Bishop, 1994; Gurney, 2018). According to Bishop (1994), the problem of determining the values for the weights in a neural network is called training, which proceeds in an analogous manner. In the case of a neural network, the most used form of error function is the sum-of-squares error, written as:

Equation 3.1: $\boldsymbol{E = \frac{1}{2}\sum_{q=1}^{n}\sum_{k=1}^{c}\{y_k(x^q; w) - t_k^q\}^2}$

Where each input vector (Eqn 3.2);

Equation 3.2: $\boldsymbol{x^q = (x_1^q, \dots, x_d^q)}$

from the data set has a corresponding target vector t^q.

The error for each output k when the network is presented with pattern q, written as: $y_k(x^q; w) - t_k^q$. The total error for the whole pattern set is then the squares of the individual errors summed over all output units and over all patterns to yield equation 3.1 above.

XGBoost

This is a scalable tree gradient boosting system widely used in machine learning, whose scalability is due to systems and algorithmic optimizations (Chen & Guestrin, 2016). It can be seen to adaptively determine local neighborhoods of a model, considering the bias-variance tradeoff during model fitting (Nielsen, 2016). To make predictions, XGBoost employs an additive model consisting of an ensemble of multiple tree models (decision trees chosen as weak learners) specifically, regression trees that produces real value output for splits and whose output can be added together, to improve residuals in the predictions leading to the final prediction (Santhanam et al., 2017). The algorithm learns the structure of the trees and the leaf scores to optimize the objective function (Dhaliwal et al., 2018). Which can be written in two ways as follows:

Equation 3.3: $obj(\theta) = TL(\theta) + R(\theta)$, where;

R is the regularization term that helps to keep the model's complexity within desired limits, eliminating problems such as over-stacking or overfitting data that can lead to a less accurate model.

TL is the training loss, that measures how predictive the model is.

According to (Li et al., 2019) the objective function can also be expressed as:

Equation 3.4: $\boldsymbol{obj = \sum_k l(\tilde{y}_i, y_i) + \sum_k \Omega(f_k)}$

where:

l is the loss function, which represents the error between the predictive value and the true value

Ω is the function used for regularization to prevent overfitting expressed as;

Equation 3.5: $\boldsymbol{\Omega(f) = \gamma T + \frac{1}{2}\lambda \, ||w||^2}$

Where:

T represents the number of leaves per tree

w represents the weight of the leaves of each tree

and the tree model (ỹ) integrated with addition method written as:

Equation 3.6: $\tilde{y} = \sum_{k=1}^{K} f_k(x_i), f_k \in F$

where:

K is the total number of trees

F represents the basic tree model.

The generalized structure of the set of decision trees (Fig. 3.19) used by XGBoost is given by

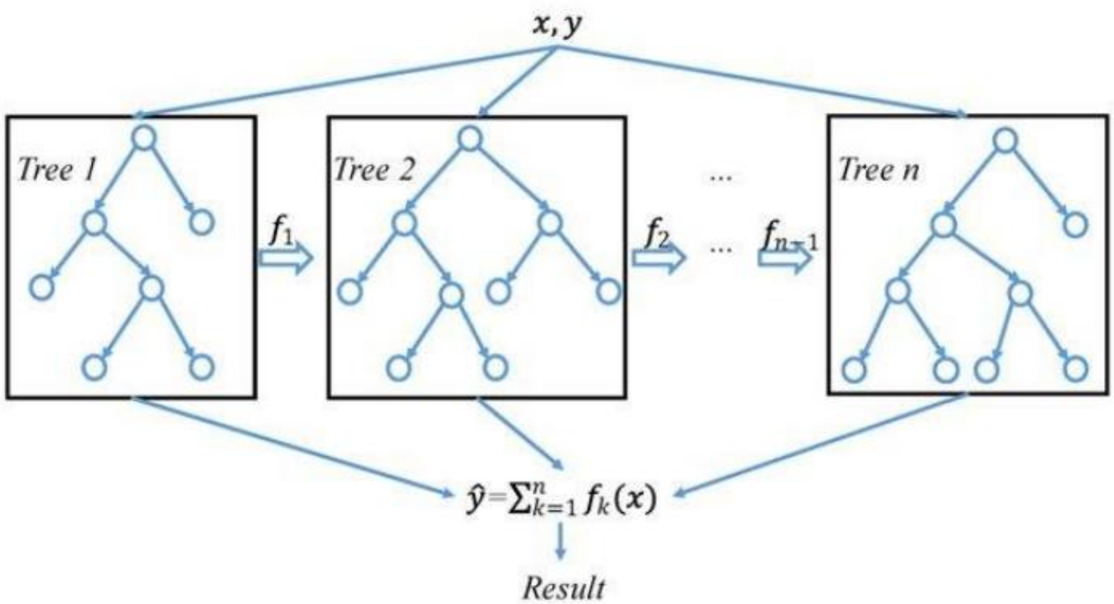

Figure 3.19: General structure of XGBoost (Kalyani et al., 2019)

Chapter 4 - Results and Discussion

4.1 Synthetic Models

The synthetic models from the 1D convolutional model were overlaid both as wiggle traces (Fig 4.1) and a raster (Fig 4.2) on the seismic data. This showed strong alignment of positive deflections, and negative deflections (wiggle overlay) and a consistent color (raster) for peak amplitude, and trough amplitudes with the already mapped Viola, Simpson and Arbuckle horizon reflections respectively. This observation is in line with the assertions of Jallow (2024) and Vohs (2016) that the Viola top, Simpson and Arbuckle formations are peak, trough and peak amplitudes respectively.

4.2 Spectral Whitening

The original frequency bandwidth of the seismic data (original) was 15Hz to 84Hz. The three enhanced amplitude spectrums obtained by spectral whitening had frequency bandwidths of 18Hz to 100Hz (Amp 18-25-80-100), 10Hz to 105Hz (Amp 10-20-65-105), and 20Hz to 100Hz (Amp 20-25-60-100) (Fig 4.3). All three enhanced spectrums had broad frequency bandwidths that fit within the amplitude spectrum of the original seismic data. However, the spectrum that had frequency bandwidth of 18Hz to 100Hz denoted as (Amp 18-25-80-100) was selected as the enhanced amplitude spectrum upon seismic section evaluations proved it illuminated to a greater detail an offshoot feature attached to a peak reflector at inline 1181 and crossline 220 at about 0.895s two-way time (TWT) (Fig 4.4). The various plot names given to each spectrally whitened amplitude spectrum (e.g. Amp 18-25-80-100) defines the frequency for the trapezoidal setup (i.e., X1, X2, X3 and X4) during the whitening process.

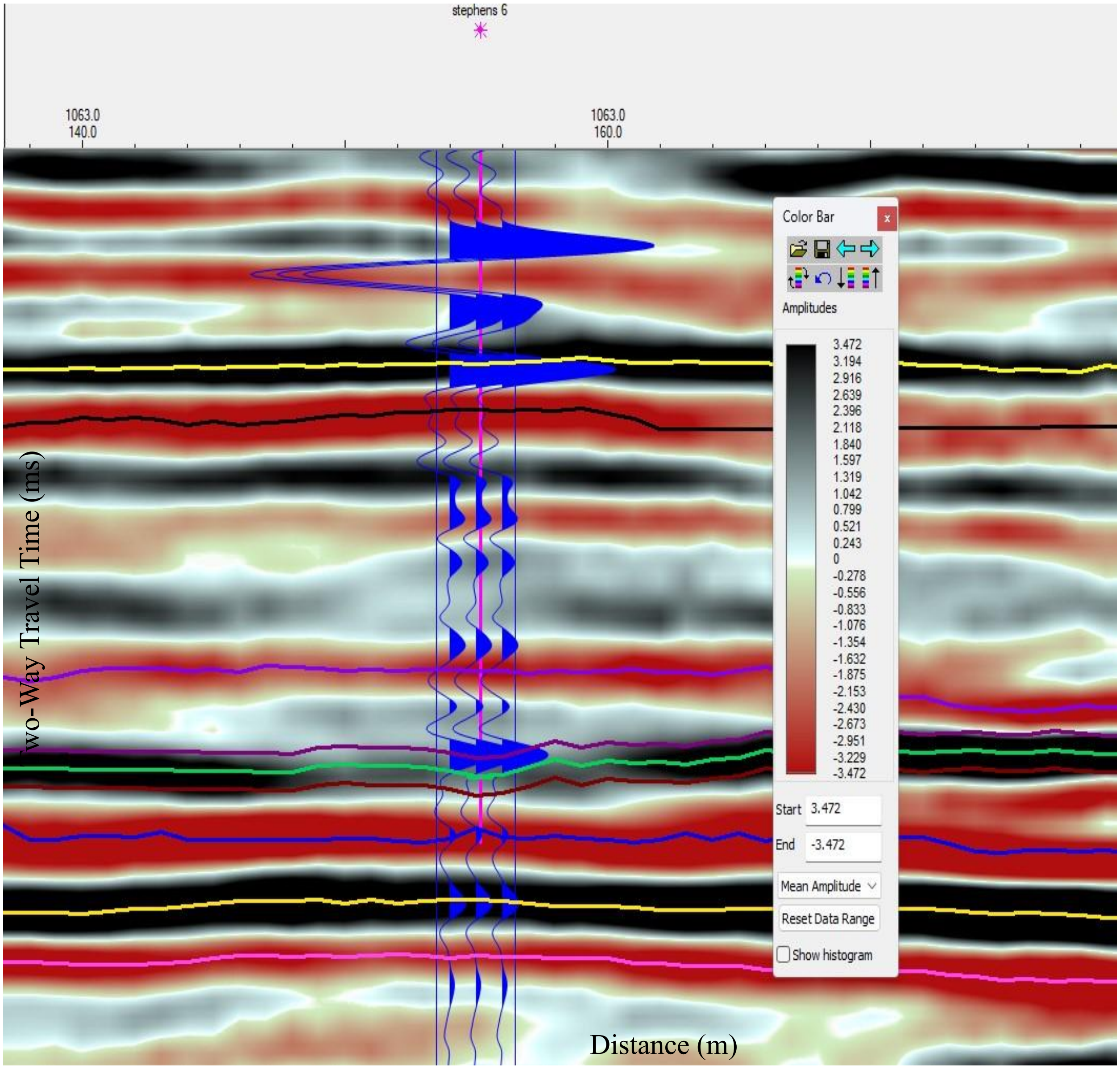

Figure 4.1: Seismic amplitude section with synthetic wiggle overlay. The background represents a seismic amplitude map, where positive amplitudes are shown in red and negative amplitudes in black. The overlaid blue synthetic wiggle trace is used to compare synthetic seismograms with actual seismic data, aiding in well-to-seismic correlation. Interpreted horizons are marked with yellow, green, purple lines etc. The color bar on the right indicates amplitude values, providing a reference for subsurface characterization.

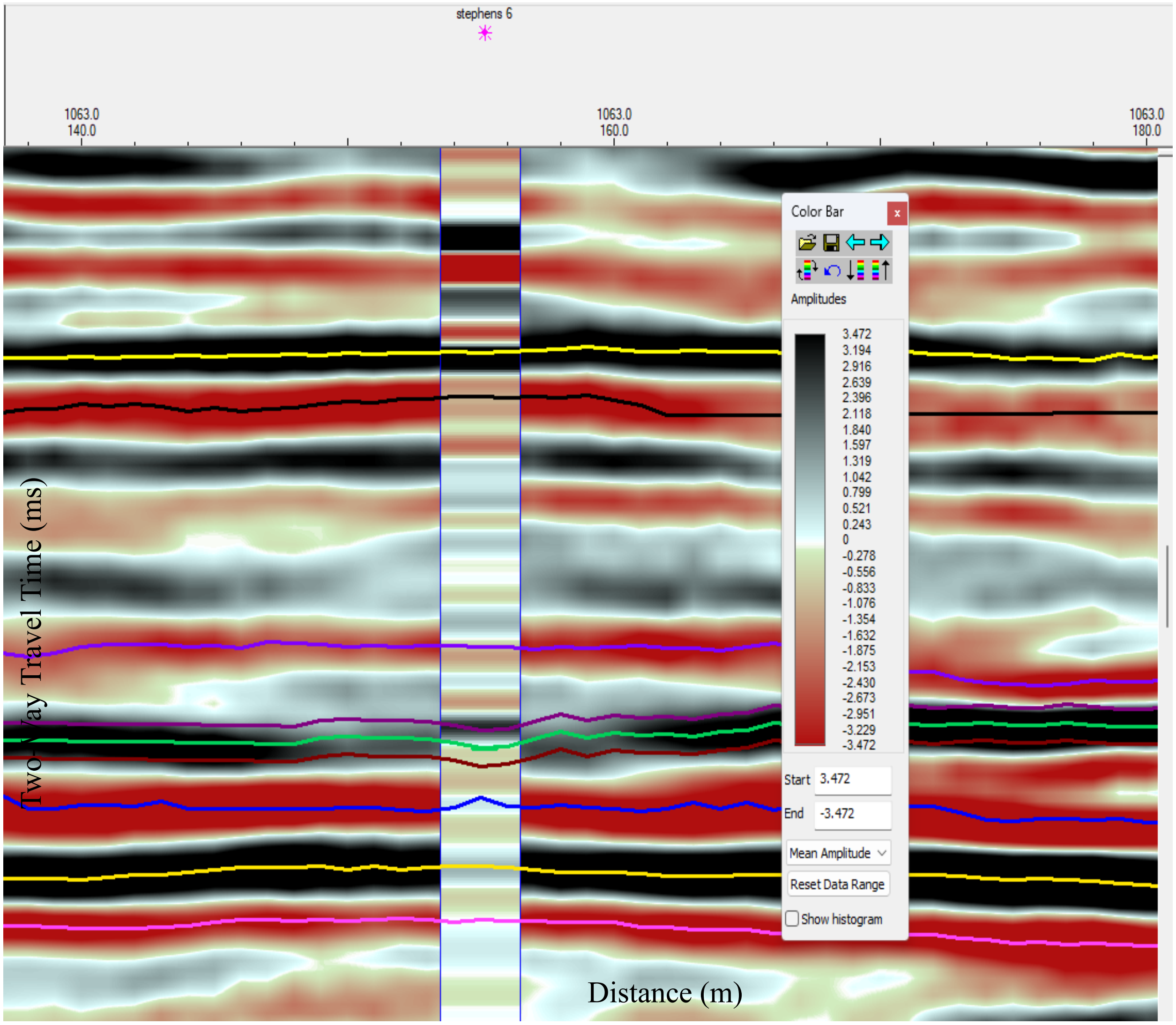

Figure 4.2: Seismic amplitude section with synthetic raster overlay. The background represents a seismic amplitude map, where positive amplitudes are shown in red and negative amplitudes in black. The overlaid raster synthetic with blue boundary is used to compare synthetic seismograms with actual seismic data, aiding in well-to-seismic correlation. Interpreted horizons are marked with yellow, green, purple lines etc. The color bar on the right indicates amplitude values, providing a reference for subsurface characterization.

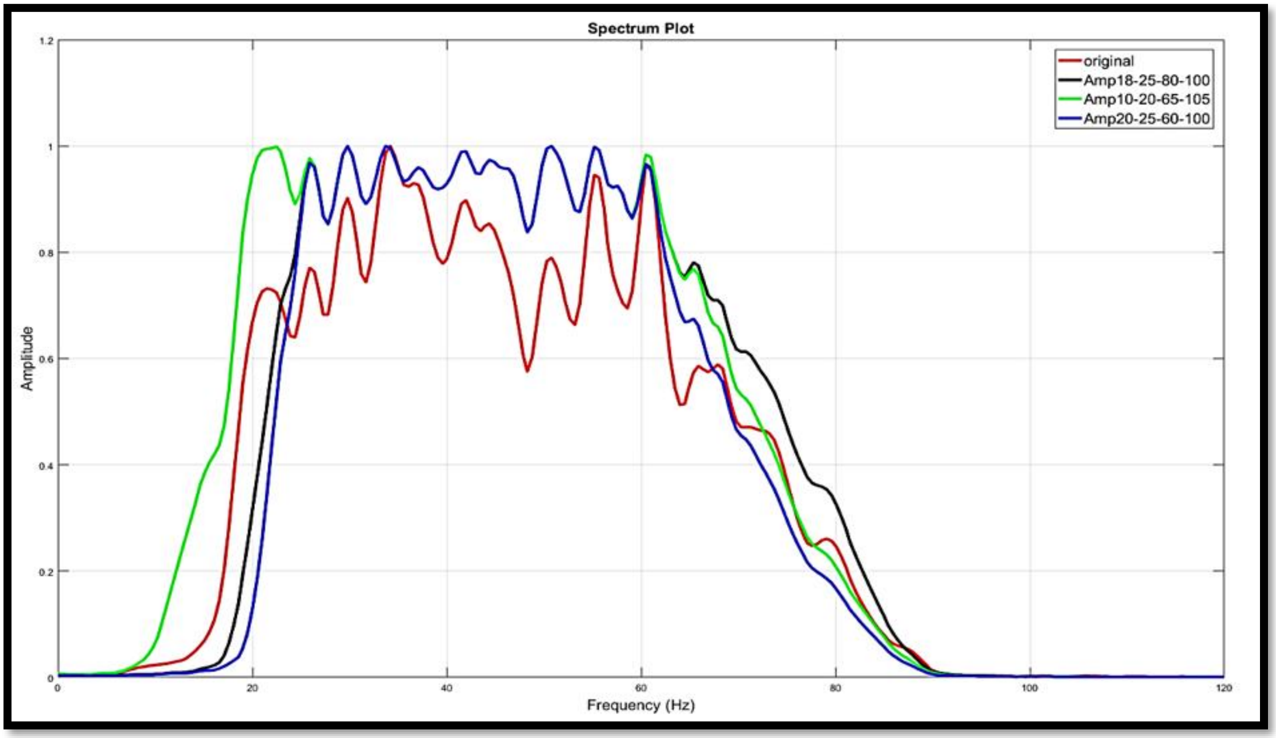

Figure 4.3: Frequency spectrum plot comparing the original signal (red) with three filtered versions using different amplitude parameters: Amp18-25-80-100 (black), Amp10-20-65-105 (green), and Amp20-25-60-100 (blue). The x-axis represents frequency in Hertz (Hz), while the y-axis denotes normalized amplitude (Matlab R2016b, Mathworks®).

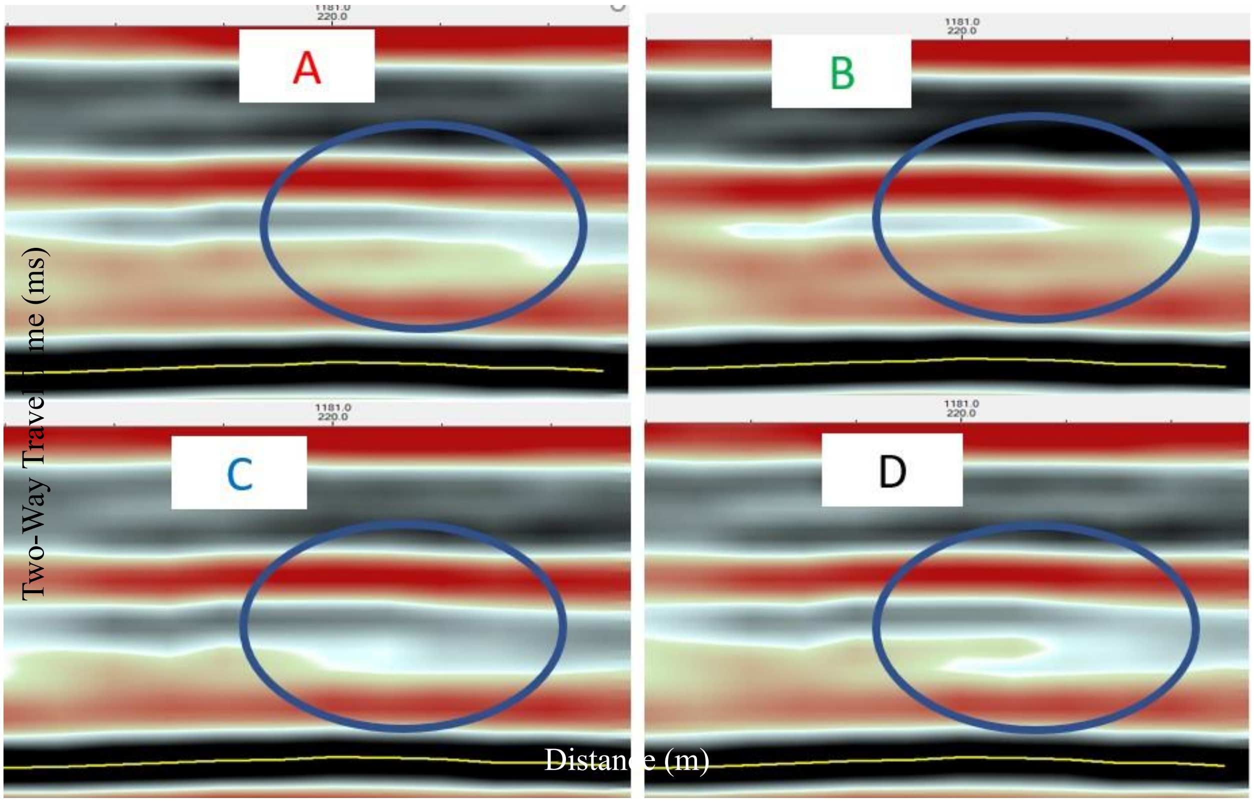

Figure 4.4: Comparison of seismic sections processed with different spectral whitening parameters for the respective amplitude spectrums in figure 4.3 above. The blue circle highlights an offshoot feature progressively resolved due increase in resolution as frequency bandwidth increases from the original spectrum (A) to spectrum (D).

4.3 Horizon Mapping

The initial interpretation of the Viola horizon using automated picking techniques resulted in inconsistencies due to the horizon's variable nature. Automated algorithms struggled to accurately follow the horizon due to changes in amplitude, continuity and signal noise, leading to mis-ties in the amplitude map. These mis-ties manifested as noticeable gaps and structural misalignments (Fig 4.5), which can negatively impact subsurface interpretation and reservoir modelling (Brown, 2011; Chopra & Marfurt, 2007).

To mitigate these discrepancies, the horizon was manually re-tracked along both inlines and crosslines using an increment of 1. This systematic re-tracking significantly improved

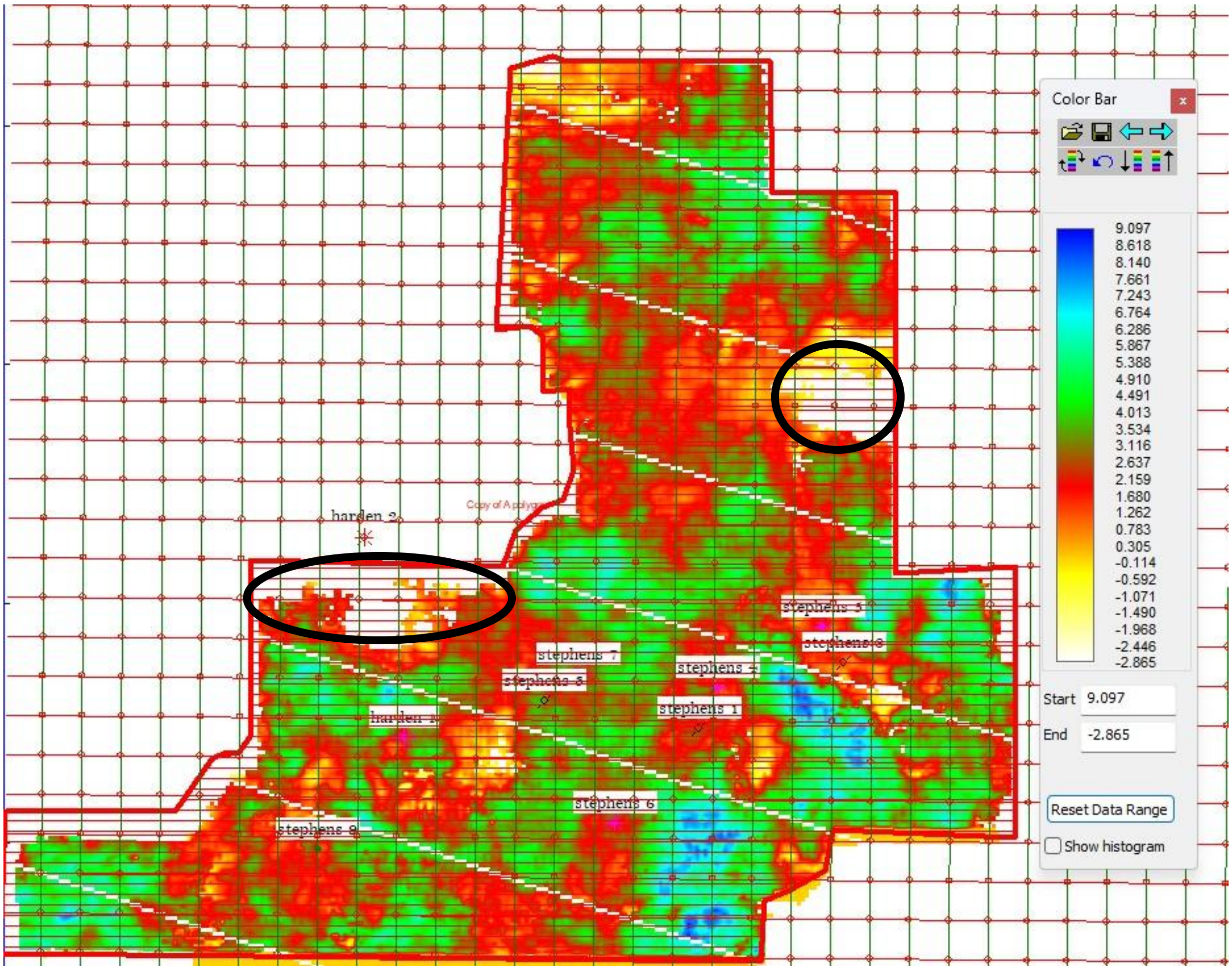

Figure 4.5: Amplitude map of the automatically picked Viola top horizon. dark circles highlight some areas of misties showing as gaps in the amplitude map. Color bar shows the values of amplitude.

structural coherence, as seen in the revised amplitude map (Fig4.6). The corrected interpretation shows well-defined and continuous horizon with closed gaps, reducing the mis-ties observed in the initial map. The overall alignment of the structure is more geologically consistent, enhancing the accuracy of depth conversion and reservoir characterization (Fossen, 2016). A direct comparison between figures 4.5 and 4.6 highlights the effectiveness of manual re-tracking in resolving interpretation errors. In the auto-picked version, the horizon exhibits multiple disjointed sections, particularly in areas where amplitude variations caused the algorithm to deviate. In contrast, the manually refined horizon shows more continuous and geologically reasonable structure, supporting the assertion that manual intervention is crucial when dealing with complex seismic data (Yilmaz, 2001).

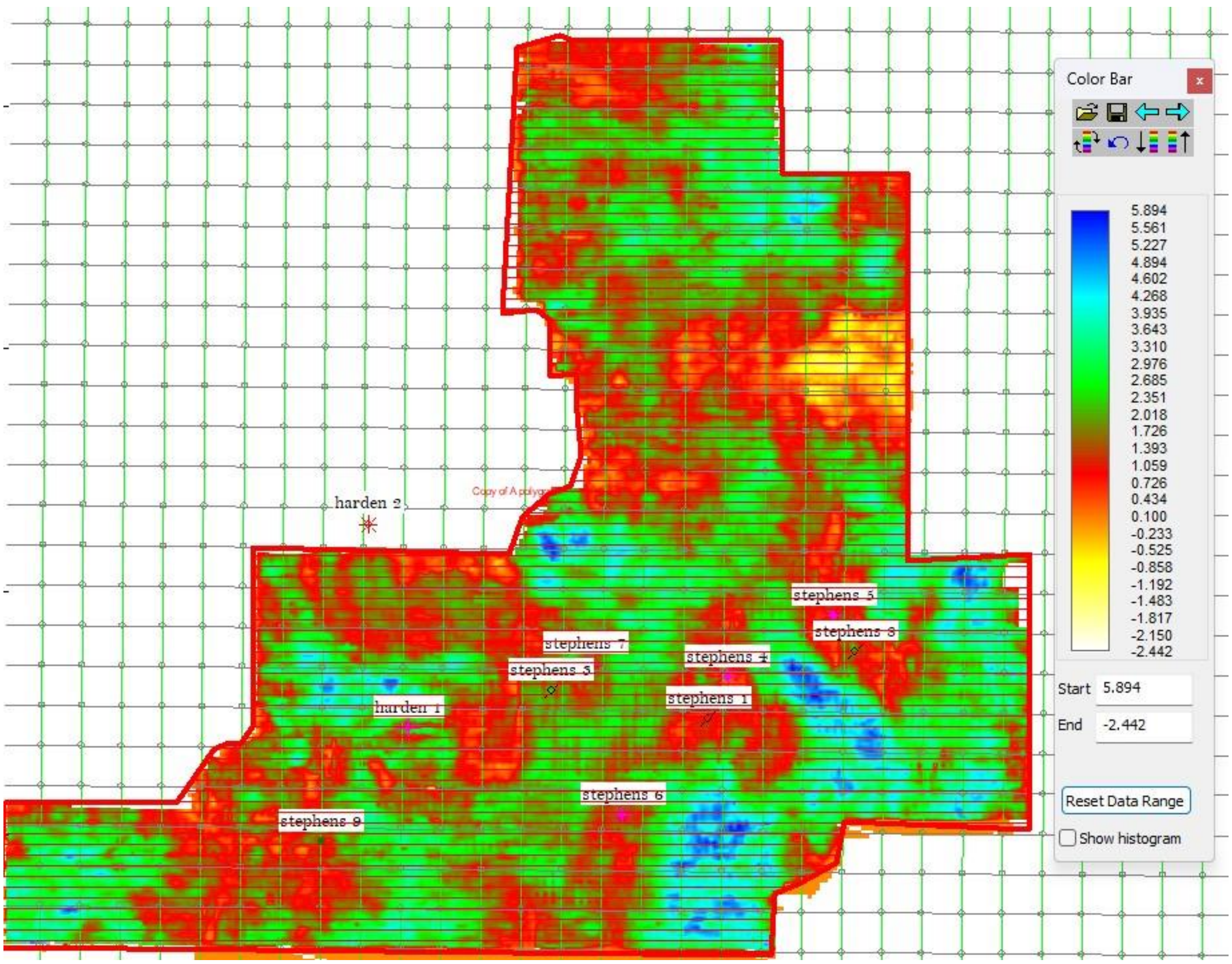

Figure 4.6: Amplitude map of the Viola horizon top manually re-tracked to close gaps that manifested out of misties during automatic picking algorithms. Color bar shows the values of amplitude.

4.4 Model Based Inversion

The inversion process was conducted at each well location by integrating multiple datasets within the S & P global Kingdom software. This workflow involved feeding the system with sonic logs, density logs, a micromodel, whitened amplitude data (Amp 18-25-80-100) and the seismic survey data to generate the inverted impedance results. The accuracy and reliability of the inversion outputs were assessed based on three quality metrics:

1. Error between the seismic trace and reconstructed trace: A lower error value indicates a strong correlation between the original seismic response and the inversion-derived trace, suggesting an accurate impedance estimation (Russell, 1990; Veeken et al., 2002).
2. Impedance log validation: the comparison between the well-derived impedance logs and the inverted impedance results served as a critical validation check. A close match between these logs suggests that the inversion process successfully captured the subsurface impedance variations (Lindseth, 1979).
3. Boundary limit adherence: the extent to which the inverted impedance log remains within the expected geological boundaries further confirms the robustness of the inversion model (Veeken & Da Silva, 2004).

The results (Fig 4.7 to Fig 4.14) indicate that the inversion is of high quality, as evidenced by the low error between the seismic trace and the reconstructed trace. Additionally, the inverted impedance logs closely matched the well-derived impedance logs, staying well within expected boundary constraints. These findings suggest that the inversion output can be reliably used for further geological and reservoir characterization.

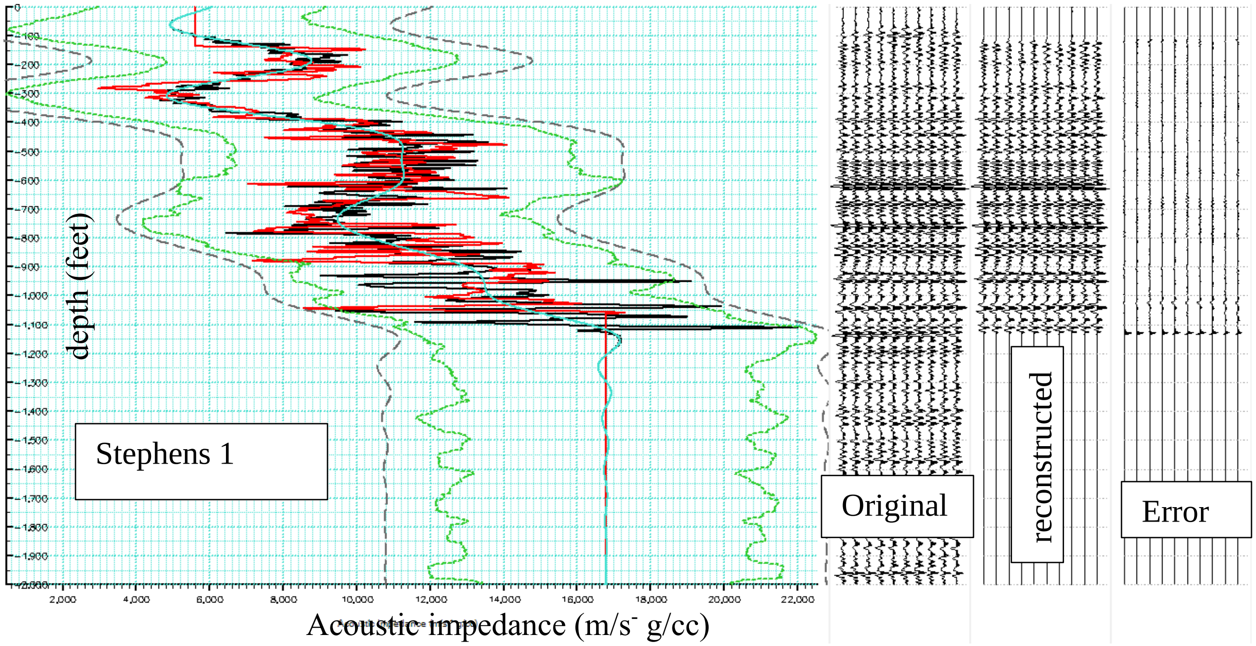

Figure 4.7: Stephens 1 well inversion results. Marked in red is the impedance results from logs, black is impedance from inversion process, cyan is macromodel, dashed black is the bounds, and green is the modified bounds. The right panel shows original seismic data, reconstructed seismic data and the error between the two.

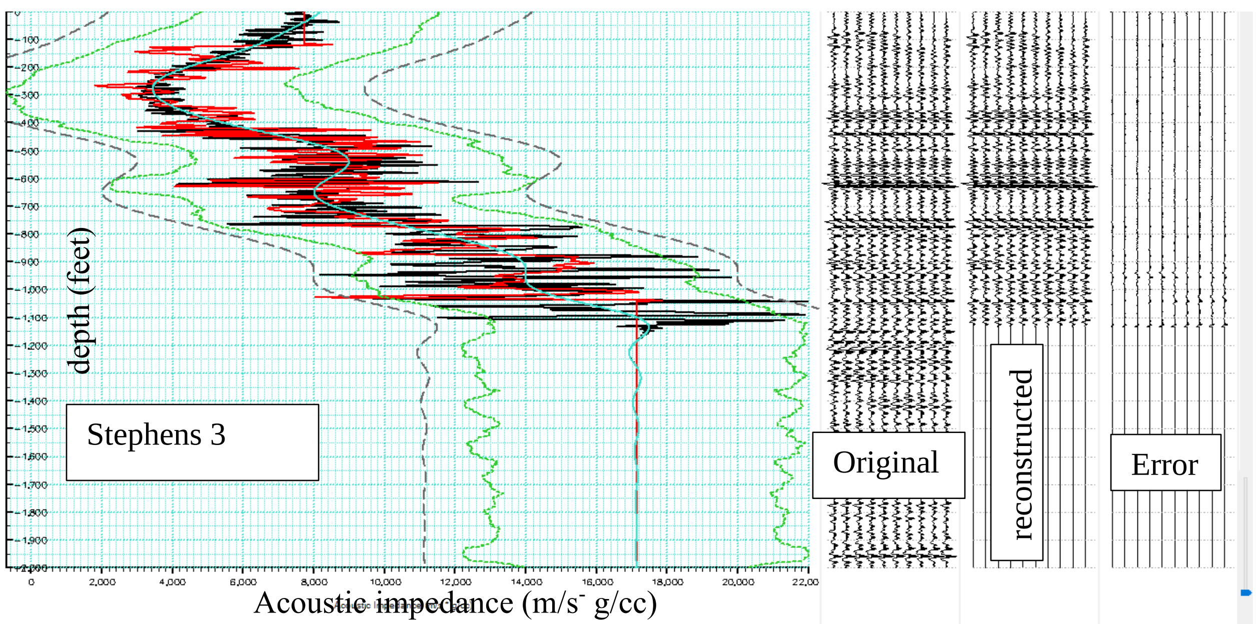

Figure 4.8: Stephens 3 well inversion results. Marked in red is the impedance results from logs, black is impedance from inversion process, cyan is macromodel, dashed black is the bounds, and green is the modified bounds. The right panel shows original seismic data, reconstructed seismic data and the error between the two.

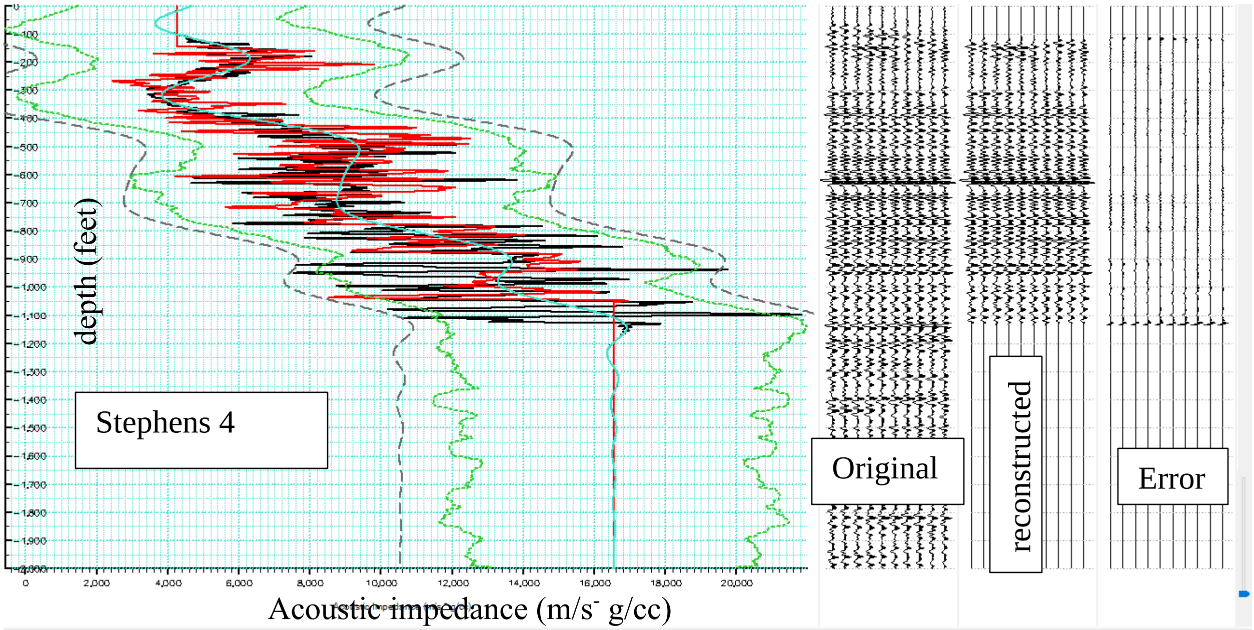

Figure 4.9: Stephens 4 well inversion results. Marked in red is the impedance results from logs, black is impedance from inversion process, cyan is macromodel, dashed black is the bounds, and green is the modified bounds. The right panel shows original seismic data, reconstructed seismic data and the error between the two.

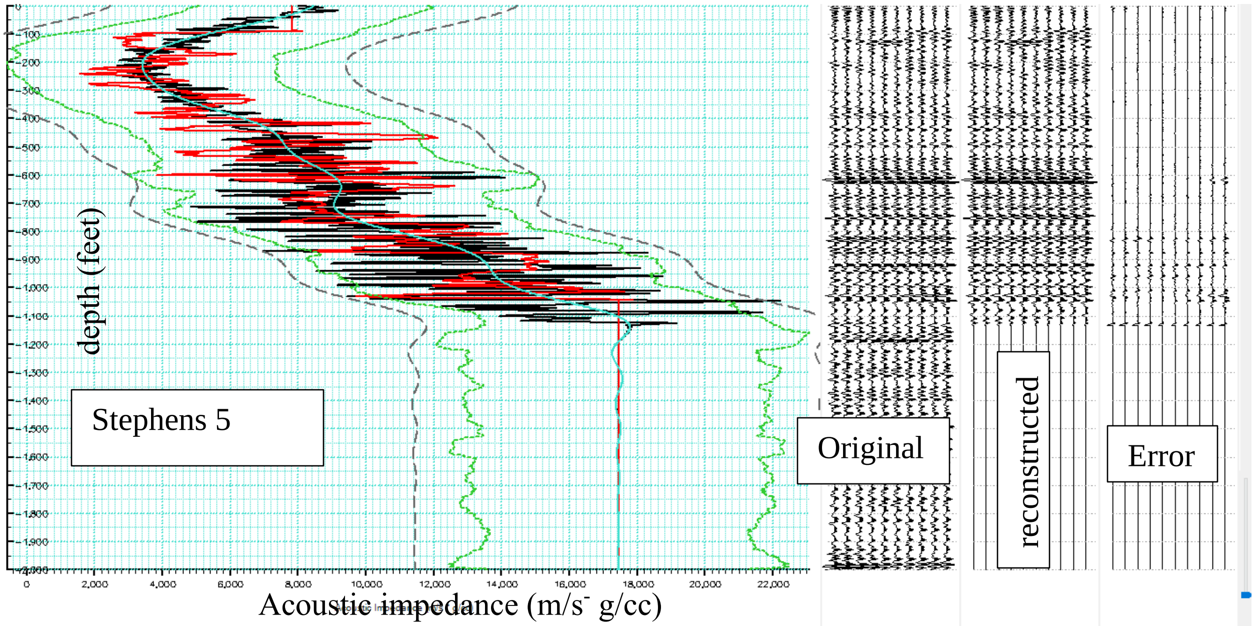

Figure 4.10: Stephens 5 well inversion results. Marked in red is the impedance results from logs, black is impedance from inversion process, cyan is macromodel, dashed black is the bounds, and green is the modified bounds. The right panel shows original seismic data, reconstructed seismic data and the error between the two.

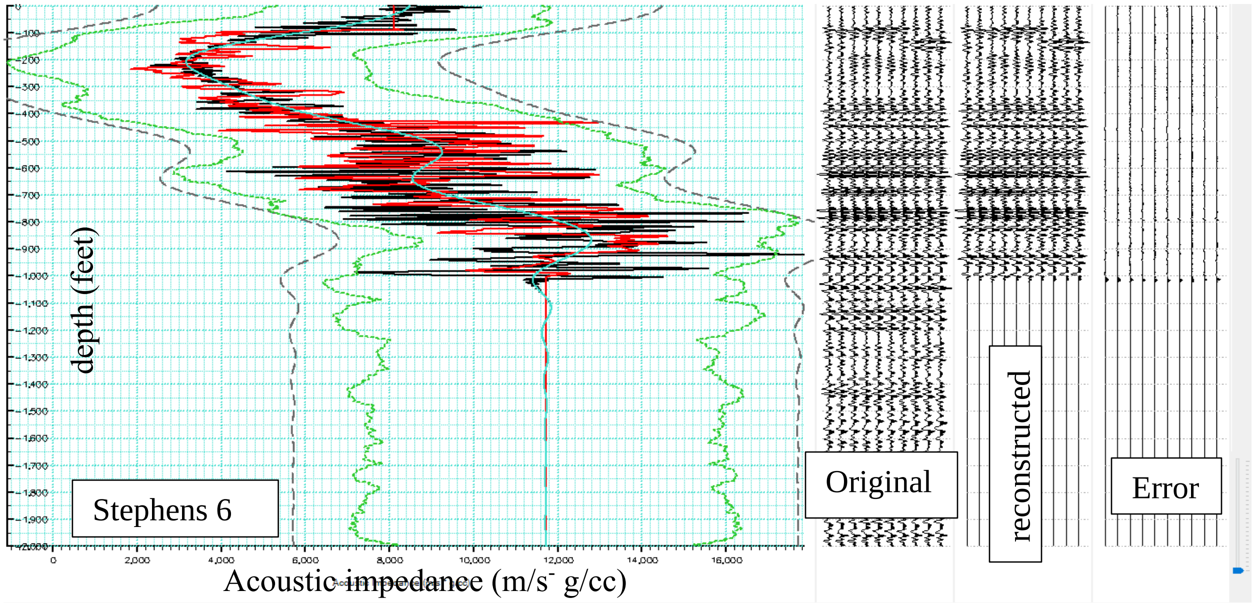

Figure 4.11: Stephens 6 well inversion results. Marked in red is the impedance results from logs, black is impedance from inversion process, cyan is macromodel, dashed black is the bounds, and green is the modified bounds. The right panel shows original seismic data, reconstructed seismic data and the error between the two.

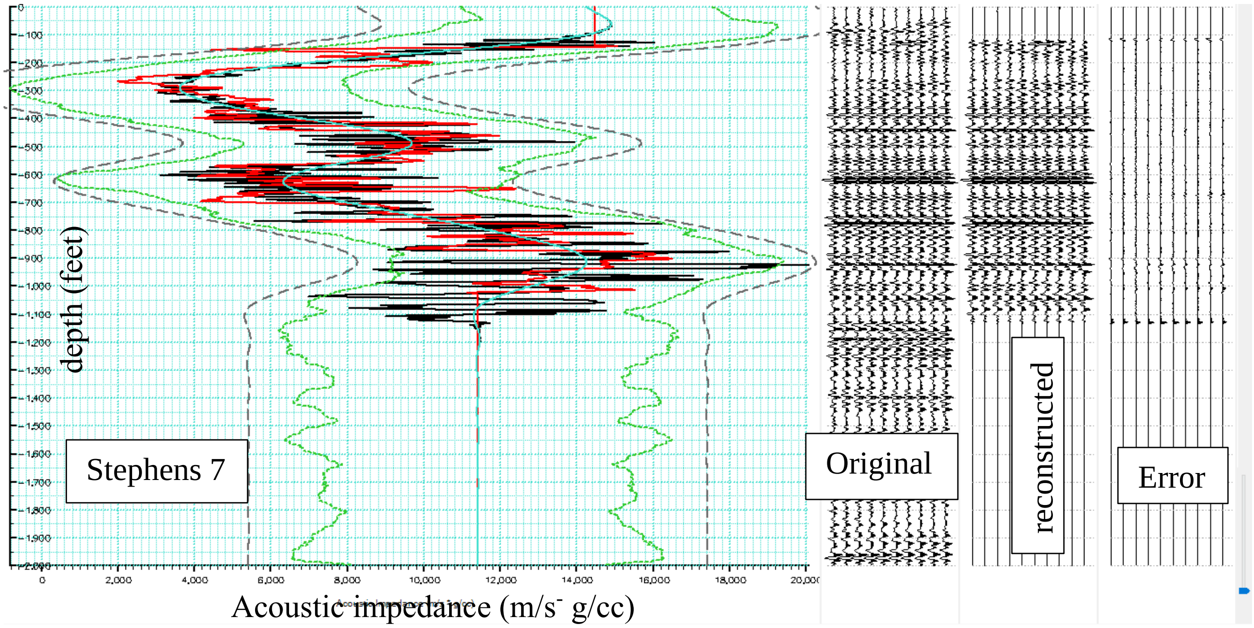

Figure 4.12: Stephens 7 well inversion results. Marked in red is the impedance results from logs, black is impedance from inversion process, cyan is macromodel, dashed black is the bounds, and green is the modified bounds. The right panel shows original seismic data, reconstructed seismic data and the error between the two.

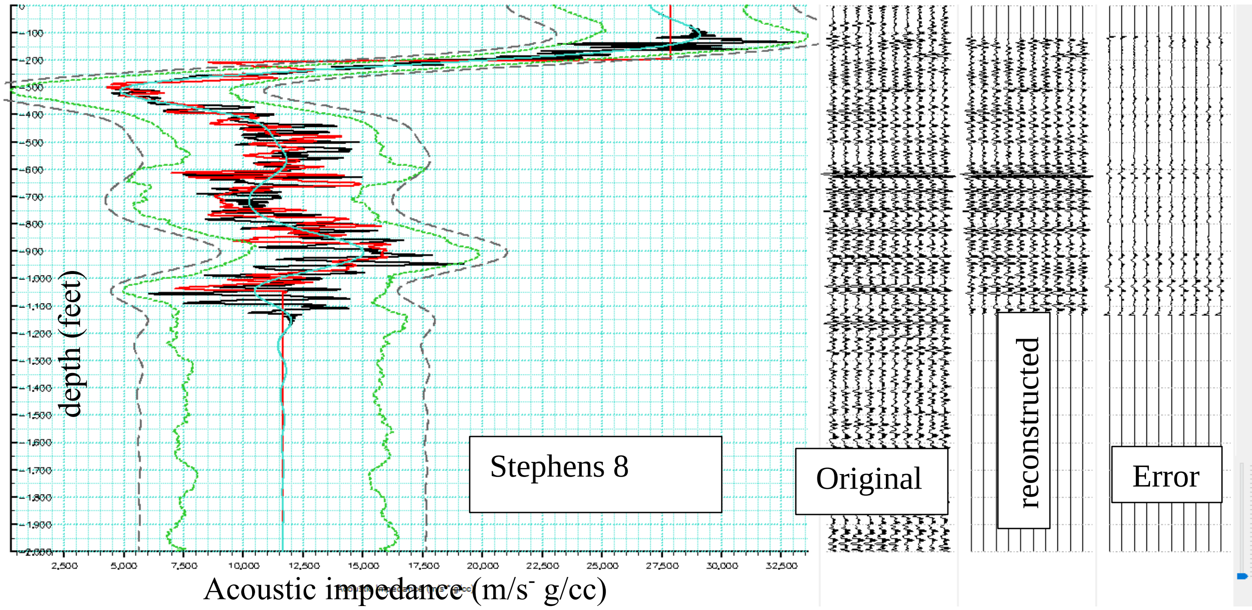

Figure 4.13: Stephens 8 well inversion results. Marked in red is the impedance results from logs, black is impedance from inversion process, cyan is macromodel, dashed black is the bounds, and green is the modified bounds. The right panel shows original seismic data, reconstructed seismic data and the error between the two.

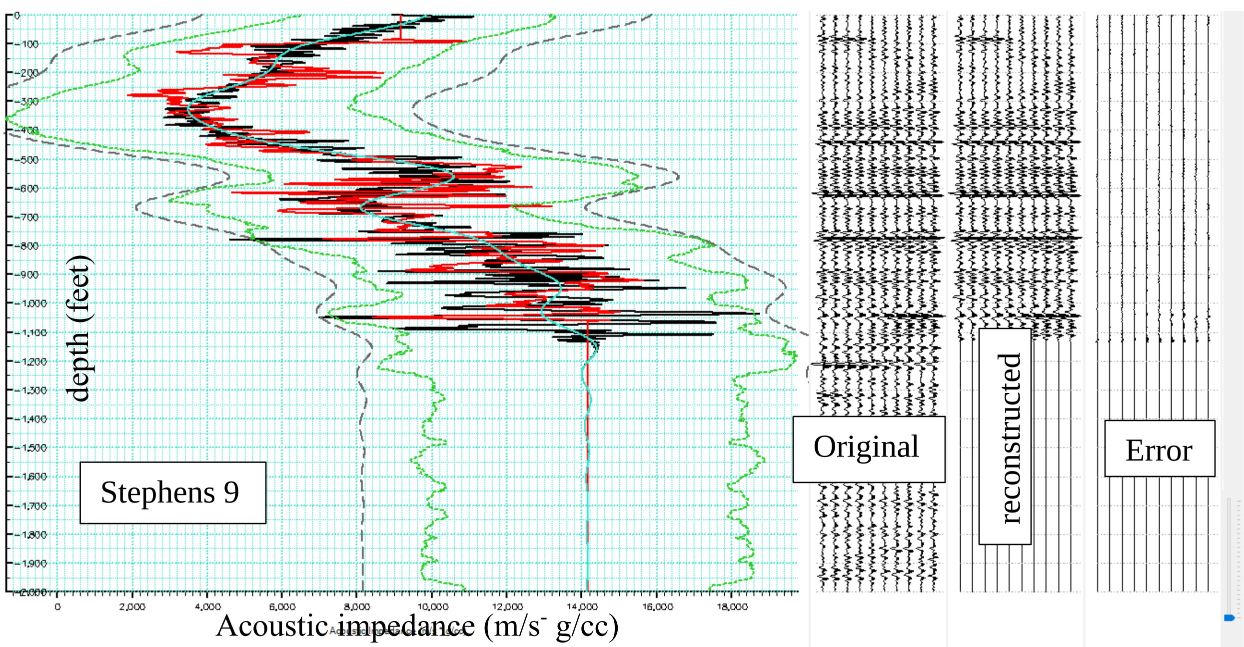

Figure 4.14: Stephens 9 well inversion results. Marked in red is the impedance results from logs, black is impedance from inversion process, cyan is macromodel, dashed black is the bounds, and green is the modified bounds. The right panel shows original seismic data, reconstructed seismic data and the error between the two.

4.5 Acoustic Impedance Prediction Using Machine Learning

The performance of XGBoost and TabNet model (a neural network-based model designed explicitly for tabular data) in predicting the standardized impedance values at well locations between the horizons above and beneath the viola were evaluated by key statistical metrics such as Mean Absolute Error (MAE), Mean Squared Error, and Root Mean Squared Error (RMSE). Figure 4.15 and figure 4.16 Illustrate predicted versus actual impedance for both models.

Model Performance Comparison

The XGBoost model shows a moderate spread of predicted values around the perfect prediction line (red dashed line); there is a noticeable deviation of several data points, indicating some degree of error in prediction, MAE (0.60), MSE (0.60) and RMSE (0.77). Despite these deviations, the overall trend aligns with the expected impedance values. In contrast, the TabNet model exhibits lower MAE (0.4895), MSE (0.3847) and RMSE (0.6202) values, suggesting improved predictive accuracy. The tighter clustering of points around the perfect prediction line indicates better impedance values reconstruction as it appears to minimize extreme deviations, which contributes to reduced error values.

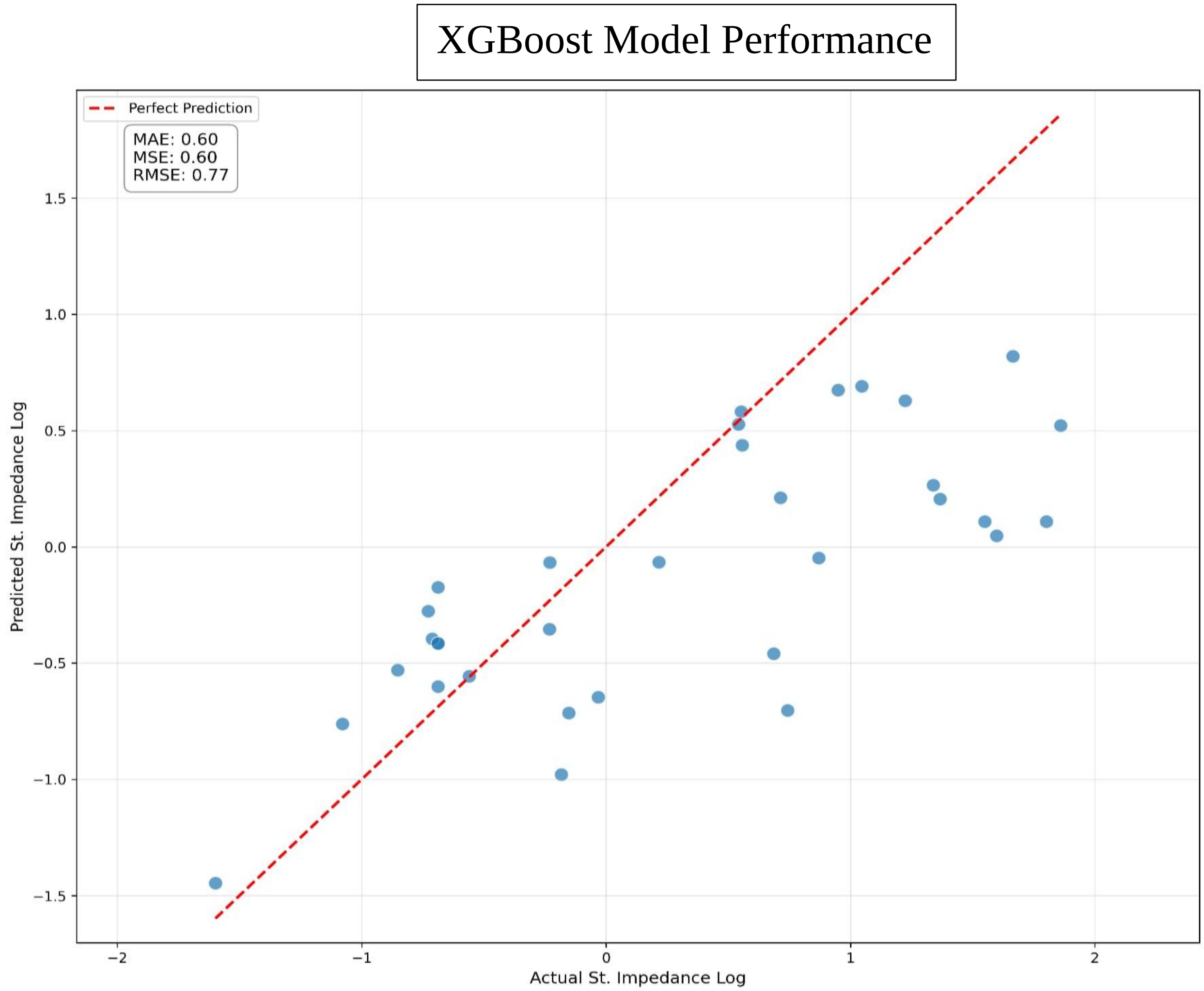

Figure 4.15: XGBoost model performance of actual standardized impedance log values against predicted impedance log values. The red dashed line represents perfect prediction, while the data points indicate model predictions.

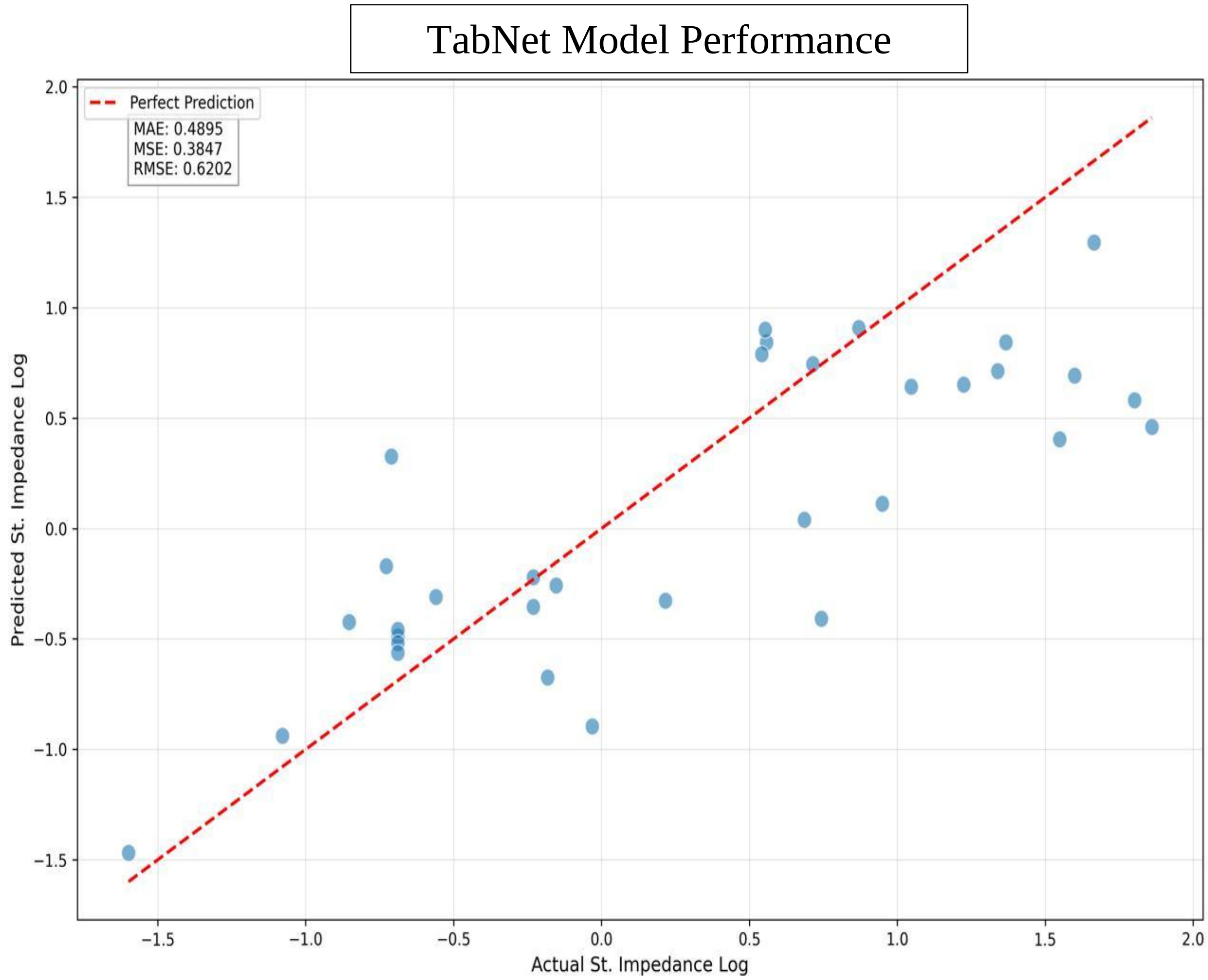

Figure 4.16: TabNet model performance of actual standardized impedance log values against predicted impedance log values. The red dashed line represents perfect prediction, while the data points indicate model predictions.

4.6 Predicted Impedance Volume

The impedance volume of the study area (Fig 4.17) obtained by applying the TabNet model to the extracted attributes data from the Viola horizon provides crucial insights into the subsurface properties. Areas with lower impedance values are indicative of higher porosity, which in turn, suggests a more significant potential for hydrocarbon saturation/entrapment.

Comparing the detuned isochrone map (Fig 4.18), time structural map (Fig 4.19), impedance volume map, amplitude map (Fig 4.6), the drilling results (Table 4.1) and mineralogy results from Jallow (2024), high thicknesses, structural highs, low amplitudes and low impedance associates with producing wells.

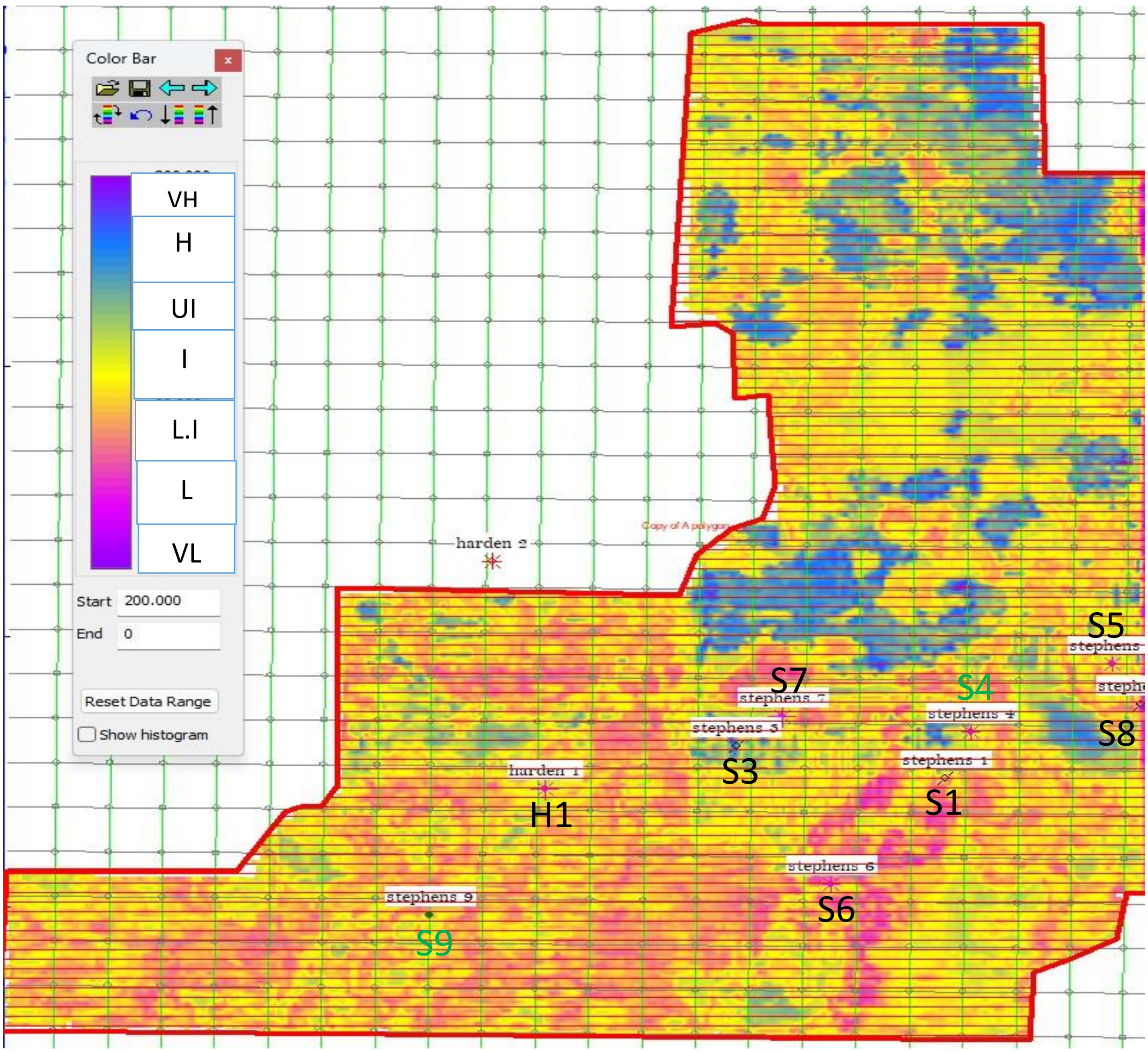

Figure 4.17: Acoustic impedance volume showing the variation in impedance across the study area. Acoustic impedance values on color bar scale normalized to show detailed resolution.

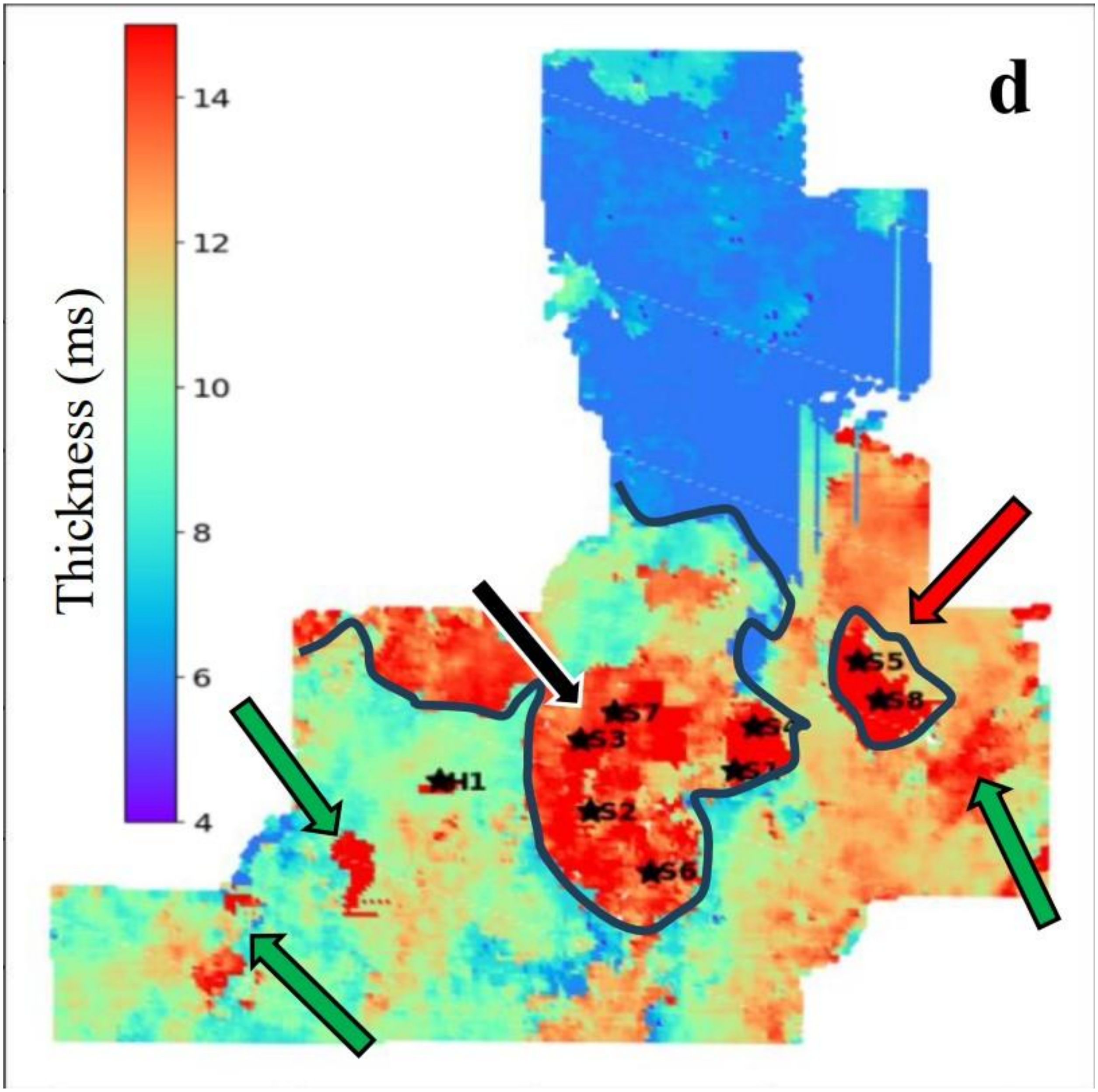

Figure 4.18: Detuned isochrone map showing thickness variations for the Viola horizon.

Drillers report for the Stephens 4 well, which is currently producing commercial hydrocarbons from the Viola formation reveals that the Viola which is the target reservoir was encountered from 6366 fts to 6392 fts. With this knowledge a sonic-density cross plot fitted to this depth interval and overlaid with a preset lithology filter and colored with photoelectric log (PE) (Fig 4.20). A similar cross plot was made for a non-producing well (Stephens 3) (Fig 4.21) shows more dolomite points than calcite, photoelectric factor (PeF) of dolomite is approximately 3.14 whilst PeF of calcite is approximately 5.08. This interpretation is based on the Kansas Geological Survey's (KGS) photoelectric curve scaled from 0 to 10 (Fig 4.22). A photoelectric (PE) log is a petrophysical well log used in formation evaluation to determine rock mineralogy rather than fluid properties. It measures the photoelectric absorption cross-section index of the formation, which depends on the atomic number (Z) of the rock's mineral components. This assertion holds true because porosity within the Viola is highly controlled by dolomitization and correlates with the mineralogy calculation done by Jallow (2024).

Stephens 6 well which is now being used as an (EOR) Enhanced Oil Recovery well has low impedance was a producing well has appreciable dolomite and quartz content as compared to limestone (calcite). This insight is important because the effectiveness EOR techniques and methods depends greatly on porosity and movement of fluids (permeability) through the rock to extract hydrocarbons (Thomas, 2007).

Areas exhibiting structural highs, high thicknesses, and low amplitudes are prospects for future well placement (Jallow, 2024). In compliance with our results, we add that these areas characterized by the aforementioned features with low impedances are potential hydrocarbon saturation zones.

Well Name	Well Status
Stephens 1	Plugged and abandoned
Stephens 3	Plugged and abandoned
Stephens 4	Producing (Oil and Gas)
Stephens 5	Converted to Saltwater Disposal Well
Stephens 6	Converted to Enhanced Oil Recovery well
Stephens 7	Plugged and abandoned
Stephens 8	Plugged and abandoned
Stephens 9	Producing (Oil)

Table 4.1: Drilling results of Stephens 1, 3, 4, 5, 6, 7, 8, and 9. Information extracted from Kansas Geological Survey (KGS) oil and gas wells database.

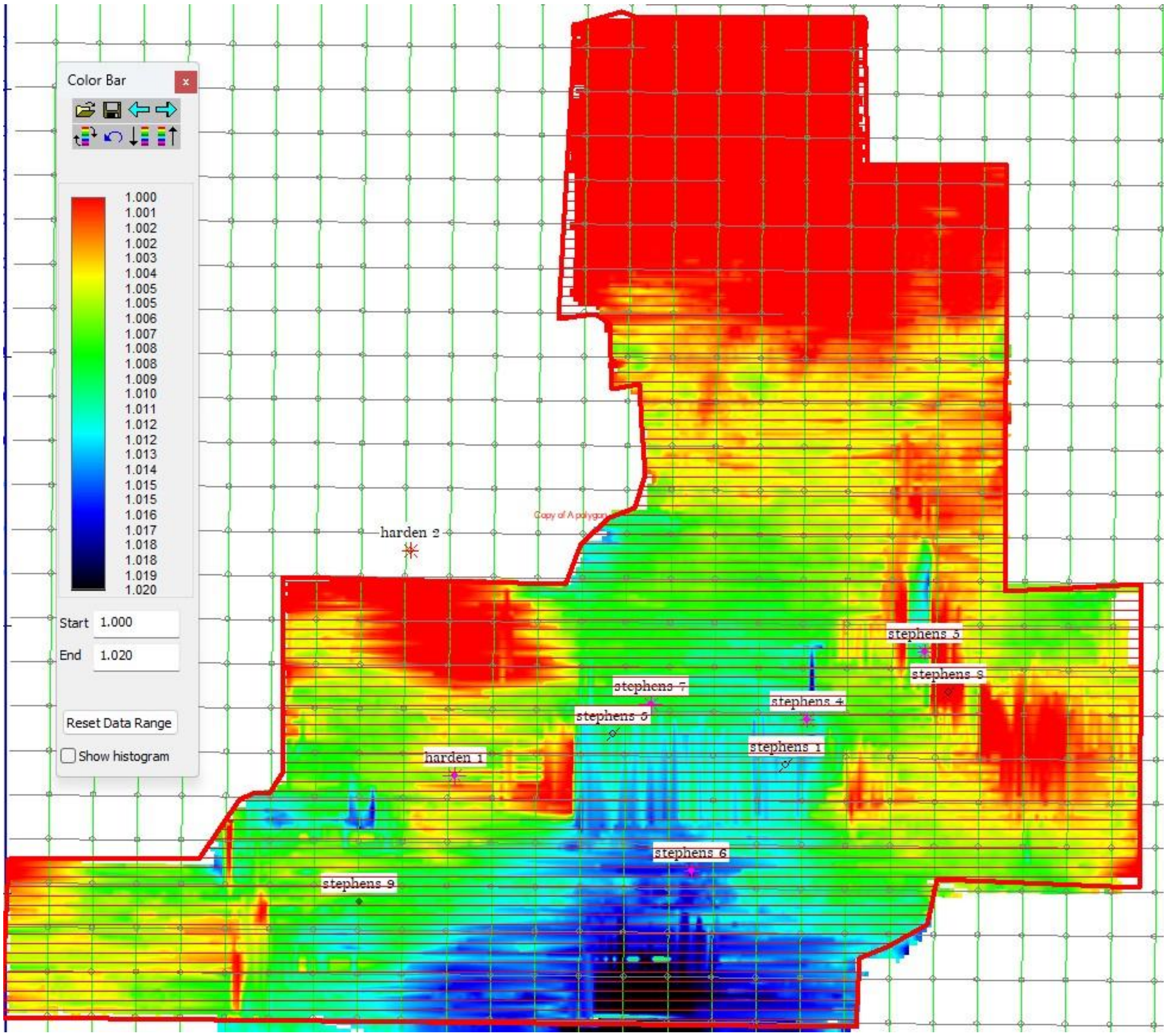

Figure 4.19: Viola time structural map. Interpretative color bar revealing structural highs and lows. Structural highs have lower time values whilst structural lows have higher time values on the displayed color bar.

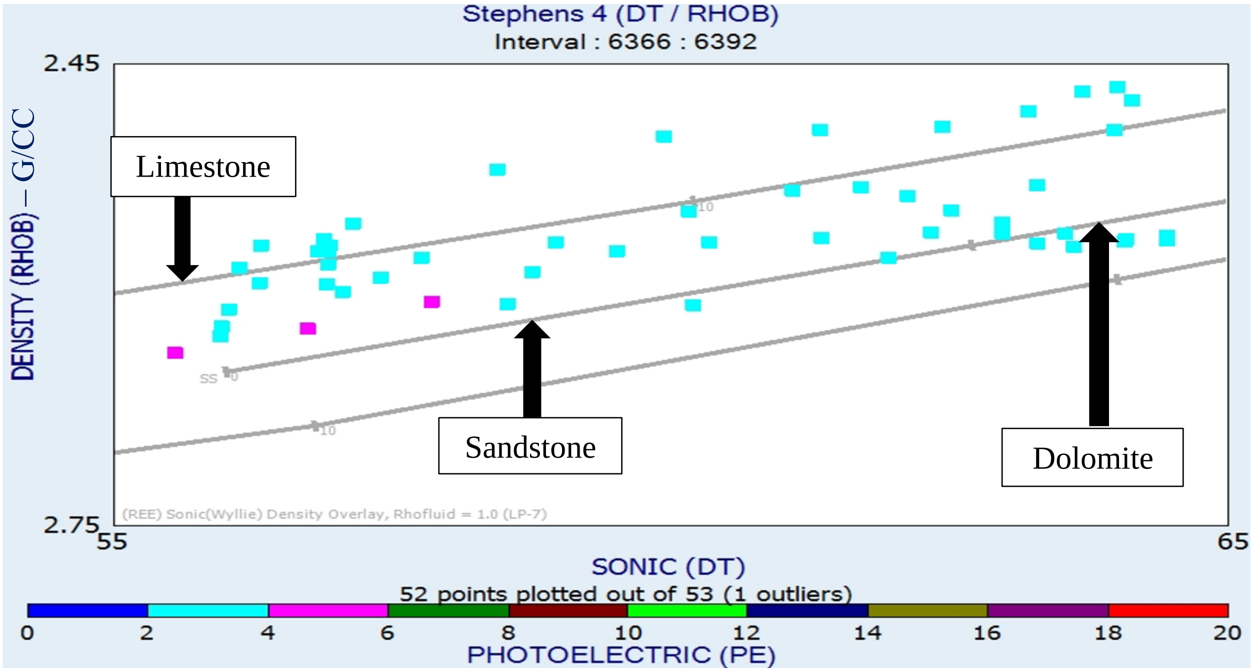

Figure 4.20: Cross plot of Stephens 4 well (producing) colored with Photoelectric log. Low PE values colored in cyan and high PE values colored in pink (calcite)

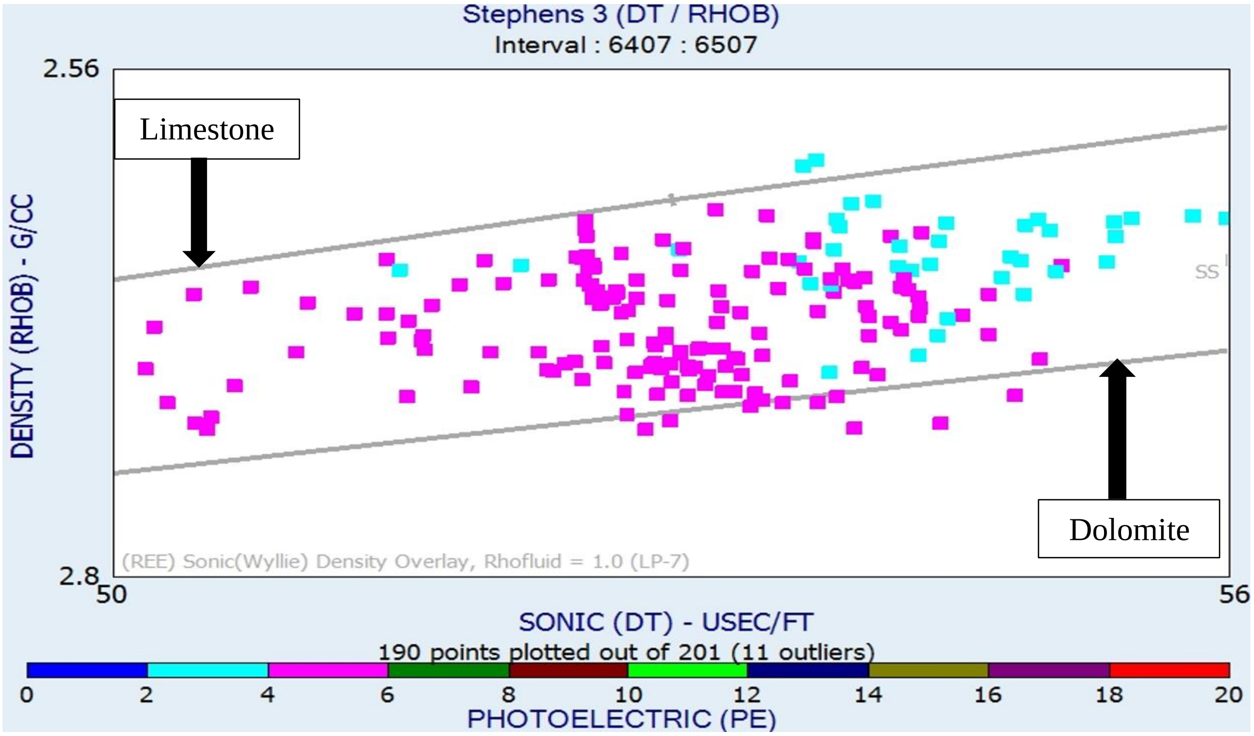

Figure 4.21: Cross plot of Stephens 3 well (Non - producing) colored with Photoelectric log. Low PE values colored in cyan and high PE values colored in pink (calcite)

The Photoelectric Factor Curve

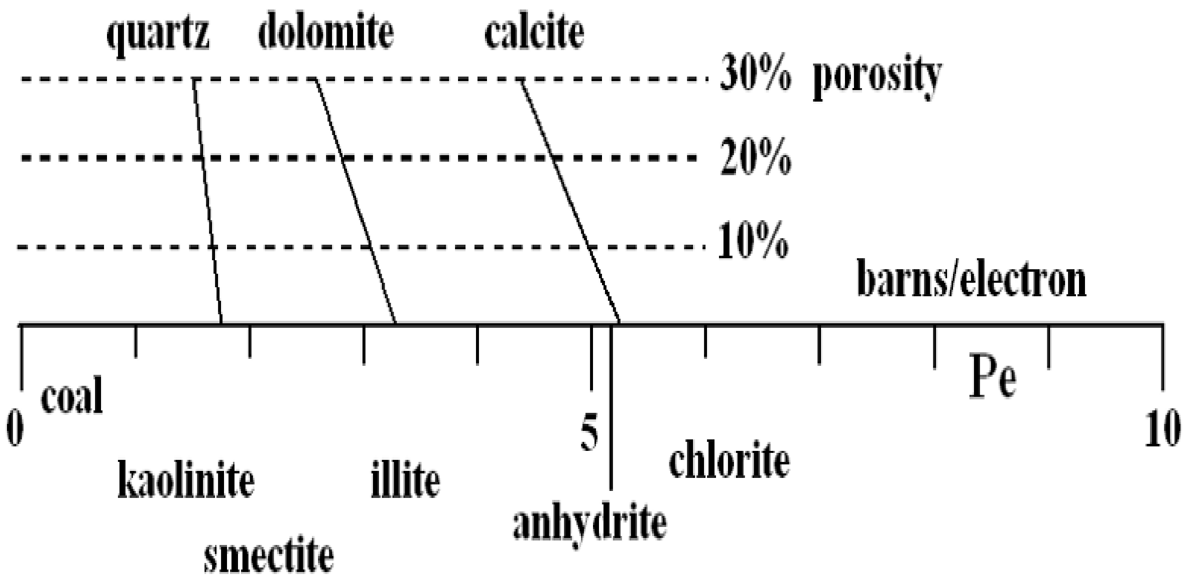

Figure 4.22: Photoelectric factor (PeF) curve scaled on a range between 0 and 10 barns/electron (from Kansas Geological Survey).

Chapter 5 - Conclusion

This study has successfully demonstrated the effectiveness of seismic inversion techniques based on machine learning models in estimating average acoustic impedance of the Viola carbonates. By integrating well log data, seismic survey data, and inversion acoustic impedance, this research project provides a better understanding of a seismic indicator to enhance reservoir quality mapping of the target Viola carbonate of Morrison NE Field. The Viola horizon interpretation revealed initial inconsistencies when auto-picking methods were employed, resulting in mis-ties in the amplitude maps. These inaccuracies were mitigated by manually retracking both inlines and crosslines, leading to a more coherent structural representation. The refinement technique improved pre-retracking amplitude maps.

Furthermore, seismic inversion was performed using S & P Global Kingdom, incorporating sonic logs, density logs, a macromodel, and whitened amplitude data. The quality of inversion results was evaluated on the error between the actual and inverted impedance logs. The results demonstrated high accuracy, as indicated by minimum error and well-constrained impedance value within expected geological limits.

Spectral whitening played a crucial role in enhancing seismic resolution. This process improved the visibility of geological features and increased the accuracy of the inversion results. The application of spectral whitening ensured better preservation of high-frequency signals, leading to a clearer distinction between different subsurface layers and reducing the effects of tuning artifacts.

This study underscores the importance of accurate horizon tracking for improved seismic attribute extraction, which forms the foundation for robust reservoir characterization.

A comparative analysis between machine learning models, including XGBoost and TabNet, was conducted to assess their performance in predicting impedance values. TabNet demonstrated better alignment with the actual impedance values as it outperformed XGBoost in terms of MAE, MSE and RMSE suggesting its deep learning-based architecture provided acceptable predicted acoustic impedance that can leverage Viola reservoir management drilling decisions. The degree of dolomitization within the Viola is essential control on the Viola's reservoir quality.

Ultimately, the most promising zones for future exploration and development within the Morrisson Northeast field are associated with lower acoustic impedance, high thickness, and structurally favorable settings.

References

Adriansyah, A., & McMechan, G. A. (2002). Analysis and interpretation of seismic data from thin reservoirs: Northwest Java Basin, Indonesia. *Geophysics*, *67*(1), 14–26. https://doi.org/10.1190/1.1451317

Ali, A., Alves, T. M., Saad, F. A., Ullah, M., Toqeer, M., & Hussain, M. (2017). Resource potential of gas reservoirs in South Pakistan and adjacent Indian subcontinent revealed by post-stack inversion techniques. *Journal of Natural Gas Science and Engineering*, *49*, 41–55. https://doi.org/10.1016/j.jngse.2017.10.010

Bishop, C. M. (1994). Neural networks and their applications. *Review of Scientific Instruments*, *65*(6), 1803–1832. https://doi.org/10.1063/1.1144830

Bornemann, E., Doveton, J. H., St.Clair, P. N., Kansas Geological Survey, Schlumberger Well Services, & Marathon Oil Company. (1982). Lithofacies analysis of the Viola Limestone in South-central Kansas. In *KGS--Petrophysical Series 3*. https://www.kgs.ku.edu/Publications/Bulletins/PS3/

Bouharket, B. (2017). *3D Seismic Attributes Analysis and inversions for prospect evaluation and characterization of Cherokee Sandstone Reservoir in the Wierman Field, Ness County, Kansas* [MS Thesis]. Kansas State University.

Brown, A. R. (2011c). *Interpretation of Three-Dimensional seismic data*. https://doi.org/10.1190/1.9781560802884

Brown, A., Wright, R., Burkart, K., Abriel, W., & McBeath, r. (1986). tuning effects, lithological effects and depositional effects in the seismic response of gas reservoirs*. *Geophysical Prospecting*, *34*(5), 623–647. https://doi.org/10.1111/j.1365-2478.1986.tb00485.x

Campbell, T. J., Richards, F. B., Silva, R. L., Wach, G., & Eliuk, L. (2015). Interpretation of the Penobscot 3D seismic volume using constrained sparse spike inversion, Sable sub-Basin, offshore Nova Scotia. *Marine and Petroleum Geology*, *68*, 73–93. https://doi.org/10.1016/j.marpetgeo.2015.08.009

Carlson, M. P., Newell, K. D., & Oklahoma Geol. Society. (1997). *Stratigraphy and Petroleum Potential of the Simpson and Viola (Ordovician) in Kansas and Nebraska. Simpson and Viola Groups, in the Southern Midcontinent, 1994 Symposium*.

Chen, T., & Guestrin, C. (2016b). XGBoost: A Scalable Tree Boosting System. *KDD '16: Proceedings of the 22nd ACM SIGKDD International Conference on Knowledge Discovery and Data Mining*, 785–794. https://doi.org/10.1145/2939672.2939785

Chopra, S., & Marfurt, K. J. (2005). Seismic attributes — A historical perspective. *Geophysics*, *70*(5), 3SO-28SO. https://doi.org/10.1190/1.2098670

Chopra, S., & Marfurt, K. J. (2007). *Seismic attributes for prospect identification and reservoir characterization*. https://doi.org/10.1190/1.9781560801900

Chopra, S., & Marfurt, K. J. (2018). Coherence Attribute Applications on Seismic Data in Various Guises. *AAPG Search and Discovery Article*, 42273. https://doi.org/10.1306/42273chopra2018

Chopra, S., Marfurt, K. J., & Misra, S. (2011). Seismic Attributes on Frequency-enhanced Seismic Data. *AAPG Search and Discovery Article*, 90173.

Cui, T., & Margrave, G. F. (2014). Seismic wavelet estimation. *CREWES Res Rep*, *26*, 1-16.

Dhaliwal, S. S., Nahid, A., & Abbas, R. (2018). Effective intrusion detection system using XGBOOST. *Information*, *9*(7), 149. https://doi.org/10.3390/info9070149

Djanawir, F. D., & Langitan, F. (2004). Application of inverse-q filter and deconvolution to improve seismic data quality in the deep section. *IPA-AAPG Proceedings, Deepwater and Frontier Exploration in Asia & Australasia Symposium*, DFE04-PO-029.

Erryansyah, M., Nainggolan, T. B., & Manik, H. M. (2020). Acoustic impedance model-based inversion to identify target reservoir: a case study Nias Waters. *IOP Conference Series Earth and Environmental Science*, *429*(1), 012033. https://doi.org/10.1088/1755-1315/429/1/012033

Figueiredo, A. M., Gattass, M., & Szenberg, F. (2007). Seismic horizon mapping across faults with Growing Neural Gas. *Tenth International Congress of the Brazilian Geophysical Society*. https://doi.org/10.1190/sbgf2007-288

Fossen, H. (2016). *Structural Geology* (2nd ed.). Cambridge University Press.

Goebel, N. E. D. (1968). Mississippian Rocks of Western Kansas. *AAPG Bulletin*, *52*. https://doi.org/10.1306/5d25c4cf-16c1-11d7-8645000102c1865d

Gurney, K. (2018). An introduction to neural networks. In *CRC Press eBooks*. https://doi.org/10.1201/9781315273570

Hagood, W. K. (2019). *Detailed Core and Log Analysis of a Producing Viola Dolomite Well in Comanche County, Kansas* [MS Thesis]. Kansas State University.

Herron, A. (2011). Resolution. In *First Steps in Seismic Interpretation* (Vol. 16, pp. 75–81). https://doi.org/10.1190/1.9781560802938.ch6

Jallow, M., (2024). *Thin Layer Effects on Horizon Attributes: Analysis Beyond Amplitude Tuning, Viola Carbonate Reservoir, Morrison NE Field, Kansas* [MS Thesis]. Kansas State University.

Koefoed, O. (1981). Aspects of vertical seismic resolution*. *Geophysical Prospecting*, *29*(1), 21–30. https://doi.org/10.1111/j.1365-2478.1981.tb01008.x

Li, W., Yin, Y., Quan, X., & Zhang, H. (2019). Gene Expression Value Prediction based on XGBOOST algorithm. *Frontiers in Genetics, 10*. https://doi.org/10.3389/fgene.2019.01077

Li, Z., & Guo, X. (2007). Predicting the distribution of thin bed reservoirs by broad frequency band seismic. *Applied Geophysics*, *4*(2), 118–126. https://doi.org/10.1007/s11770-007-0017-8

Linares, A., & Totten, M. (2016). *Petrographic Analysis and Diagenetic History of The Viola Limestone At Stephen's Ranch, In The Morrison Northeast Field Of Clark County, Kansas* [MS Thesis]. Kansas State University.

Lindseth, R. O. (1979). Synthetic sonic logs—a process for stratigraphic interpretation. *Geophysics*, *44*(1), 3–26. https://doi.org/10.1190/1.1440922

Liu, G., Fomel, S., Jin, L., & Chen, X. (2009). Stacking seismic data using local correlation. *Geophysics*, *74*(3), V43–V48. https://doi.org/10.1190/1.3085643

Liu, X., Zheng, X., Xu, G., Wang, L., & Yang, H. (2010). Locally linear embedding-based seismic attribute extraction and applications. *Applied Geophysics*, *7*(4), 365–375. https://doi.org/10.1007/s11770-010-0260-2

Maulana, A. D., Safira, Prayoga, Wijaksono, & Ascaria, A. (2022). Seismic inversion resolution enhancement with (3S) spectral blueing, spectral balancing, and stochastic inversion on fluvio deltaic environment. In *Proceedings, Indonesian Petroleum Association*.

Morris, J. R. (1995). Seismic Detection of the Rose Run Sandstone in South-Central Ohio: Structural Influences on Oil and Gas Reservoirs. *Ohio Geological Society: Third Annual Technical Symposium*.

Nestvold, E. O., (1996). The impact of 3-D seismic data on exploration, field development, and production, in P. Weimer and T. L. Davis, eds., *AAPG Studies in Geology No. 42 and SEG Geophysical Developments Series No. 5*, AAPG/SEG, Tulsa, p. 1–8

Nielsen, D. (2016). *Tree boosting with XGBoost-why does XGBoost win" every" machine learning competition?* [MS Thesis]. Norwegian University of Science and Technology.

Papageorgiou, G. and Chapman, M., (2021). Seismic tuning of dispersive thin layers. Geophysical Prospecting, 69(3), pp.622-628.

Patel, S. Bruckner, I. Viola and E. M. Gröller, "Seismic volume visualization for horizon extraction," *2010 IEEE Pacific Visualization Symposium (PacificVis)*, Taipei, Taiwan, 2010, pp. 73-80, doi: 10.1109/PACIFICVIS.2010.5429605.

Peacock, K. L., & Treitel, S. (1969). Predictive deconvolution: theory and practice. *Geophysics*, *34*(2), 155–169. https://doi.org/10.1190/1.1440003

Raef, A. E., Totten, M. W., Linares, A., & Kamari, A. (2019). Lithofacies control on reservoir quality of the Viola limestone in southwest Kansas and unsupervised Machine Learning Approach of Seismic Attributes FACIES-Classification. *Pure and Applied Geophysics*, *176*(10), 4297–4308. https://doi.org/10.1007/s00024-019-02205-4

Review of basic concepts. (1984). In *Developments in petroleum science* (pp. 1–28). https://doi.org/10.1016/s0376-7361(08)70415-1

Richardson, L. J. (2013). The Herd Viola Trend, Comanche County, Kansas. *AAPG Search and Discovery Article*, 20220.

Ricker, N. (1953). wavelet contraction, wavelet expansion, and the control of seismic resolution. *Geophysics*, *18*(4), 769–792. https://doi.org/10.1190/1.1437927

Roden, R., Smith, T. A., Santogrossi, P., Sacrey, D., & Jones, G. (2017). Seismic interpretation below tuning with multiattribute analysis. *The Leading Edge*, *36*(4), 330–339. https://doi.org/10.1190/tle36040330.1

Rost, S., & Thomas, C. (2009). Improving seismic resolution through array processing techniques. *Surveys in Geophysics*, *30*(4–5), 271–299. https://doi.org/10.1007/s10712-009-9070-6

Russell, B. H. (1990). *Introduction to Seismic Inversion Methods. (n.d.)* (No.2, S.N Domenico, Series Editor). Society of Exploration Geophysicists, Course Notes Series. https://books.google.com/books?id=uUIx-89aifwC

Santhanam, R., Uzir, N., Raman, S., & Banerjee, S. (2017). Experimenting XGBoost Algorithm for Prediction and Classification of Different Datasets. *Conference: National Conference on Recent Innovations in Software Engineering and Computer Technologies (NCRISECT) 2017At: Chennai*.

Schoepp, A. R., Margrave, G. F., & The CREWES Project, University of Calgary. (1998). Merging inverse-Q filtering and deconvolution. In *GEO-TRIAD '98*.

Sheriff, R. E. (1994). *Encyclopedic Dictionary of Exploration Geophysics.* Society of Exploration Geophysics.

Singh, Y. (2008). Phase distortion and time shifts due to seismic attenuation and application to well ties. *First Break*, *26*(2). https://doi.org/10.3997/1365-2397.2008001

Thomas, S. (2007). Enhanced oil Recovery - an overview. *Oil & Gas Science and Technology – Revue D'IFP Energies Nouvelles*, *63*(1), 9–19. https://doi.org/10.2516/ogst:2007060

Veeken, P., & Da Silva, M. (2004). Seismic Inversion Methods and some of their constraints. *First Break*, *22*(6). https://doi.org/10.3997/1365-2397.2004011

Veeken, P., Rauch-Davies, M., Gallardo, R., Vera, E. G., & Villasenor, R. V. (2002). Seismic inversion of the Fortuna National 3D survey (Tabaso, Mexico). *First Break. Geology*. https://doi.org/10.1046/J.1365-2397.2002.00257.X

Vohs, A. B., (2016). *3D Seismic Attributes Analysis in reservoir characterization: The Morrison NE Field & Morrison Field, Clark County Kansas* [MS Thesis]. Kansas State University.

Wang, M., Liu, Y., Zou, G., Teng, D., & She, J. (2022). Application of model-based acoustic impedance inversion in the prediction of thin interbedded coal seams: a case study in the Yuwang colliery, Yunnan Province. *Exploration Geophysics*, *54*(4), 407–415. https://doi.org/10.1080/08123985.2022.2155514

White, R., & Simm, R. (2003). Tutorial: good practice in well ties. *First Break*, *21*(10). https://doi.org/10.3997/1365-2397.21.10.25640

Xiong, R., Huang, X., Guo, L., Zou, X., & Tian, H. (2024). Seismic attribute extraction and application based on the Gabor wavelet transform. *IEEE Access*, 1. https://doi.org/10.1109/access.2024.3359696

Yilmaz, O. (2001). *Seismic Data Analysis: Processing, Inversion, and Interpretation of Seismic Data*. (Vol. 2). SEG.

Zhang, X., Zhang, Z., Xu, T., Bai, Z., & Harris, J. M. (2012). Phase shift approximation for the post-critical seismic wave. *Journal of Geophysics and Engineering*, *9*(5), 482–493. https://doi.org/10.1088/1742-2132/9/5/482

Zhonghua, N. M. (2017). Seismic data attribute extraction based on Hadoop platform. *IEEE*, 180–184. https://doi.org/10.1109/icccbda.2017.7951907

Appendix A - Sonic / Density Cross-plots

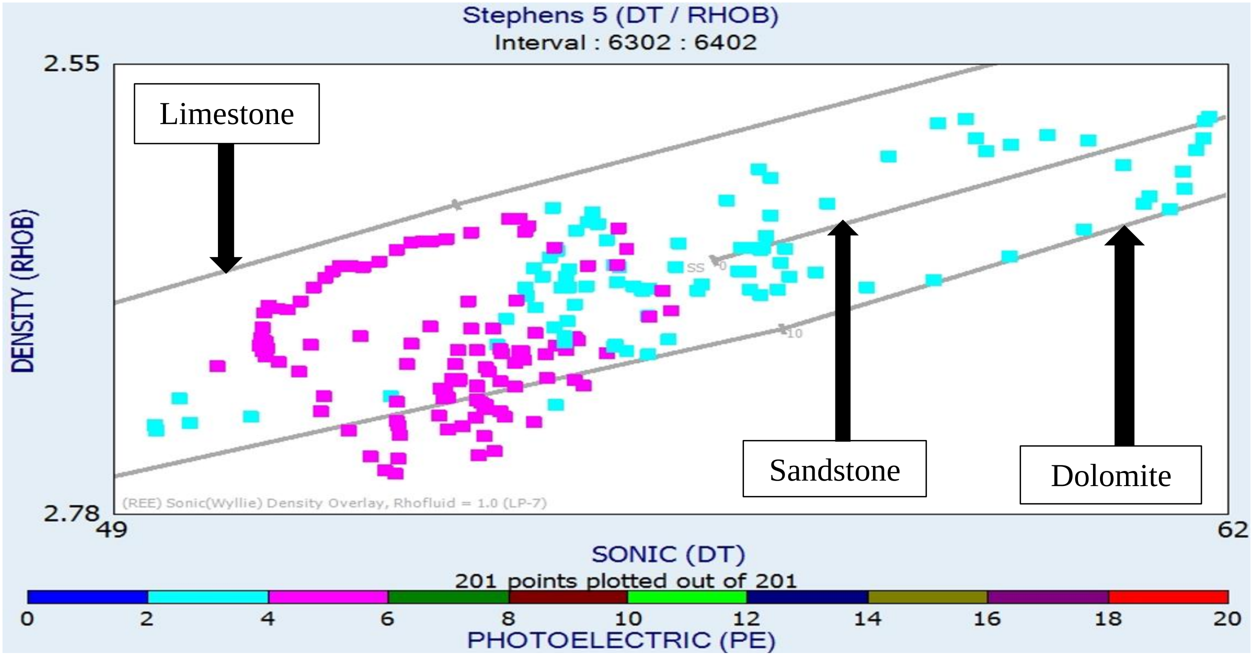

Appendix Figure A.1: Cross plot of Stephens 5 well (SWD) colored with Photoelectric log. Low PE values colored in cyan and high PE values colored in pink (calcite).

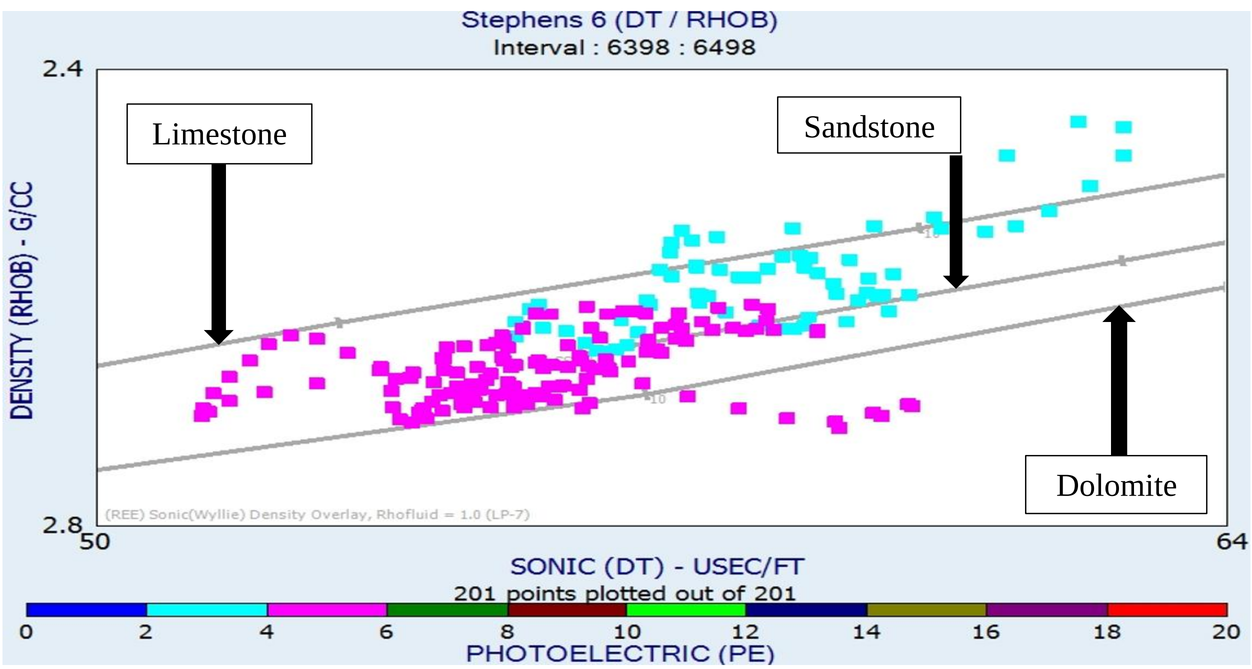

Appendix Figure A.2: Cross plot of Stephens 6 well (EOR) colored with Photoelectric log. Low PE values colored in cyan and high PE values colored in pink (calcite).

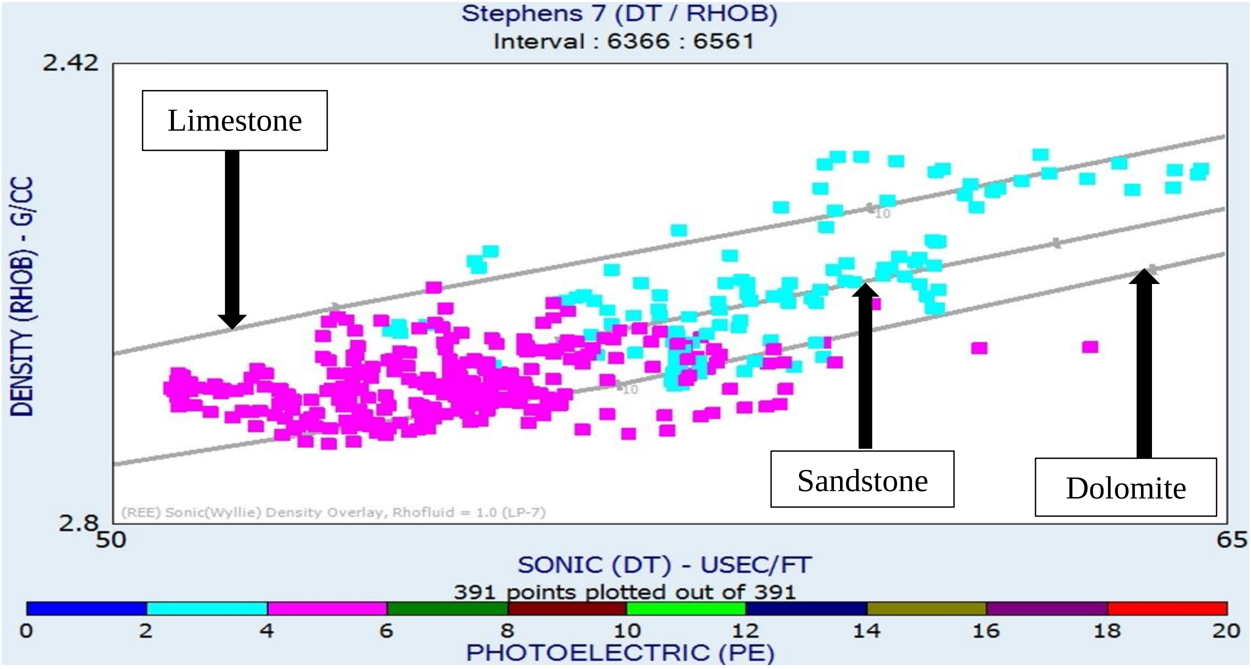

Appendix Figure A.3: Cross plot of Stephens 7 well (Non - producing) colored with Photoelectric log. Low PE values colored in cyan and high PE values colored in pink (calcite).

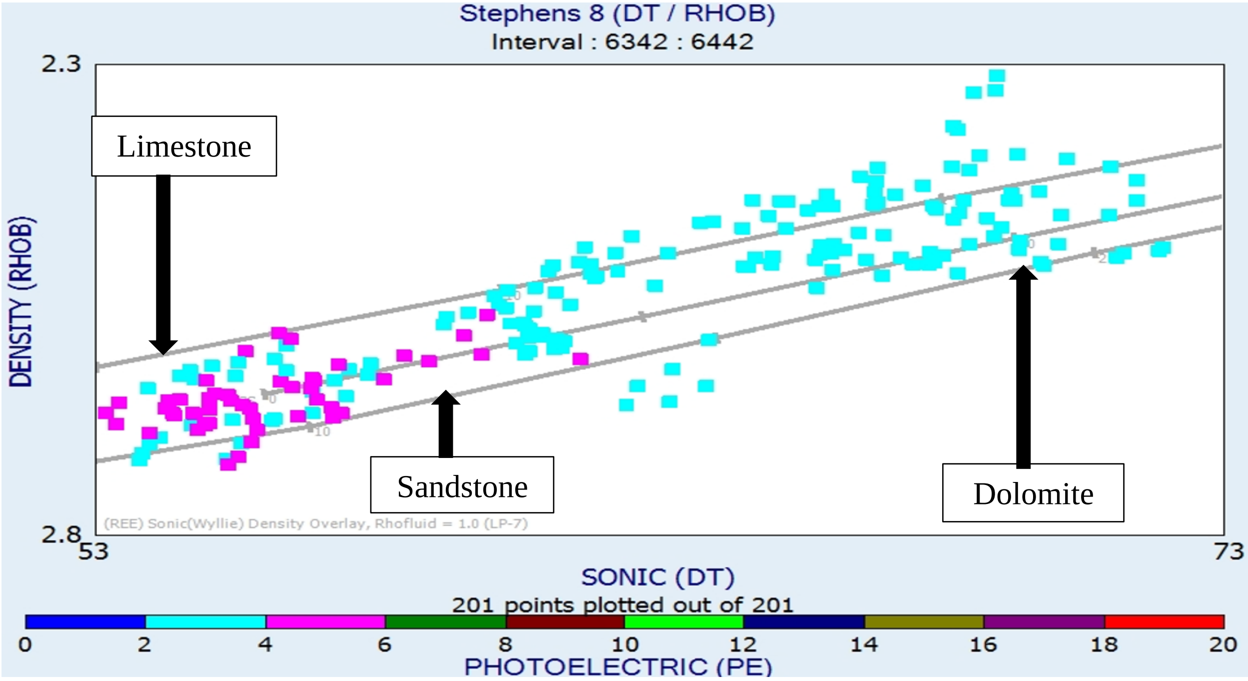

Appendix Figure A.4: Cross plot of Stephens 8 well (Non - producing) colored with Photoelectric log. Low PE values colored in cyan and high PE values colored in pink (calcite).

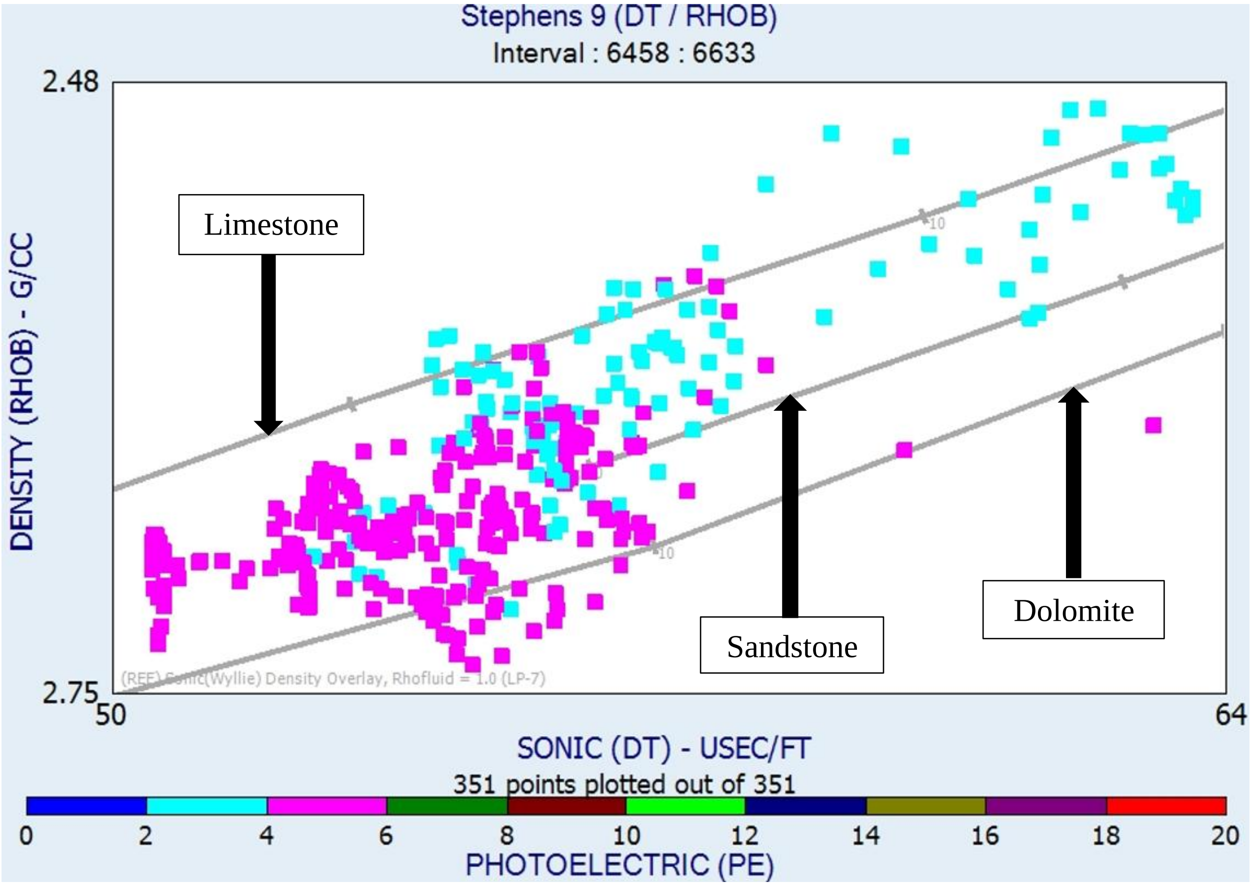

Appendix Figure A.5: Cross plot of Stephens 9 well (Producing) colored with Photoelectric log. Low PE values colored in cyan and high PE values colored in pink (calcite)